Development of Improved Surface Integral Methods for Jet Aeroacoustic Predictions

Anthony R. Pilon
University of Minnesota
Minneapolis, Minnesota

Anastasios S. Lyrintzis
Purdue University
West Lafayette, Indiana

Final Report: NASA–Langley Grant No. NAG-1660

June 1997

Preface

The research described in this report was carried out at the School of Aeronautics and Astronautics at Purdue University and was funded by NASA Grant NAG 1-1660. Dr. Kristine Meadows was the technical monitor. The authors would like to express their appreciation to Dr. Meadows for her useful comments and suggestions throughout the course of this research. Dr. Fereidoun Farassat and Dr. Kenneth Brentner of NASA Langley also provided insight and valuable assistance with the theoretical development in this work.

The Principal Investigator for this sponsored research activity was Professor A. Lyrintzis. Much of this report (except chapter 5) is based on the first author's Ph.D. thesis, with several improvements and corrections.

The authors are grateful to Dr. S. H. Shih, and Dr. R. R. Mankbadi of NASA Lewis Research Center, as well as Dr. J. N. Scott and Mr. T. J. Rozmajzl of The Ohio State University, for providing the results of their CFD calculations, which were used in this work.

This research was supported in part by grant number ASC950019P from the Pittsburgh Supercomputing Center, sponsored by the National Science Foundation (NSF).

Abstract

The accurate prediction of aerodynamically generated noise has become an important goal over the past decade. Aeroacoustics must now be an integral part of the aircraft design process.

The direct calculation of aerodynamically generated noise with CFD–like algorithms is plausible. However, large computer time and memory requirements often make these predictions impractical. It is therefore necessary to separate the aeroacoustics problem into two parts, one in which aerodynamic sound sources are determined, and another in which the propagating sound is calculated. This idea is applied in acoustic analogy methods. However, in the acoustic analogy, the determination of far–field sound requires the solution of a volume integral. This volume integration again leads to impractical computer requirements.

An alternative to the volume integrations can be found in the Kirchhoff method. In this method, Green's theorem for the linear wave equation is used to determine sound propagation based on quantities on a surface surrounding the source region. The change from volume to surface integrals represents a tremendous savings in the computer resources required for an accurate prediction.

This work is concerned with the development of enhancements of the Kirchhoff method for use in a wide variety of aeroacoustics problems. This enhanced method, the modified Kirchhoff method, is shown to be a Green's function solution of Lighthill's equation. It is also shown rigorously to be identical to the methods of Ffowcs Williams and Hawkings. This allows for development of versatile computer codes which can easily alternate between the different Kirchhoff and Ffowcs Williams–Hawkings formulations, using the most appropriate method for the prob-

lem at hand.

The modified Kirchhoff method is developed primarily for use in jet aeroacoustics predictions. Applications of the method are shown for two dimensional and three dimensional jet flows. Additionally, the enhancements are generalized so that they may be used in any aeroacoustics problem.

Contents

List of Figures

Chapter 1

Introduction

Over the past several decades, air travel has become popular. Along with the increase in the use of aircraft has come a marked awareness of the tremendous amounts of aerodynamically generated noise associated with air travel. A relatively new field of study, *aeroacoustics*, has developed as a result. Aeroacoustics is concerned with the investigation of noise generated by moving fluids and surfaces. As the field of aeroacoustics progressed, so did the development of computer hardware and numerical methods to be used in the solution of complex problems in science and engineering. This report is concerned with the development of new numerical techniques, *Kirchhoff methods*, for use in the prediction of noise generated by air and surfaces in motion. The techniques are developed for use in the prediction of noise from high speed jets. However, the development is generalized so that the methods can be easily applied to other aeroacoustics problems, e.g. helicopter rotor noise, fan noise, propeller noise, etc.

1.1 Computational Aeroacoustics

The field of computational aeroacoustics (CAA) is concerned with numerical prediction of the production and propagation of aerodynamically generated sound. The governing equations of fluid mechanics (the Navier–Stokes equations) govern these phenomena. Recent advances in computer hardware and computational fluid dynamics (CFD) methodology have made the direct calculation of aerodynamic noise plausible, but there are several technical difficulties involved in extending CFD technology to CAA applications.[1] Aerodynamic noise generation is governed by nonlinear processes, and the problems of interest are normally associated with high Reynolds number turbulent flows. CAA requires the determination of time dependent flow fluctuations. Thus, conventional approaches to the calculation of turbulent flows based on Reynolds averaging are not applicable, since they cannot resolve the temporal history or spectra of the fluctuations. Direct numerical simulation (DNS) can be used to resolve relevant length and temporal scales without the need of modeling. However, these calculations are currently limited to low Reynolds number flows, because of the large amounts of computational resources required.[2] In many applications, it may be desirable to perform a large eddy simulation (LES) instead. In these calculations the large turbulent structures are calculated directly, as in DNS calculations, but the smaller scales are modeled. It is believed that larger scales are the most efficient in generating noise.[3–6] Mankbadi, et. al.[7–8] have used this approach to calculate the unsteady sound source in an axisymmetric supersonic jet.

With the sound source calculated, several approaches are available to describe the propagation. An obvious strategy is to extend the computational domain in the

calculations used to predict the source. However, if the objective is to predict noise in the acoustic far–field, this direct approach requires prohibitive storage and leads to unrealistic computation time.[7] The acoustic fluctuations are also quite small, usually several orders of magnitude less than mean flow fluctuations. The use of CFD–like algorithms to calculate these disturbances will result in dispersion and dissipation errors. Highly accurate Dispersion Relation Preserving (DRP) schemes have been developed to deal with these difficulties,[9] but storage limitations prohibit their use in the calculation of far–field sound. Thus, the most attractive approach is to separate the calculation into two domains, one for the prediction of the nonlinear sound source, and the other to describe the linear sound propagation.

There are different means of describing the sound propagation after prediction of the source. The most prevalent of these is Lighthill's acoustic analogy.[10] Other alternatives, which have become more popular recently, are surface integral methods. These methods are based on a formulation of Green's theorem for the linear wave equation. Development of new types of surface integral methods for use in jet acoustics studies is the main focus of this work. The developments are related to acoustic analogy methods, so a brief discussion of each is in order.

1.2 Lighthill's Acoustic Analogy

One of the earliest and most influential developments in aeroacoustic theory was presented in 1952,[10] and further developed in 1954 by Lighthill.[11] In this work, Lighthill re–arranged the mass and momentum conservation equations of fluid mechanics to form an inhomogeneous wave equation. In this arrangement, the fluid medium was assumed to be at rest. The fluid motion was taken to be part of the

acoustic source term. This produced a means of determining the noise produced by the turbulent velocity fluctuations in a flow field. The noise produced by solid surfaces and their effect of the turbulent velocity fluctuations were not included in Lighthill's theory. The resultant indeterminant, inhomogeneous wave equation, the *acoustic analogy*, was a very important development. It provided many useful scaling relations at that time. With the later development of CFD methods, the acoustic analogy was used as a basis for the numerical calculation of turbulence generated noise. In this case, CFD methods are used to determine the turbulent velocity fluctuations, and thus the acoustic source term.

Since it's initial development, Lighthill's theory of aerodynamically generated sound has been modified and extended to more accurately account for the effects of source convection, etc. Examples of this work are presented by Phillips,[12] Lilley,[13] Ribner,[14] and many others. An in–depth survey is not in the scope of this project, but two excellent reviews of classical jet noise theory are presented by Ribner,[15] and Lilley.[16]

1.3 Surface Integral Theory

The first attempt to extend Lighthill's acoustic analogy to account for the effects of surfaces in the flow field was presented by Curle.[17] This extension was expanded to include the effects of arbitrary surface and turbulence motion by Ffowcs Williams and Hawkings.[18] Both of these studies utilized the boundary solution to the homogeneous wave equation presented by Kirchhoff.[19] Ffowcs Williams and Hawkings were the first to present a version of Kirchhoff's solution valid for moving boundaries. This solution had been previously attempted by Morgans,[20] and

Khromov.[21] Morgans' solution was shown to have an ambiguity, while that of Khromov was incorrect.[22–23]

While the work of Ffowcs Williams and Hawkings did a great deal to advance the theory behind noise generation by surfaces, their results were not presented in a manner that made them easily applicable in numerical applications. Farassat and Succi,[24] and others, presented the Ffowcs Williams–Hawkings equation in terms of *source* (i.e. the surface) coordinates and time, as opposed to the observer (listener) coordinates and time. This expression allows for efficient numerical predictions of sound generated by moving surfaces. Farassat's formulation of the Ffowcs Williams–Hawkings equation is the predominant method currently being employed in the prediction of rotor and propeller noise. A popular example of these applications is the WOPWOP code developed by Brentner.[25]

1.4 Traditional Kirchhoff Method

The moving surfaces described above which generate noise need not be real, solid surfaces. Hawkings[26] was the first to demonstrate the notion of using a mathematically defined surface to determine mid–field and far–field sound. If this surface is allowed to enclose all sound sources, and is placed in a region where the linear wave equation is valid, the sound at points outside this surface is completely defined in terms of quantities on the surface. This is a result of Kirchhoff's boundary solution to the linear wave equation.[19] In numerical studies, the surface acoustic quantities are usually determined through the use of a suitable CFD algorithm. The combination of a near–field CFD computation with Kirchhoff's boundary integral solution to determine mid–field and far–field sound was proposed by Hawkings,[26]

and has come to be known as the *Kirchhoff Method.* In this work it is often referred to as the *Traditional Kirchhoff Method.*

As mentioned above, Ffowcs Williams and Hawkings[18] derived a version of Kirchhoff's boundary solution which is valid for moving boundaries. Farassat and Myers[27] expressed this solution in terms of source quantities. Their solution is valid for a surface moving or deforming in an arbitrary manner. Their result is easily applicable in numerical methods, and is the basis for many modern Kirchhoff methods.

The traditional Kirchhoff method is attractive as a tool for numerical acoustic prediction because it utilizes surface integrals, and not volume integrals, over a source region to determine mid–field and far–field acoustics. Additionally, the Kirchhoff method does not suffer the dissipation and dispersion errors found when the mid–field and far–field sound is directly calculated with an algorithm similar to those used in computational fluid dynamics studies. A review of the theory and application of Kirchhoff methods is presented by Lyrintzis.[28]

There are difficulties with using the Kirchhoff and related methods for some aeroacoustic problems. For an accurate prediction, the Kirchhoff control surface must completely enclose the aerodynamic source region. This may be difficult or impossible to accomplish if the source region is large. The validity of each method is also dependent on the control surface being placed in a region where the linear wave equation is valid. Difficulties meeting these criteria frequently arise in jet acoustics and similar studies.

Despite these limitations, the traditional Kirchhoff method has been used recently in jet noise predictions. Lyrintzis and Mankbadi[29] calculated the noise due

to a supersonic round jet. They avoided the difficulties discussed above by using an open Kirchhoff surface. That is, no near–field acoustic data was used in regions where the linear wave equation was not valid. This left the predictions invalid in some regions of the calculation domain. Mitchell, et. al.[30] performed similar calculations, with a slightly different formulation of Kirchhoff integral equation and an open surface. Freund et. al.[31] investigated the effects of using an open surface, and proposed corrections for the missing surface using asymptotic approximations and stationary phase assumptions. The current work is devoted to correction of these effects in a different manner. The corrections come from extensions of the traditional Kirchhoff and Ffowcs Williams–Hawkings equations to account for nonlinearities at and outside of the surface.

1.5 Scope of this Work

The main goal of this work is to develop extensions to the traditional Kirchhoff method for use in jet noise aeroacoustics calculations. However, the extensions are quite generalized, so that the newly derived methods will be applicable to a wide range of problems. A secondary goal is to show rigorously the relationship between the traditional Kirchhoff method, the newly derived methods, and the Ffowcs Williams–Hawkings based methods. Numerical calculations will be used to verify the derivations. Results obtained from sample jet acoustics calculations will be presented as well.

It is conceivable that versatile codes can be developed with the results of this report. The codes will be able to alternate between the use of the traditional Kirchhoff method, traditional Ffowcs Williams–Hawkings methods, or the modified

methods developed here. Researchers will then have the choice of the optimum acoustic prediction obtainable with input from any aerodynamic prediction code.

The report is divided into six chapters. Chapter two discusses the development of the traditional Kirchhoff method. Chapter three describes the proposed extensions to the Kirchhoff method. Test and validation calculation results, obtained with simple acoustic sources, are presented in each of these chapters. Sample jet noise calculation results are presented in chapter four. Chapter five presents corrections for the refraction caused by mean flow gradients, and chapter six contains conclusions, and a discussion of additional issues and proposed future work. Portions of this work were presented by the authors in references 32-35.

Chapter 2

The Traditional Kirchhoff Method

A description of the development and uses of the traditional Kirchhoff method will be presented in this chapter. While some of this material (the Kirchhoff formula for a moving and deformable surface in three dimensions) has been presented previously, the the remainder of the results are new. The methods and concepts involved in the derivations are unique enough to warrant a review, as the mathematical development here will serve as a basis for that to be used in the following chapter.

2.1 Generalized Wave Equation

2.1.1 Time Domain

Consider a closed and bounded smooth surface S, the "Kirchhoff Surface." Let $f = 0$ describe the surface such that $f > 0$ in the exterior of the surface. Now assume a function ϕ, which is continuous and has continuous first derivatives over

$f > 0$, satisfies the linear wave equation

$$\frac{1}{a_o^2}\frac{\partial^2\phi}{\partial t^2} - \frac{\partial^2\phi}{\partial x_i^2} = \Box^2\phi = 0 \tag{2.1}$$

outside the surface. Further assume that ϕ and it's first derivatives are given on S for all time. Now, let ϕ be extended to the interior of the surface by setting $\phi = 0$ inside of S. The extended function $\tilde{\phi}(\vec{x}, t)$ is defined as

$$\tilde{\phi}(\vec{x}, t) = \phi(\vec{x}, t)H(f) = \begin{cases} \phi(\vec{x}, t) & f > 0 \\ 0 & f < 0 \end{cases} \tag{2.2}$$

Where $H(f)$ is the Heaviside function. It follows that $\Box^2\tilde{\phi} = 0$ is valid everywhere but at the surface. The function $\tilde{\phi}$ is discontinuous at the surface, and it's derivatives do not exit there. Generalized derivatives,[36–38] however, can be defined. If generalized derivatives are used in equation (2.1), then it is valid over all space. An overbar denotes generalized derivation.

$$\overline{\Box}^2\tilde{\phi} \neq 0 \tag{2.3}$$

The source terms that appear on the right side of (2.3) will lead to the traditional Kirchhoff formulation. The generalized derivatives in (2.3) can be expanded as

$$\begin{aligned} \frac{\overline{\partial}\tilde{\phi}}{\partial t} &= \frac{\partial\tilde{\phi}}{\partial t} + \tilde{\phi}\frac{\partial f}{\partial t}\delta(f) = \frac{\partial\tilde{\phi}}{\partial t} \\ \frac{\overline{\partial}^2\tilde{\phi}}{\partial t^2} &= \frac{\partial^2\tilde{\phi}}{\partial t^2} \end{aligned} \tag{2.4}$$

$$\begin{aligned} \frac{\overline{\partial}\tilde{\phi}}{\partial x_i} &= \frac{\partial\tilde{\phi}}{\partial x_i} + \tilde{\phi}\frac{\partial f}{\partial x_i}\hat{n}_i\delta(f) \\ \frac{\overline{\partial}^2\tilde{\phi}}{\partial x_i^2} &= \frac{\partial^2\tilde{\phi}}{\partial x_i^2} + \frac{\partial\phi}{\partial n}\delta(f) + \frac{\overline{\partial}}{\partial x_i}\left[\phi\hat{n}_i\delta(f)\right] \end{aligned} \tag{2.5}$$

where $\delta(f)$ is the Dirac delta function, and the surface normal vector $\hat{n}_i = \partial f/\partial x_i$. Quantities ϕ and $\partial\phi/\partial n$ are taken in the limit as $f \to 0^+$. Using (2.1), (2.4) and (2.5) in (2.3) gives

$$\overline{\Box}^2\tilde{\phi} = -\frac{\partial\phi}{\partial n}\delta(f) - \frac{\overline{\partial}}{\partial x_i}\left[\phi\hat{n}_i\delta(f)\right] \tag{2.6}$$

This generalized wave equation is valid over all space and time. The source terms on the right side are due to the discontinuities in $\tilde{\phi}$ and its derivatives at S.

2.1.2 Frequency Domain

Through use of the Fourier transform, equation (2.1) can be expressed in the frequency domain as the Helmholtz equation,

$$\frac{\partial^2 \hat{\phi}}{\partial x_i^2} + k^2 \hat{\phi} = 0 \tag{2.7}$$

where ω is the cyclic frequency, k is the wave number, $k = \omega/a_o$, and $\hat{\phi}$ is the complex Fourier transform of ϕ

$$\hat{\phi} = \int_{-\infty}^{\infty} \phi\, e^{i\omega t} dt \qquad \phi = \frac{1}{2\pi} \int_{-\infty}^{\infty} \hat{\phi}\, e^{-i\omega t} d\omega$$

Then, following the analysis above, the generalized form of the Helmholtz equation is

$$\frac{\overline{\partial}^2}{\partial x_i^2} \left(\hat{\phi} H(f)\right) + k^2 \hat{\phi} H(f) = -\frac{\partial \hat{\phi}}{\partial n} \delta(f) - \frac{\overline{\partial}}{\partial x_i} \left[\hat{\phi} \hat{n}_i \delta(f)\right] \tag{2.8}$$

The generalized wave equations can be solved through the use of appropriate Green's functions to produce the Kirchhoff's integral equation. The necessary Green's function is dependent on the formulation (time or frequency), and the dimension of the problem. Green's functions for two dimensional and three dimensional problems are presented here.

2.2 Green's Functions

If source coordinates and time are denoted by (y_i, τ) and observer coordinates and time are denoted with (x_i, t), $r = |x_i - y_i|$, and a_o is the ambient wave speed,

the free–space Green's function for the three dimensional wave equation (i.e. indices i and j are $1-3$) is[27]

$$G_3 = \frac{\delta(g)}{4\pi r} \quad \text{where} \quad g = \tau - t + \frac{r}{a_o} \tag{2.9}$$

In the frequency domain, the Green's function may be expressed as

$$\widehat{G}_3 = \frac{\exp(i\omega r/a_o)}{4\pi r} \tag{2.10}$$

However, if the problem of interest is two dimensional ($i, j = 1-2$) then the time domain free–space Green's function is[39]

$$G_2 = \frac{H(a_o t - r)}{2\pi a_o (a_o^2 t^2 - r^2)} \tag{2.11}$$

and in the frequency domain,

$$\widehat{G}_2 = \frac{H_0^{(2)}(kr)}{4i} \tag{2.12}$$

where $H_0^{(2)}$ is the Hankel function of the second kind of order zero.[40] Convolution of these functions with the corresponding generalized wave equations will lead to the different forms of the Kirchhoff integral equation.

2.3 Stationary Kirchhoff Integral

2.3.1 Time Domain – 3D

Convolution of the three dimensional, time domain, free–space Green's function, (2.9) with (2.6), and integration over all space and over $(-\infty, t]$ in time gives

$$4\pi\widetilde{\phi}(\vec{x}, t) = -\int \frac{1}{r}\frac{\partial\phi}{\partial n}\delta(f)\,\delta(g)\,d\vec{y}\,d\tau - \frac{\overline{\partial}}{\partial x_i}\int \frac{\phi\hat{n}_i}{r}\delta(f)\,\delta(g)\,d\vec{y}\,d\tau \tag{2.13}$$

The volume element $d\vec{y}$ is equal to $dS\,df$, where dS is the element of area on S. τ may now be transformed to g. The Jacobian of this transformation, for a stationary

surface is 1. Integration over space is restricted to S, due to the nature of the delta functions, and integration over g introduces the retarded time.

$$4\pi\tilde{\phi}(\vec{x},t) = -\int \frac{1}{r}\left[\frac{\partial\phi}{\partial n}\right]_{\tau^*} dS - \frac{\overline{\partial}}{\partial x_i}\int \frac{[\phi\hat{n}_i]_{\tau^*}}{r}\, dS \tag{2.14}$$

Here the subscript τ^* indicates evaluation of the quantities in brackets at the retarded (emission) time

$$[\phi]_{\tau^*} \equiv \phi(y_i, t - r/a_\circ)$$

The gradient operator can be brought inside the second integral. Then the traditional Kirchhoff integral for a stationary surface is

$$4\pi\phi(\vec{x},t)H(f) = \int_S \frac{1}{r}\left[\frac{1}{a_\circ}\frac{\partial\phi}{\partial\tau}\cos\theta - \frac{\partial\phi}{\partial n}\right]_{\tau^*} dS + \int_S \frac{[\phi]_{\tau^*}}{r^2}\, dS \tag{2.15}$$

where $\cos\theta = \vec{r}\cdot\hat{n}/|\vec{r}|$.

Due to the nature of the Heaviside function, this formula will produce a null sound field for any observer inside of S. As a result, ϕ, $\partial\phi/\partial n$, and $\partial\phi/\partial\tau$ are not independent on S. Equation (2.15) can be used to determine the sound signal at any observer point outside of S based on quantities on S. Alternatively, the observer can be placed on the surface. In this case, (2.15) becomes an integral equation governing ϕ on S. This is the basis for boundary element methods.[41] The derivation here follows that of Farassat and Myers.[27]

2.3.2 Frequency Domain – 3D

The frequency domain formulation of the Kirchhoff integral equation is developed in the same manner as that presented above. Convolution of (2.10) with (2.8), and integration over all space gives

$$4\pi\hat{\phi}(\vec{x},\omega)H(f) = -\int \frac{1}{r}\frac{\partial\hat{\phi}}{\partial n}\delta(f)\, e^{i\omega r/a_\circ}\, d\vec{y} - \frac{\overline{\partial}}{\partial x_i}\int \frac{\hat{\phi}\hat{n}_i}{r}\delta(f)\, e^{i\omega r/a_\circ}\, d\vec{y} \tag{2.16}$$

As in the previous section, the divergence operator is brought inside the integral to produce the Kirchhoff integral in the frequency domain,

$$4\pi\widehat{\phi}(\vec{x},\omega)H(f) = \int_S e^{i\omega r/a_\circ}\left[\frac{1}{r}\left(-\frac{i\omega}{a_\circ}\cos\theta\,\widehat{\phi} - \frac{\partial\widehat{\phi}}{\partial n}\right) + \frac{\widehat{\phi}\cos\theta}{r^2}\right] dS \qquad (2.17)$$

This frequency domain formulation of Kirchhoff's integral equation is often used in applications.[42] Recently, the developments of Farassat and Myers[27] made time domain applications more easily applicable. Farassat and Myers mention that the developments of this section (producing the frequency domain Kirchhoff integral from a generalized form of the Helmholtz equation) are valid, but do not actually carry out the necessary steps, which are shown here.

2.3.3 Frequency Domain – 2D

The two dimensional formulations of Kirchhoff's integral equation can be developed in the same manner as those for three dimensional problems presented above. However, the free–space Green's function for the wave equation in two dimensions, equation (2.11), does not contain a Dirac delta function which would lead to the notion of a retarded time. Alternatively, it can be said that Huygens' principle[42] is not valid in two dimensions. The lack of a retarded time makes the time domain formulation unattractive for 2D cases. The frequency domain formulation, however, is useful in applications and is shown here. Atassi and his associates have used a two dimensional frequency domain formulation in studies of acoustic radiation from airfoils.[43–45]

The two dimensional frequency domain formulation is derived in the same manner as that presented above. The generalized 2D Helmholtz equation (2.8) is convolved with the free–space Green's function, (2.12). The integration is over all

space in two dimensions.

$$4i\widehat{\phi}(\vec{x},\omega)H(f) = -\int \frac{\partial\widehat{\phi}}{\partial n} H_0^{(2)}(kr)\delta(f)\,d\vec{y} - \frac{\overline{\partial}}{\partial x_i}\int \widehat{\phi}\hat{n}_i\, H_0^{(2)}(kr)\delta(f)\,d\vec{y} \qquad (2.18)$$

The divergence operator acts only on the Hankel function, so the two dimensional form of the frequency domain Kirchhoff integral is

$$4i\widehat{\phi}(\vec{x},\omega)H(f) = -\int_S \left[\frac{\partial\widehat{\phi}}{\partial n} H_0^{(2)}(kr) - \cos\theta\, k\,\widehat{\phi}\, H_1^{(2)}(kr)\right] dS \qquad (2.19)$$

Here the integral over S is understood to be a line integral in two dimensional space.

2.4 Moving/Deforming Kirchhoff Integral

The analysis used above can also be used to determine the Kirchhoff integral for an arbitrarily moving or deforming surface. In this case the function f, which defines the surface, is a function of time. Thus, the temporal derivatives in (2.6) become

$$\begin{aligned}\frac{\overline{\partial}\widetilde{\phi}}{\partial t} &= \frac{\partial\widetilde{\phi}}{\partial t} + \widetilde{\phi}\frac{\partial f}{\partial t}\delta(f) = \frac{\partial\widetilde{\phi}}{\partial t} - \phi\, v_n\delta(f)\\ \frac{\overline{\partial}^2\widetilde{\phi}}{\partial t^2} &= \frac{\partial^2\widetilde{\phi}}{\partial t^2} - \frac{\partial\phi}{\partial t_x} v_n\delta(f) - \frac{\overline{\partial}}{\partial t}\left[\phi\, v_n\delta(f)\right]\end{aligned} \qquad (2.20)$$

where $v_n = -\partial f/\partial t$ is the local normal velocity of the surface. The subscript x on the temporal derivative is to indicate differentiation at the observer time and coordinates. The generalized Laplacian of $\widetilde{\phi}$ is given by equation (2.5) above. Using (2.20) and (2.5) in (2.6) results in

$$\begin{aligned}\overline{\Box}^2\left[\phi H(f)\right] = &-\left(\frac{\partial\phi}{\partial n} + \frac{1}{a_o}M_n\frac{\partial\phi}{\partial t_x}\right)\delta(f)\\ &-\frac{1}{a_o}\frac{\overline{\partial}}{\partial t}\left[M_n\,\phi\,\delta(f)\right] - \frac{\overline{\partial}}{\partial x_i}\left[\phi\,\hat{n}_i\,\delta(f)\right]\end{aligned} \qquad (2.21)$$

Here $M_n = v_n/a_\circ$ is the local normal Mach number of the surface motion. This equation is also valid over all space and time, so that the above procedure can be followed. Use of the free-space Green's function for the temporal wave equation, equation (2.9), gives

$$\begin{aligned} 4\pi\tilde{\phi}(\vec{x},t) = &- \int \frac{1}{r}\Big(\frac{\partial\phi}{\partial n} + \frac{1}{a_\circ}M_n\frac{\partial\phi}{\partial\tau_y}\Big)\delta(f)\,\delta(g)\,d\vec{y}\,d\tau \\ &- \frac{1}{a_\circ}\frac{\overline{\partial}}{\partial t}\int \frac{1}{r}M_n\,\phi\,\delta(f)\,\delta(g)\,d\vec{y}\,d\tau \\ &- \frac{\overline{\partial}}{\partial x_i}\int \frac{1}{r}\phi\,\hat{n}_i\,\delta(f)\,\delta(g)\,d\vec{y}\,d\tau \end{aligned} \tag{2.22}$$

The subscript y on the temporal derivative now indicates evaluation of the derivative at the source time and coordinates. It is now possible to evaluate the integrals, and transform τ to g to obtain a valid form of the Kirchhoff integral equation. However, this would leave the temporal derivative and divergence operators outside of the integrals. Such a formulation would be difficult to utilize in numerical applications. However, Farassat and Myers[27] show how the operators may be expressed in terms of source quantities. Their derivation is followed here.

First, note that the generalized divergence operator acts only on the term $\delta(g)/r$. This term may be re–written as[27]

$$\frac{\overline{\partial}}{\partial x_i}\left[\frac{\delta(g)}{r}\right] = -\frac{1}{a_\circ}\frac{\overline{\partial}}{\partial t}\left[\frac{\hat{r}_i\,\delta(g)}{r}\right] - \frac{\hat{r}_i\,\delta(g)}{r^2} \tag{2.23}$$

where $\hat{r} = (\vec{x}-\vec{y})/r$ is the unit radiation vector. Using this relation in (2.22) leads to

$$\begin{aligned} 4\pi\tilde{\phi}(\vec{x},t) = &- \int \frac{1}{r}\Big(\frac{\partial\phi}{\partial n} + \frac{1}{a_\circ}M_n\frac{\partial\phi}{\partial\tau_y}\Big)\delta(f)\,\delta(g)\,d\vec{y}\,d\tau \\ &+ \int \frac{\phi}{r^2}\cos\theta\,\delta(f)\,\delta(g)\,d\vec{y}\,d\tau \\ &+ \frac{1}{a_\circ}\frac{\overline{\partial}}{\partial t}\int \frac{\phi}{r}\left(\cos\theta - M_n\right)\delta(f)\,\delta(g)\,d\vec{y}\,d\tau \end{aligned} \tag{2.24}$$

The temporal derivative in observer time of the third integral must also be expressed in a different form to create a useful formulation. Thus, it is transformed to source time, and brought inside the integral. First, $\vec{y}$ is transformed to coordinates local to the surface, (u^1, u^2, u^3). (u^1, u^2) describe the surface, and $u^3 = f$. Then τ is transformed to g. The Jacobians of the transformations are 1 and $1/(1 - M_r)$ respectively, where $M_r = M_i \hat{r}_i$ is the Mach number of the surface motion in the radiation direction. Integration over $\vec{u}$ and g gives

$$\begin{aligned} 4\pi\tilde{\phi}(\vec{x},t) = &- \int_{D(S)} \left[\frac{\sqrt{g_{(2)}}}{r(1-M_r)} \left(\frac{\partial \phi}{\partial n} + \frac{1}{a_o} M_n \frac{\partial \phi}{\partial \tau_y} \right) \right]_{\tau^*} du^1\, du^2 \\ &+ \int_{D(S)} \left[\frac{\phi \cos\theta \sqrt{g_{(2)}}}{r^2(1-M_r)} \right]_{\tau^*} du^1\, du^2 \\ &+ \int_{D(S)} \left\{ \frac{1}{a_o r\,(1-M_r)} \frac{\partial}{\partial \tau} \left[\frac{(\cos\theta - M_n)\,\phi}{(1-M_r)} \sqrt{g_{(2)}} \right] \right\}_{\tau^*} du^1\, du^2 \end{aligned} \tag{2.25}$$

The determinant of the coefficients of the first fundamental form on the surface S is $g_{(2)} = g_{11}g_{22} - g_{12}^2$, where g_{ij} are the metric tensor components for $(i, j = 1, 2)$. Details on differential geometry can be found in a book by Aris.[46] $g_{(2)}$ is a function of $\vec{u}$ and the source time, τ. The surface integral is over $D(S)$, the domain of S in the space defined by (u^1, u^2). Subscript τ^* again indicates evaluation of the integrand at the emission time τ^*, which is now the root of

$$g = \tau - t + \frac{|\vec{x} - \vec{y}(u^1, u^2, 0, \tau)|}{a_o} = 0 \tag{2.26}$$

If the surface velocity is subsonic (2.26) has a unique solution. However, (2.25) is still valid for supersonically moving surfaces. Farassat and Myers[47] have developed an "emission surface" formulation that deals with the singularities caused when $(1 - M_r) \longrightarrow 0$. However, this formulation is lengthy and quite complicated, so it is not used here. Doppler singularities are not encountered in the cases of interest shown here. Farassat and Myers[27] evaluated the time derivative in the

third integral of (2.25) analytically, to cast the integral in a form that is useful in numerical applications. Their notation is used here, for the moving surface version of the traditional Kirchhoff formula

$$4\pi\phi(\vec{x},t)H(f) = \int_{D(S)} \left[\frac{E_1\sqrt{g_{(2)}}}{r\,(1-M_r)} + \frac{\phi\,E_2\sqrt{g_{(2)}}}{r^2\,(1-M_r)} \right]_{\tau^*} du^1\,du^2 \tag{2.27}$$

where

$$\begin{aligned} E_1 = &\left(M_n^2 - 1\right)\frac{\partial\phi}{\partial n} + M_n\vec{M}_t\cdot\nabla_2\phi - \frac{M_n}{a_\circ}\dot{\phi} \\ &+ \frac{1}{a_\circ(1-M_r)^2}\left[\dot{M}_r\,(\cos\theta - M_n)\,\phi\right] \\ &+ \frac{1}{a_\circ(1-M_r)}\Big[\left(\dot{n}_r - \dot{M}_n - \dot{n}_M\right)\phi \\ &+ (\cos\theta - M_n)\,\dot{\phi} + (\cos\theta - M_n)\,\phi\,\dot{\sigma}\Big] \\ E_2 = &\frac{(1-M^2)}{(1-M_r)^2}\,(\cos\theta - M_n) \end{aligned} \tag{2.28}$$

Here $\vec{M}_t$ is the Mach number vector tangent to the surface, and ∇_2 is the surface gradient operator. Also, (a dot indicates a source time derivative, with (u^1, u^2, u^3) kept fixed)

$$\dot{M}_r = \dot{M}_i\hat{r}_i \qquad \dot{n}_r = \dot{n}_i\hat{r}_i \qquad \dot{M}_n = \dot{M}_i\hat{n}_i$$

$$\dot{n}_M = \dot{n}_i M_i \qquad \dot{\sigma} = (1/\sqrt{g_{(2)}})\partial\sqrt{g_{(2)}}/\partial\tau$$

The convective derivative $\dot{\phi}$ is defined by

$$\dot{\phi} = a_\circ M_n\frac{\partial\phi}{\partial n} + a_\circ\vec{M}_t\cdot\nabla_2\phi + \frac{\partial\phi}{\partial\tau_y}$$

The form of (2.28) and E_1, E_2 were given by Farassat and Myers.[27] E_2 was presented in the simplified form shown here by Myers and Hausmann.[48] If the control surface is assumed to be rigid, then $[\sqrt{g_{(2)}}]_{\tau^*}du^1\,du^2$ is equal to the differential surface element dS. This form of Kirchhoff's integral equation is the most popular, and

is widely used in aeroacoustic calculations,[28] particularly rotor and propeller noise studies.

It is also possible to develop frequency domain and two dimensional formulations of the Kirchhoff integral for generally moving and deforming surfaces. The process would be identical to that shown above. However, general surface deformation and motion is time dependent and not periodic. Mixing these time dependent quantities with frequency dependent quantities in a "mixed formulation" seems to be counter productive. It seems to be most efficient to keep all quantities in terms of either frequency or time. Therefore, the full Kirchhoff formula for a generally moving and deforming surface will only be presented for the time domain, three dimensional case. Development of other formulations in the manner described above would be valid however. One special case of interest where a frequency domain formulation can be developed is that of uniform rectilinear motion by a rigid surface. This formulation is presented next.

2.5 Uniform Rectilinear Motion

2.5.1 Time Domain

A case of interest in aeroacoustics and aerodynamics is that of uniform rectilinear motion, i.e. the Kirchhoff surface and observer points are both moving in the same direction, with the same constant velocity. Myers and Hausmann[49] used a reduced form of the Farassat and Myers[27] formulation to calculate acoustic scattering due to bodies moving in this fashion. Morino[41] developed an equivalent formulation for use in unsteady aerodynamics. Here, the traditional Kirchhoff formulation is shown for the case of rectilinear motion. This formula can be used in the study

of forward flight effects on jet acoustics.

The control surface is assumed to be rigid and, due to the rectilinear nature of the motion, $\dot{M}$, $\dot{\sigma}$, $\dot{n}$, etc. are zero. It is convenient to express the integrals in a frame of reference that is moving with the surface and observer. Let (x_1, x_2, x_3) and (y_1, y_2, y_3) now denote the cartesian observer and source coordinates in the moving frame, and let (X_1, X_2, X_3) and (Y_1, Y_2, Y_3) be the stationary observer and source coordinates. Then

$$X_i(t) = x_i + tV \qquad Y_i(\vec{u}, \tau) = y_i(\vec{u}) + \tau V$$

where V is the speed of the surface motion. If the motion is assumed to be in the x_1 direction, Equation (2.26) can now be written explicitly as[49]

$$a_o(t - \tau^*) = \left\{\left[(x_1 - y_1) + V\left(t - \tau^*\right)\right]^2 + (x_2 - y_2)^2 + (x_3 - y_3)^2\right\}^{\frac{1}{2}} \tag{2.29}$$

Solving for τ^* gives

$$\tau^* = t - \frac{r_o + M\left(x_1 - y_1\right)}{a_o\left(1 - M^2\right)} \tag{2.30}$$

where

$$r_o = \left\{(x_1 - y_1)^2 + (1 - M^2)\left[(x_2 - y_2)^2 + (x_3 - y_3)^2\right]\right\}^{\frac{1}{2}}$$

Equation (2.27) can now be applied as for an arbitrary surface. The simplified form is

$$4\pi\phi(\vec{x}, t)H(f) = \int_S \left[\frac{\tilde{E}_1}{r\left(1 - M_r\right)} + \frac{\phi\, E_2}{r^2\left(1 - M_r\right)}\right]_{\tau^*} dS \tag{2.31}$$

where

$$\tilde{E}_1 = \left(M_n^2 - 1\right)\frac{\partial\phi}{\partial n} + M_n\vec{M}_t \cdot \nabla_2\phi - \frac{M_n}{a_o}\dot{\phi} + \frac{1}{a_o(1 - M_r)}\left(\cos\theta - M_n\right)\dot{\phi} \tag{2.32}$$

This expression is the Kirchhoff formula appropriate for use in studies of jet noise in which there is a non–zero free stream velocity.

2.5.2 Frequency Domain

The frequency domain counterpart to equation (2.32) can be derived in a similar manner to that shown above. An equivalent frequency domain formulation for rectilinear motion was presented by Lyrintzis and Mankbadi.[29] The equivalent to (2.32) in the frequency domain is

$$4\pi\widehat{\phi}(\vec{x},\omega)H(f) = \int_S e^{i\omega r/a_\circ}\left[\frac{K_1}{r\,(1-M_r)} + \frac{\widehat{\phi}\,E_2}{r^2\,(1-M_r)}\right]dS \qquad (2.33)$$

where

$$K_1 = \left(M_n^2 - 1\right)\frac{\partial\widehat{\phi}}{\partial n} + M_n\vec{M}_t\cdot\nabla_2\widehat{\phi} + \frac{iM_n\omega}{a_\circ}\,\widehat{\phi} - \frac{i\omega\widehat{\phi}}{a_\circ(1-M_r)}\,(\cos\theta - M_n) \qquad (2.34)$$

Validation calculations using the various Kirchhoff integral formulations are presented next.

2.6 Validation Calculations

Several calculations have been performed in order to validate the surface integral methodology and the computer codes used in this research. Results of these calculations are presented in this section.

2.6.1 Three Dimensional Calculations

The easiest means of testing the numerical implementation of Kirchhoff's integral equation is to place a point acoustic source inside of a simply defined surface. The point acoustic source is defined by the right side of

$$\Box^2\phi = Q\delta(\vec{y}_\circ) \qquad (2.35)$$

where Q is the source function, and $\delta(\vec{y}_o)$ is the Dirac delta function with support at $\vec{y}_o$. Equation (2.35) can be solved through the use of the free–space Green's function. The solution in terms of observer variables is

$$\phi(\vec{x},t) = \frac{[Q]_{\tau^*}}{4\pi r} \tag{2.36}$$

where $r = |\vec{x} - \vec{y}_o|$. Equation (2.36) can be used to determine ϕ, ϕ_n, and ϕ_τ on a Kirchhoff surface which surrounds $\vec{y}_o$. Because it is most appropriate for use in jet acoustics predictions, a cylindrical Kirchhoff surface is used in most of the calculations here. The Kirchhoff surface and point source geometry are shown in figure 2.1.

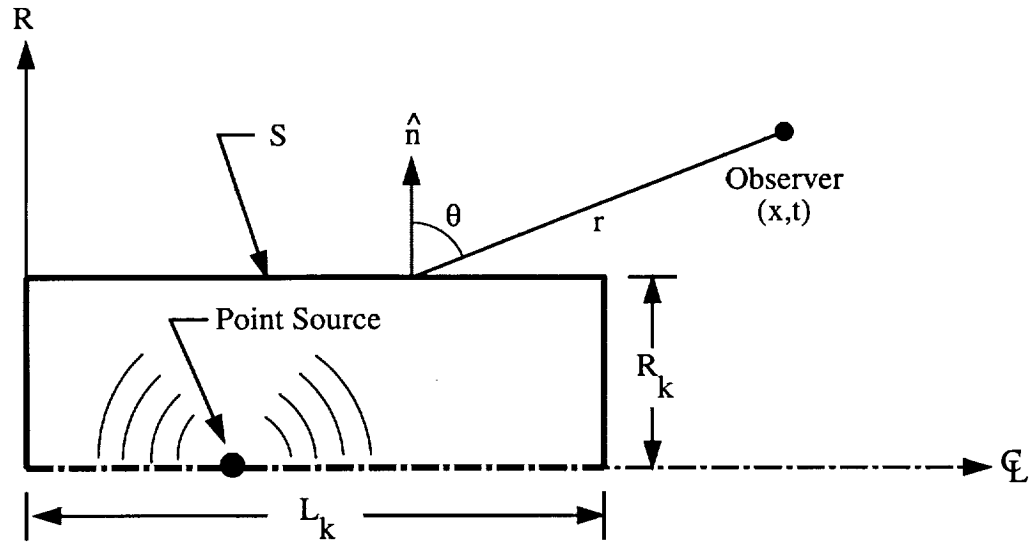

Figure 2.1. Point source and Kirchhoff surface geometry for the validation calculations.

The first calculations were performed to validate the traditional Kirchhoff method in the time domain. A point monopole was used as the acoustic source

at $\vec{y}_o$. That is, $Q = A\sin(\omega_o \tau)$, where ω_o is the angular frequency of the acoustic radiation, and A is a scalar amplitude. $\vec{y}_o$ was chosen so that the point monopole was on the centerline of the cylindrical Kirchhoff surface, $3.5\,\lambda$ from the left end of the surface; where the wavelength λ is $\omega_o/2\pi a_o$. The Kirchhoff surface had a length, L_k of $10\,\lambda$, and a radius, R_k of $2\,\lambda$. First order, mid–panel quadrature[50] was used to solve the integrals in equation (2.31). 201, 81, and 73 quadrature points were used on the surface in the axial, radial and azimuthal directions respectively. There were 64 discrete temporal points per acoustic period, $T = 2\pi/\omega_o$. Figure 2.2 shows exact and predicted temporal acoustic signals at an observer located at $(x, R) = (5\,\lambda, 5\,\lambda)$. Both the Kirchhoff surface and the observer are stationary. The predicted signal, calculated with the traditional Kirchhoff method, and the exact signal, from equation (2.36) show excellent agreement.

Figure 2.3 shows the exact and predicted signals for identical conditions to those used to generate figure 2.2, except that both the Kirchhoff surface and the observer are moving in the negative x direction with a Mach number of $M = 0.40$. The signals again show excellent agreement. The traditional Kirchhoff method should thus be valid for control surfaces and observers which are stationary, or in rectilinear motion, as long as all acoustic sources are contained within the Kirchhoff surface, and there is a suitable number of quadrature and temporal points used. The frequency domain version of the three dimensional Kirchhoff integral was also used to calculate the acoustic field of a point acoustic monopole. In this case, equation (2.36) is written as

$$\widehat{\phi}(\vec{x}, \omega_o) = \frac{A e^{i\omega_o r/a_o}}{4\pi r} \tag{2.37}$$

Figure 2.4 shows two iso–contours of the real part of $\widehat{\phi}$, at angular frequency ω_o, in the acoustic near–field and mid–field of the point acoustic source. The source

remained on the centerline, $3.5\,\lambda$ from the left end of the surface. The Kirchhoff surface dimensions and number of quadrature points were kept constant from those used in the earlier figures.

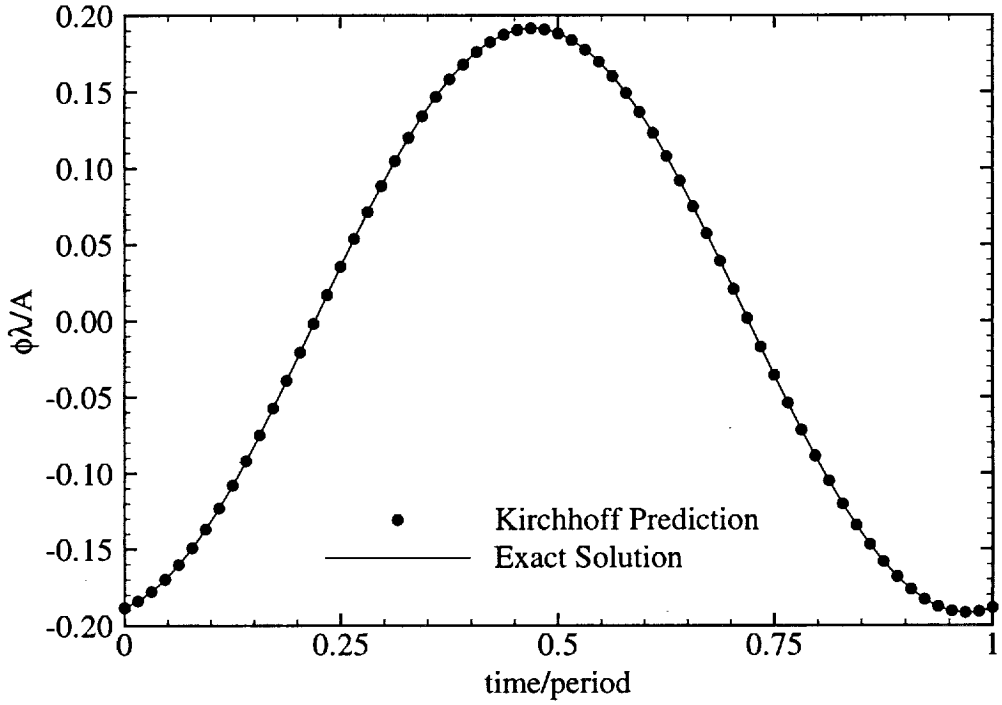

Figure 2.2. Predicted and exact acoustic signals at $(x, R) = (5\,\lambda, 5\,\lambda)$. $M = 0.00$. Time domain formulation.

The contours shown above the centerline are those predicted with the traditional Kirchhoff method, while those below the centerline were calculated with (2.37). The Kirchhoff control surface is shown as well. The contours appear to match quite well, except for observation points inside the Kirchhoff surface, where there is a null sound field. This null field is a consequence of the causality condition imposed on the free–space greens function, and the nature of the Heaviside function found

on the left side of equations (2.31) and (2.33). The effects of rectilinear motion are shown in figure 2.5. Here the conditions are the same as those of figure 2.4, except that the Kirchhoff surface, and all observation points, are moving in the $-x$ direction at $M = 0.4$. The Doppler effect is noticeable, as is the excellent agreement between the exact and predicted signals.

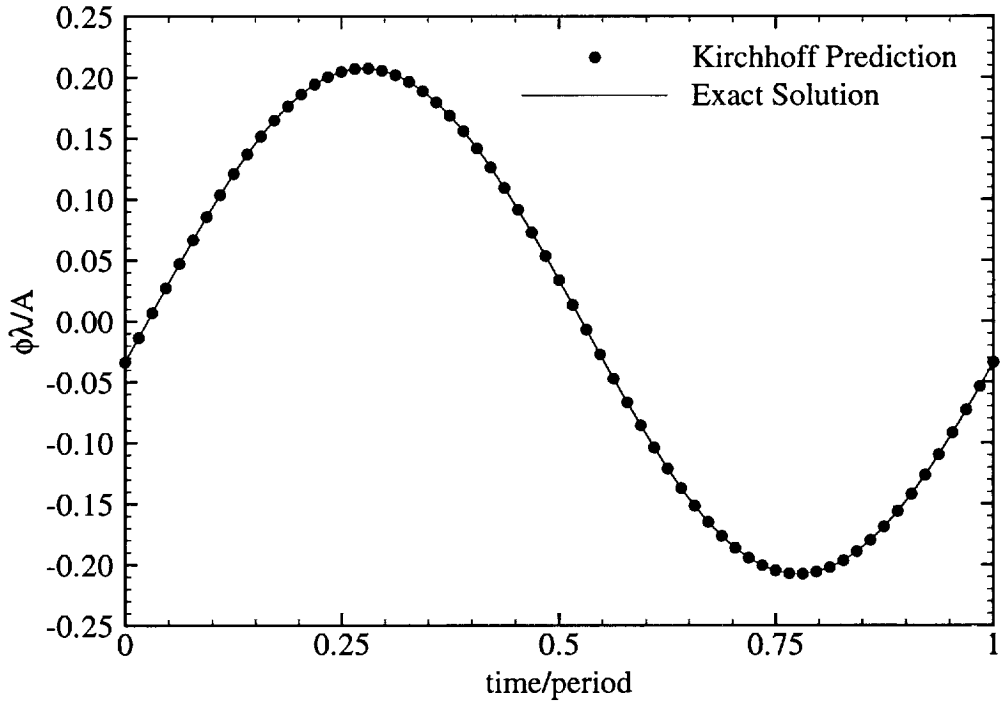

Figure 2.3. Predicted and exact acoustic signals at $(x, R) = (5\,\lambda, 5\,\lambda)$. $M = -0.40$. Time domain formulation.

The ability of the Kirchhoff method to capture the directivity of an acoustic signal was also tested. In this test, the conditions used in figures 2.5, and 2.4 were kept constant. But, the point monopole source was changed to a point dipole. In

this case, (2.37) is written

$$\widehat{\phi}(\vec{x},\omega_o) = \nabla \cdot \left(\frac{A e^{i\omega_o r/a_o} \vec{dl}}{4\pi r} \right) \tag{2.38}$$

where $\vec{dl}$ is a unit vector which points in the direction of the dipole's axis.

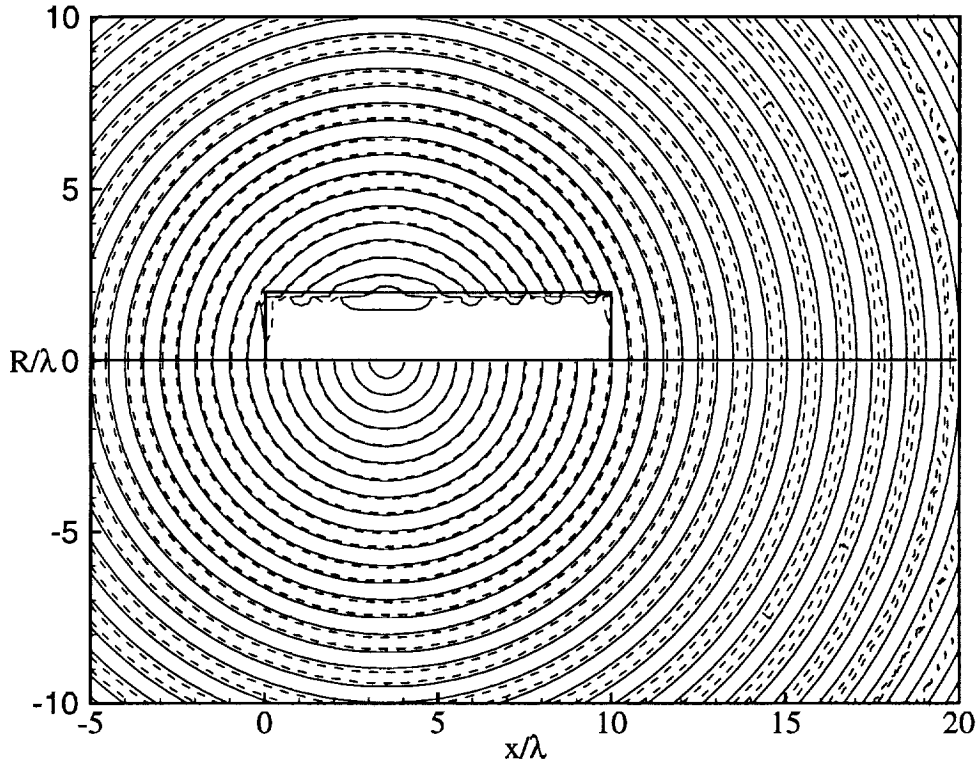

Figure 2.4. Real part of predicted and exact monopole acoustic field. $R > 0$: Traditional Kirchhoff prediction, $R < 0$: Exact solution. Solid line is $\Re(\widehat{\phi}\,\lambda/A) = 0.32$. Dashed line is $\Re(\widehat{\phi}\,\lambda/A) = -1.63$. $M = 0.00$. Frequency domain formulation.

Figure 2.6 shows two iso–contours of the real part of $\widehat{\phi}$, at angular frequency ω_o, in the acoustic near–field and mid–field of the point acoustic dipole. The point dipole remained in the same position as the point monopole used above. The Kirchhoff surface dimensions and number of quadrature points were also kept constant.

The contours again appear to match quite well, with the exception of observation points inside the Kirchhoff surface. This agreement serves to validate the ability of the traditional Kirchhoff method to capture the directivity of acoustic radiation. The effects of rectilinear motion on dipole radiation are shown in figure 2.7. The surface and observation points again moves with $M = -0.40$. The traditional Kirchhoff method again does an excellent job of capturing the radiated sound field.

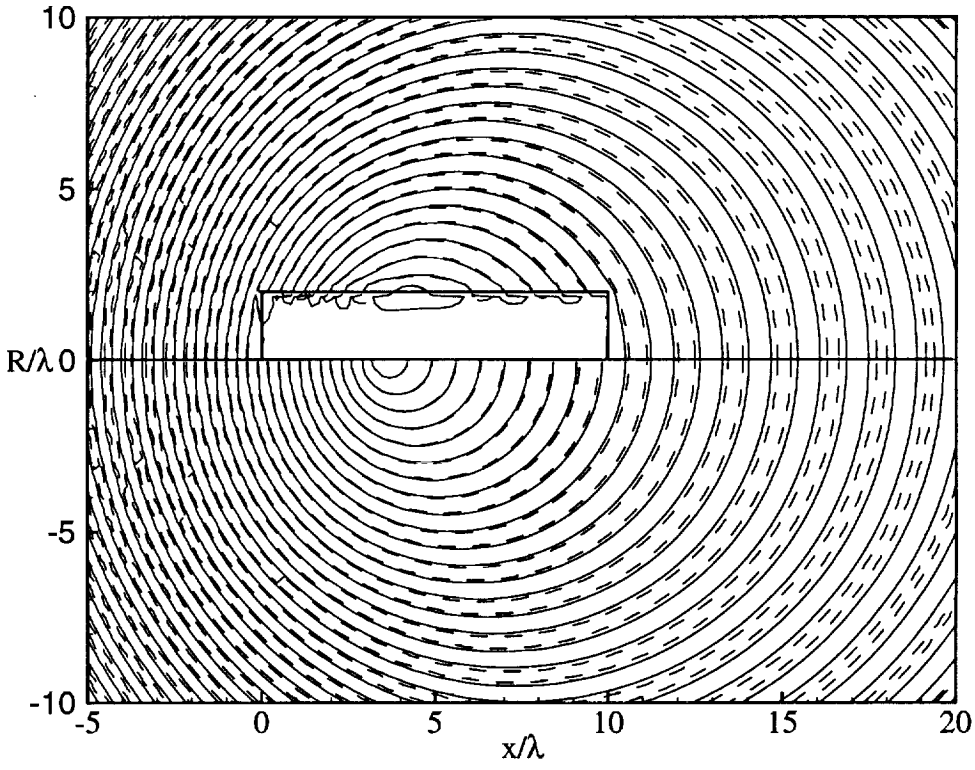

Figure 2.5. Real part of predicted and exact monopole acoustic field. $R > 0$: Traditional Kirchhoff prediction, $R < 0$: Exact solution. Solid line is $\Re(\widehat{\phi}\,\lambda/A) = 0.32$. Dashed line is $\Re(\widehat{\phi}\,\lambda/A) = -1.63$. $M = -0.40$. Frequency domain formulation.

The results presented to this point have shown that the traditional Kirchhoff method does an excellent job of predicting acoustic radiation, provided the Kirchhoff

surface is rigid, and in rectilinear motion. A suitable surface discretization and quadrature scheme must be used as well. Other researchers have determined the validity of the Kirchhoff method for rigid rotating, control surfaces.[28] However, to date a deformable Kirchhoff surface has not been used to calculate acoustic radiation. The implementation of the surface discretization and quadrature scheme will be discussed next.

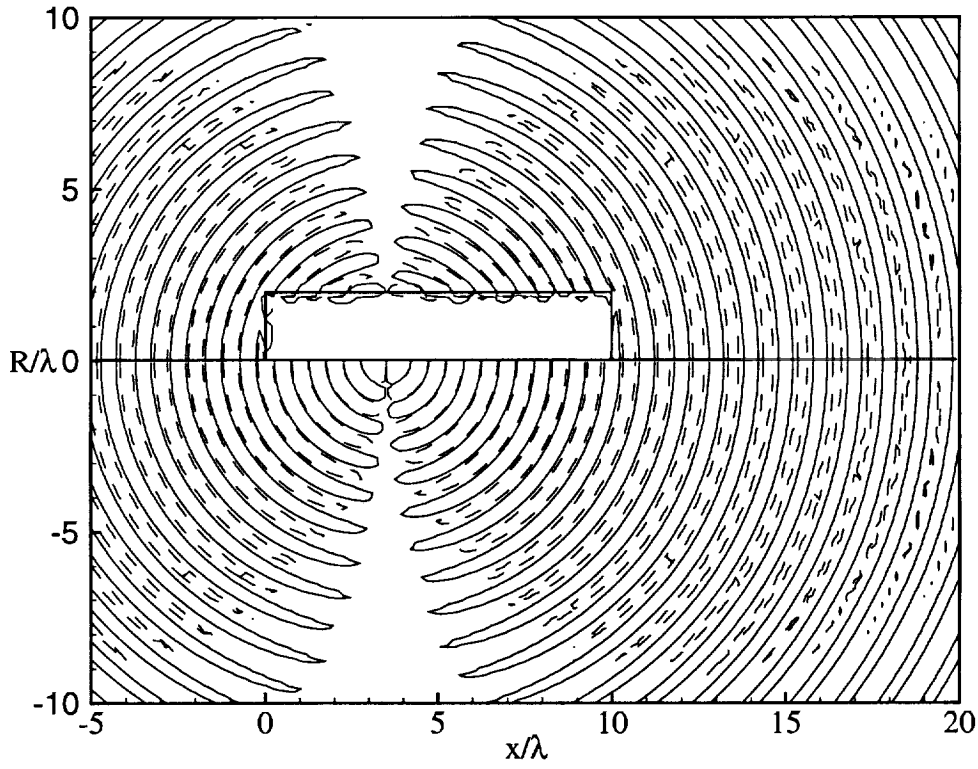

Figure 2.6. Real part of predicted and exact dipole acoustic field. $R > 0$: Traditional Kirchhoff prediction, $R < 0$: Exact solution. Solid line is $\Re(\widehat{\phi}\,\lambda^2/A) = 4.27$. Dashed line is $\Re(\widehat{\phi}\,\lambda^2/A) = -10.66$. $M = -0.40$. Frequency domain formulation.

The first order mid–panel quadrature scheme[50] used in the predictions shown above produced excellent results. However, in practical studies, it is not a simple

matter to allocate an arbitrary number of discrete quadrature points, as was done above. Most often, the surface quadrature points are determined by the computational mesh used in the near-field CFD/CAA calculations. Thus, in order to increase the number of quadrature points on the surface, a researcher would have to perform an additional costly CFD calculation. It is therefore important to know a priori the amount of discrete spatial and temporal points required for a desirable level of accuracy.

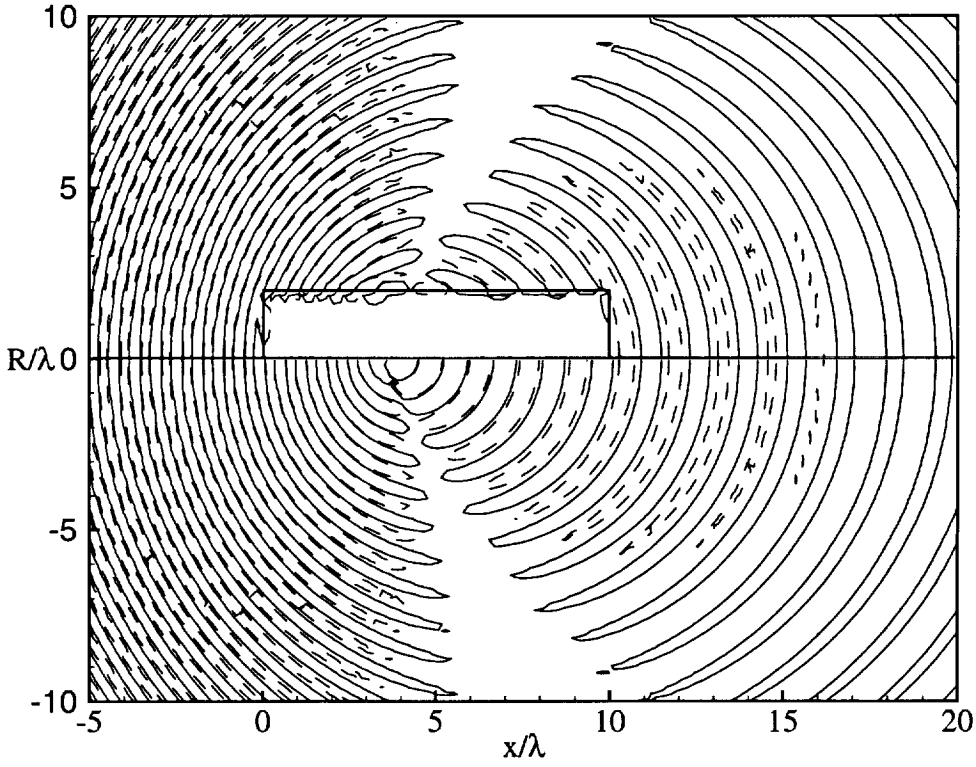

Figure 2.7. Real part of predicted and exact dipole acoustic field. $R > 0$: Traditional Kirchhoff prediction, $R < 0$: Exact solution. Solid line is $\Re(\widehat{\phi}\,\lambda^2/A) = 4.27$. Dashed line is $\Re(\widehat{\phi}\,\lambda^2/A) = -10.66$. $M = -0.40$. Frequency domain formulation.

The three dimensional, frequency domain, traditional Kirchhoff method has

been used to determine the relative errors caused by decreasing amounts of discrete quadrature points on the Kirchhoff surface. For these tests, the source region is defined by a point monopole located at $(y_o, R_o) = (0.3\pi\,\lambda, 0)$. The length, L_k, and radius, R_k of the cylindrical control surface are chosen so that the surface length is equal to it's circumference: $R_k = 0.3\,\lambda$, $L_k = 0.6\pi\,\lambda$. The surface and observer are stationary. The observer is moved to $(x, R) = (0.3\pi\,\lambda, 0.5\,\lambda)$, so that the majority of the radiated sound comes from the constant radius portion of the control surface. The number of points in the azimuthal, 19, and radial directions, 40, on the end surfaces of the cylinder are held constant. The number of points in the axial and azimuthal directions is then varied from 15 × 15 to 400 × 400. The number of points per wavelength is approximated by dividing the total number of points on the constant radius portion of the surface by it's area, and taking the square root of the quotient. Figure 2.8 shows the relative error in amplitude as a function of the amount of points per wavelength on the surface. For this calculation, approximately 15 discrete quadrature points per wavelength is sufficient to obtain 0.1% error. Even the use of ~ 8 points per wavelength yields an acceptable relative error of 0.25%.

The errors caused by decreasing the total number of points per acoustic period used in the three dimensional, time domain, Kirchhoff integral were also investigated. The conditions used are the same as those used to generate the previous figure, except that the number of discrete points on the control surface is held constant at 100 × 100 (approximately 53 points per wavelength), and the number of temporal points per acoustic period is varied from 8 to 256. Figure 2.9 shows the relative RMS error in amplitude as a function of the number of points per acoustic period. The figure indicates a relative error of approximately 0.15% with 16 points per period and $\sim 2\,\%$ with 8 points per period. Thus, the 64 points used in the

remainder of this study should be adequate.

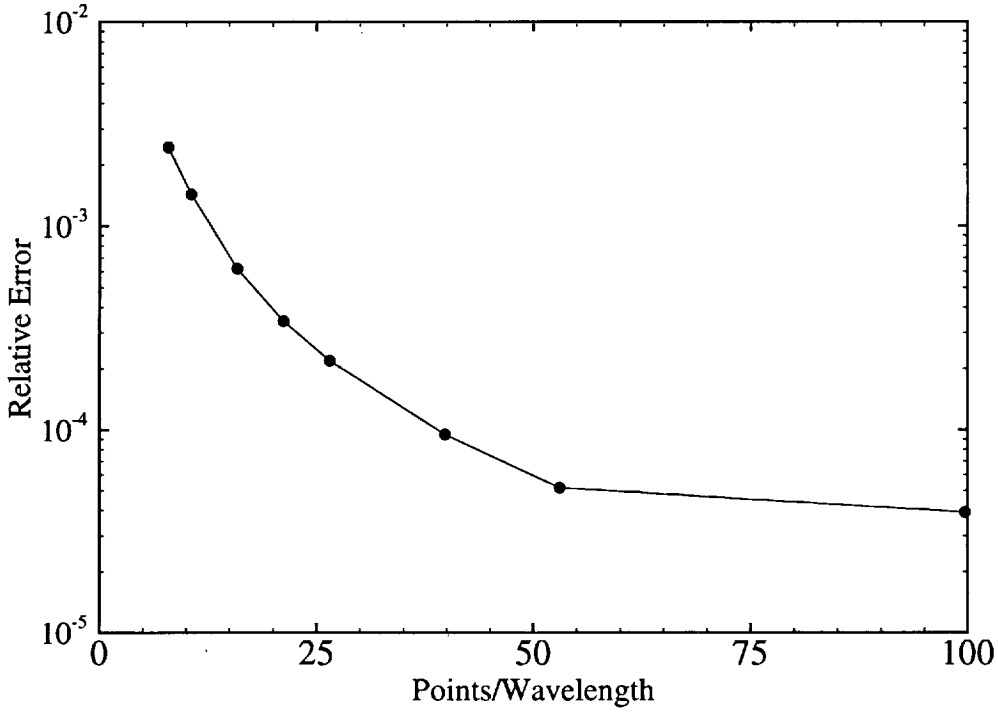

Figure 2.8. Relative Error, $|\widehat{\phi} - \widehat{\phi}_{exact}|/\widehat{\phi}_{exact}$, verses points per wavelength for the 3D, frequency domain traditional Kirchhoff method. $M = 0.00$.

2.6.2 Two Dimensional Calculations

Testing of the two dimensional, frequency domain implementation of the traditional Kirchhoff integral proceeds in a similar fashion as that in the previous section. A rectangular "surface" of length $L_k = 10\,\lambda$, and width $R_k = 4\,\lambda$ is used to surround a two dimensional point acoustic monopole placed at $(y_o, R_o) = (3.5\,\lambda, 0)$. 200 quadrature points are used along the length of the rectangular surface, and 50 along the width.

Figure 2.10 shows two iso–contours of the real part of $\widehat{\phi}$, at angular frequency ω_o, in the acoustic near–field and mid–field of a 2D point acoustic monopole. The portion above the x axis is the prediction obtained with the Kirchhoff method, while that below the axis is the exact solution. The exact solution is obtained via

$$\widehat{\phi}(\vec{x},t) = \frac{A\,H_0^{(2)}(kr)}{4\,i} \tag{2.39}$$

where $r = |\vec{x} - \vec{y}_o|$, and $k = \omega_o/a_o$. The portion of the Kirchhoff surface above the x axis is shown. The figure shows excellent agreement between the exact solution and the prediction obtained with the two dimensional Kirchhoff integral formulation.

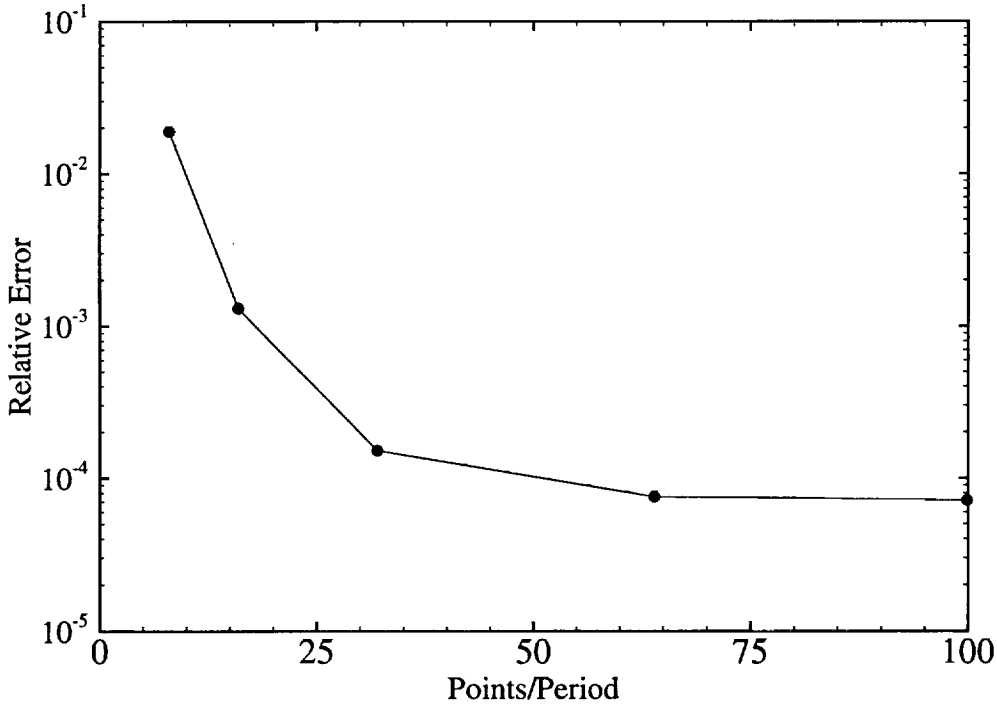

Figure 2.9. Relative Error, $|\phi - \phi_{exact}|_{RMS}/\phi_{exact_{RMS}}$, verses points per period for the 3D, time domain traditional Kirchhoff method. $M = 0.00$.

It is also necessary to determine the required number of discrete quadrature points along the line in two dimensions which defines S. For this determination, a two dimensional point acoustic monopole is placed at $(y_o, R_o) = (0.3\pi\,\lambda, 0)$. The length, L_k, and width, R_k of the rectangular control surface are chosen so that the surface length was $L_k = 0.6\pi\,\lambda$, and $R_k = 0.2\,\lambda$, to loosely match the dimensions used in the similar three dimensional test. The observer is chosen as $(x, R) = (0.3\pi\,\lambda, 0.15\,\lambda)$, so that again the majority of the predicted sound came from the constant R portion of the surface. The number of points along the width of the surface, 80, is held constant. The number of points in the lengthwise direction is then varied from 10 to 460. The number of points per wavelength is then determined by dividing the total number of points in the lengthwise direction on the surface by it's length.

Experience has shown that a larger number of quadrature points are required per wavelength in the two dimensional version of the Kirchhoff integral than in three dimension. To help alleviate the burden caused by this requirement, a higher order quadrature algorithm, Gauss–Legendre quadrature,[51] is employed. The increased accuracy afforded by the use of this quadrature method does provide for some increase in the accuracy of Kirchhoff predictions. As mentioned previously, acoustic data on the surface is most often obtained through the use of a CFD calculation in the acoustic near–field. The researcher performing acoustical analysis may not have control over the amount of grid points and temporal discretization in the CFD calculation. Furthermore, mesh refinement is often prohibitively expensive. However, there are methods available which can help increase the accuracy of Kirchhoff calculations using CFD inputs.

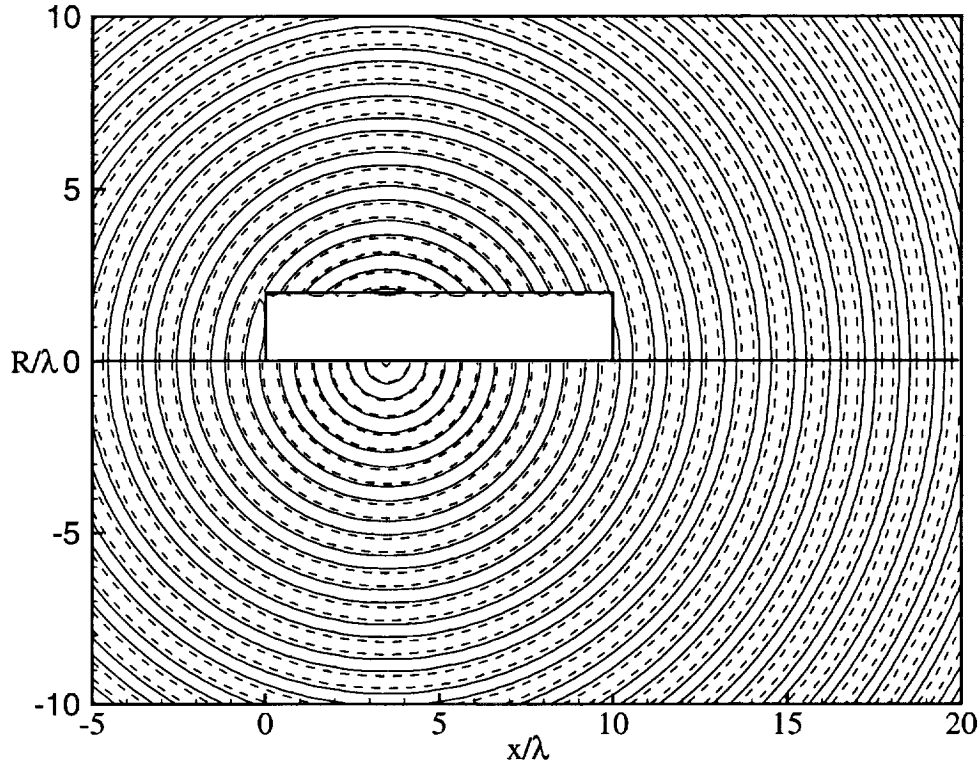

Figure 2.10. Real part of predicted and exact 2D acoustic monopole field. $R > 0$: Traditional Kirchhoff prediction, $R < 0$: Exact solution. Solid line is $\Re(\hat{\phi}/A) = 0.01$. Dashed line is $\Re(\hat{\phi}/A) = -0.01$. $M = 0.00$.

Meadows and Atkins[52] have developed a procedure to increase the accuracy of Kirchhoff integral predictions without performing a mesh refinement. This procedure, which they refer to as "mesh enrichment," consists of the addition of quadrature points on the Kirchhoff surface. The data on the additional points is obtained through a polynomial interpolation over the CFD calculation data. A high order quadrature algorithm is then used with the additional data points. They showed the ability to obtain accurate acoustic predictions from relatively coarse-grid CFD

calculations.

Figure 2.11 shows the relative error in amplitude as a function of the amount of points per wavelength in the lengthwise direction on the surface. Second, fourth, and eighth order Gauss-Legendre quadrature were used to solve the Kirchhoff integral on the control surface, with the values of the integrand determined at the mesh enrichment locations through third order polynomial interpolation.

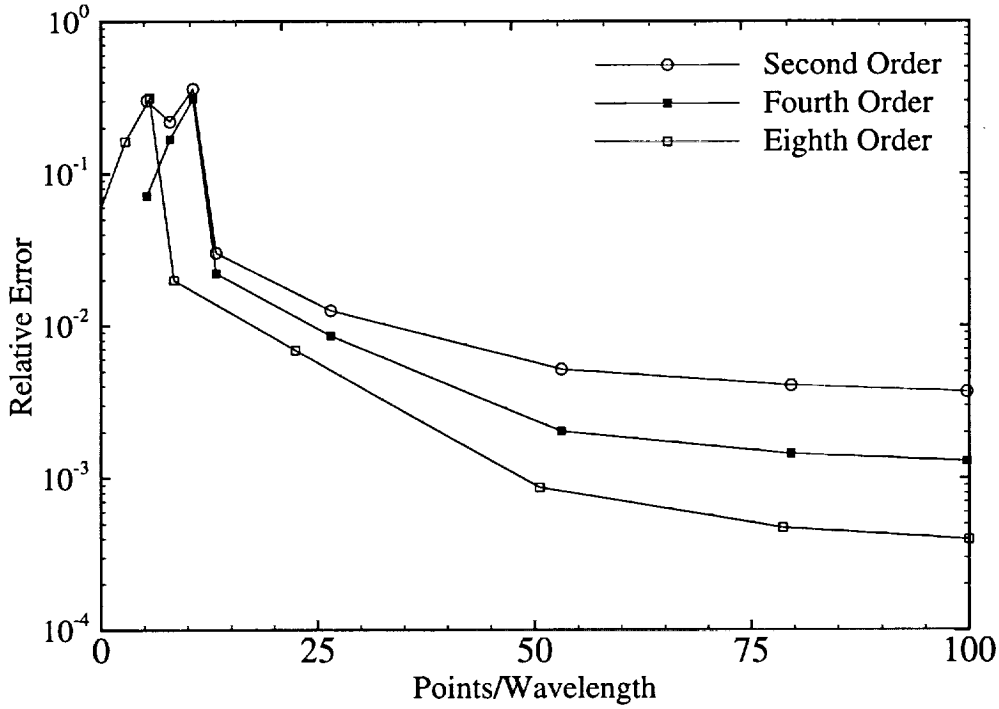

Figure 2.11. Relative Error, $|\widehat{\phi} - \widehat{\phi}_{exact}|/\widehat{\phi}_{exact}$, verses points per wavelength for the 2D, frequency domain traditional Kirchhoff method. $M = 0.00$.

In these calculations, the second order quadrature scheme produced 1% error with approximately 35 points per acoustic wavelength, while the eighth order scheme produced the same error with approximately 20 points per wavelength. Since there

is no additional cost in the CFD predictions, and very little additional cost in the Kirchhoff calculations, the mesh enrichment procedure is a very beneficial means of producing accurate Kirchhoff calculations. It should be noted that in this case more points are required per wavelength than in the three dimensional version of the code. However, this is not a burden, since the dimension of the problem has been decreased by one.

2.6.3 Related Issues

The mesh enrichment procedure discussed above is an important development in surface integral prediction methodology. A similar procedure, "quadrature adaptation," has been developed by Brentner.[50] In this algorithm, the amount of temporal or spatial quadrature points is increased or decreased, based on solution estimates, during the quadrature procedure. He recommends using an error approximation in the algorithm to increase efficiency as well.

Since the calculations shown in this chapter were based on linear inputs at an arbitrary number of points, the mesh enrichment and quadrature adaptation development were not actively pursued in the three dimensional calculations presented in this work. The mesh enrichment algorithm is straightforward to implement in two dimensions, however, so it is used in the rest of the two dimensional calculations shown here. The reader should also be aware that these quadrature techniques may be necessary in acoustics calculations which utilize output from a CFD code as inputs to the Kirchhoff routine.

Chapter 3

The Modified Kirchhoff Method

The main focus of this work is the development of modifications to the traditional Kirchhoff method so that it is more applicable for use in jet aeroacoustic calculations. These modifications are outlined in this chapter. The improvements are based on the Ffowcs Williams–Hawkings equation used in the prediction of noise generated by moving surfaces. Additionally, the Kirchhoff integral will be shown to be equivalent to a solution of the Ffowcs Williams–Hawkings equation, under certain conditions.

3.1 Porous Ffowcs Williams–Hawkings Equation

In this section the Ffowcs Williams–Hawkings equation[18] for a moving, porous surface is presented. The original developments of Ffowcs Williams and Hawkings were based on an impermeable surface, but a porous surface version was presented by Ffowcs Williams in reference 53. The derivation is similar to that of

Lighthill's equation,[10] except that there are surfaces of discontinuity that must be dealt with. These discontinuities are again handled through the use of generalized functions.[36–38]

Let the surface again be defined by $f(\vec{x},t) = 0$ such that $f > 0$ in the fluid outside the surface, and $f < 0$ inside the surface. The surface may be a real, solid surface, or a computational control surface. The mathematics are identical. The continuity equation is

$$\frac{\partial}{\partial t}(\rho - \rho_\circ) + \frac{\partial}{\partial x_j}(\rho u_j) = 0 \tag{3.1}$$

Here, ρ is the fluid density, and u_i are the cartesian components of the fluid velocity vector. Subscript $\circ$ denotes evaluation of the variables at ambient conditions. To create an equation valid over all space and time, (3.1) is multiplied by the Heaviside function, $H(f)$. That is, ambient conditions are mathematically enforced inside the surface.

$$\frac{\partial}{\partial t}\left[(\rho - \rho_\circ) H(f)\right] + \frac{\partial}{\partial x_j}(\rho u_j H(f)) = \rho(u_j - v_j)\frac{\partial H(f)}{\partial x_j} + \rho_\circ v_j \frac{\partial H(f)}{\partial x_j} \tag{3.2}$$

where $\vec{v}$ is the local velocity of the surface

$$v_j = -\frac{1}{\hat{n}_j}\frac{\partial f}{\partial t}$$

The momentum equation is

$$\frac{\partial}{\partial t}(\rho u_i) + \frac{\partial}{\partial x_j}(\rho u_i u_j + (p - p_\circ)\delta_{ij} - \sigma_{ij}) = 0 \tag{3.3}$$

where p is the fluid pressure, σ_{ij} is the viscous stress tensor, and δ_{ij} is the Kronecker delta. The Heaviside function is used to make this equation valid over all space,

$$\begin{aligned}\frac{\partial}{\partial t}(\rho u_i H(f)) + \frac{\partial}{\partial x_j}\left[(\rho u_i u_j + (p - p_\circ)\delta_{ij} - \sigma_{ij}) H(f)\right] \\ = \left[(p - p_\circ)\delta_{ij} - \sigma_{ij} + \rho u_i (u_j - v_j)\right]\frac{\partial H(f)}{\partial x_j}\end{aligned} \tag{3.4}$$

Taking the time derivative of (3.2), subtracting the generalized divergence of (3.4), and subtracting $a_o^2\nabla^2\left[(\rho-\rho_o)H(f)\right]$ from both sides yields

$$\begin{aligned}\Box^2\left[p'H(f)\right] = &\frac{\partial^2}{\partial x_i \partial x_j}\left[T_{ij}H(f)\right] + \frac{\partial}{\partial x_i}\left[L_i\delta(f)\right] \\ &+ \frac{\partial}{\partial t}\left[\rho_o v_n \delta(f)\right] + \frac{\partial}{\partial t}\left[\rho\left(u_n - v_n\right)\delta(f)\right] \\ &- \frac{\partial}{\partial x_i}\left[\rho u_i\left(u_n - v_n\right)\delta(f)\right]\end{aligned} \tag{3.5}$$

where $\rho' = \rho - \rho_o$, $p' = a_o^2(\rho - \rho_o)$, $u_n = u_i\hat{n}_i$, $v_n = v_i\hat{n}_i$. Lighthill's stress tensor and the surface loading are

$$T_{ij} = \rho u_i u_j - \sigma_{ij} + \left((p-p_o) - a_o^2\rho'\right)\delta_{ij}$$

$$L_i = -\left((p-p_o)\,\delta_{ij} - \sigma_{ij}\right)\hat{n}_j$$

Note that the definition of p' is different here than that normally encountered in the literature. ($p - p_o = a_o^2\rho'$ only in linear, isentropic regions.) Equation (3.5) is the Ffowcs Williams–Hawkings equation[18] for a moving, porous surface. The first three terms on the right side of equation (3.5) compose the original Ffowcs Williams–Hawkings equation, while the last two terms are the contributions to the radiated sound caused by the porosity of the surface. Note also that if there is no surface, $H(f) = 1$, $\delta(f) = 0$, and equation (3.5) is identical to Lighthill's equation.

Equation (3.5) is not easily employed in computational simulations as shown above. This is due to the derivatives being taken at the observer time and location. Farassat,[24] solved the first three terms on the right side of (3.5) with the free-space Green's function for the wave equation (2.9). With the additional terms, the solution to (3.5) is

$$\begin{aligned}4\pi p'H(f) = &\frac{\partial^2}{\partial x_i \partial x_j}\int T_{ij}H(f)\,\delta(g)\,d\vec{y} + \frac{\partial}{\partial x_i}\int L_i\delta(f)\,\delta(g)\,d\vec{y} \\ &+ \frac{\partial}{\partial t}\int \rho_o v_n\delta(f)\,\delta(g)\,d\vec{y} + \frac{\partial}{\partial t}\int \rho\left(u_n - v_n\right)\,\delta(f)\,\delta(g)\,d\vec{y} \\ &- \frac{\partial}{\partial x_i}\int \rho u_i\left(u_n - v_n\right)\,\delta(f)\,\delta(g)\,d\vec{y}\end{aligned} \tag{3.6}$$

He then expressed the resultant derivatives in terms of the source time and location. He referred to this solution as formulation 1A. The expression of the solution in this manner makes it easily applicable in numerical predictions.[25] Following Farassat's derivation, while accounting for the additional source terms gives

$$4\pi p'(\vec{x},t)H(f) = \int_S \left[\frac{A_1 + A_3}{r\left(1-M_r\right)^2}\right]_{\tau^*} dS + \int_S \left[\frac{A_2 + A_4}{r^2\left(1-M_r\right)^2}\right]_{\tau^*} dS + \int_{f>0} \left[\frac{1}{r(1-M_r)}\frac{\partial^2 T_{ij}}{\partial y_i \partial y_j}\right]_{\tau^*} dV \tag{3.7}$$

where

$$A_1 = \rho_o \dot{v}_n + \dot{L}_i \hat{r}_i / a_o$$

$$A_2 = L_i \hat{r}_i - L_i M_i + \Lambda \left(1-M_r\right)^{-1} \left(\rho_o v_n + L_i \hat{r}_i / a_o\right)$$

$$A_3 = \rho \left(u_n - v_n\right) \dot{\mathcal{M}}_i \hat{r}_i$$

$$A_4 = \rho \left(u_n - v_n\right)\left(u_r - u_i M_i\right) + \rho \left(u_n - v_n\right) \Lambda \left(1 + \dot{\mathcal{M}}_r\right)\left(1-M_r\right)^{-1} + \left(1 + \mathcal{M}_r\right)\left(\rho\left(\dot{u}_n - \dot{v}_n\right) + \dot{\rho}\left(u_n - v_n\right)\right)$$

$$\Lambda = \left(r\dot{M}_i \hat{r}_i + a_o M_r - a_o M^2\right)$$

Here $\mathcal{M}_i = u_i/a_o$ is the local Mach number of the flow at the surface, and $\mathcal{M}_r$ is the flow Mach number in the radiation direction. A dot over a quantity indicates derivation with respect to source time. In the volume integral, M_r is the local Mach number of the motion of the source coordinate system with respect to a stationary reference frame, in the radiation direction. Note also that the definitions of $\dot{M}_n$ and $\dot{M}_r$ are different here than those presented in the last chapter. The terms A_1 and A_2 compose the original formulation 1A. The terms A_3 and A_4 are the contribution to the radiated sound from flow through the surface. These terms were presented for the first time by the authors in reference 33. It should be noted here that p' is the acoustic pressure perturbation, $p - p_o$, only in the linear, acoustic far–field. More details on the derivation can be found in references 24 and 25.

Equation (3.7), an extension of Farassat's formulation 1A, can be used in the calculation of far–field sound based on near–field aerodynamic data. This may be an attractive alternative, because there is no need to calculate spatial derivatives at the surface, as there is with the Kirchhoff method. Additionally, terms A_3 and A_4 can be easily added to an existing FWH prediction code (e.g. WOPWOP[25]). In the next section, equation (3.6) will be modified in order to produce an equivalent to (3.7). This equivalent can then be used with existing Kirchhoff codes.

3.2 Modified Kirchhoff Equation

At this point it is desirable to re–write equation (3.5) in a different form. The new form will produce an integral solution equivalent to the Kirchhoff integral solution to the wave equation, provided $p' = a_\circ^2 \rho'$ is used as the dependent variable. Additional terms are also introduced by the porosity of the surface.

To derive an equivalent expression, first note that

$$\frac{\partial}{\partial x_i}\left[L_i \delta(f)\right] - \frac{\partial}{\partial x_i}\left[\rho u_i u_n\right] = -\frac{\partial}{\partial x_i}\left[T_{ij}\hat{n}_j \delta(f)\right] - \frac{\partial}{\partial x_i}\left[a_\circ^2 \rho' \hat{n}_j \delta(f)\right]$$

$$\frac{\partial}{\partial t}\left[\rho_\circ v_n \delta(f)\right] + \frac{\partial}{\partial t}\left[-\rho v_n \delta(f)\right] = -\frac{\partial}{\partial t}\left[\rho' v_n \delta(f)\right]$$

Equation (3.5) can then be re–cast as

$$\begin{aligned}\Box^2\left[a_\circ^2 \rho' H(f)\right] = {} & \frac{\partial^2}{\partial x_i \partial x_j}\left[T_{ij} H(f)\right] - \frac{\partial}{\partial x_i}\left[T_{ij}\hat{n}_j \delta(f)\right] \\ & - \frac{\partial}{\partial x_i}\left[a_\circ^2 \rho' \hat{n}_i \delta(f)\right] - \frac{\partial}{\partial t}\left[\rho' v_n \delta(f)\right] \\ & + \frac{\partial}{\partial x_i}\left[\rho u_i v_n \delta(f)\right] + \frac{\partial}{\partial t}\left[\rho u_n \delta(f)\right]\end{aligned} \tag{3.8}$$

The chain rule allows the last two terms to be written as

$$\begin{aligned}\frac{\partial}{\partial x_i}\left[\rho u_i v_n \delta(f)\right] + \frac{\partial}{\partial t}\left[\rho u_n \delta(f)\right] = {} & \frac{\partial}{\partial x_i}\left[\rho u_i\right] v_n \delta(f) + \rho u_i \frac{\partial}{\partial x_i}\left[v_n \delta(f)\right] \\ & + \frac{\partial}{\partial t}\left[\rho u_i\right] \hat{n}_i \delta(f) + \rho u_i \frac{\partial}{\partial t}\left[\hat{n}_i \delta(f)\right]\end{aligned}$$

Note also that

$$\rho u_i \frac{\partial}{\partial x_i}\left[v_n \delta(f)\right] + \rho u_i \frac{\partial}{\partial t}\left[\hat{n}_i \delta(f)\right] = -\rho u_i \left[\frac{\partial}{\partial x_i}\left(\frac{\partial f}{\partial t}\delta(f)\right) - \frac{\partial}{\partial t}\left(\frac{\partial f}{\partial x_i}\delta(f)\right)\right] = 0$$

and, from the conservation equations,

$$\frac{\partial}{\partial x_i}\left[\rho u_i\right] v_n \delta(f) = -\frac{\partial \rho'}{\partial t} v_n \delta(f) \tag{3.9}$$

$$\begin{aligned} \frac{\partial}{\partial t}\left[\rho u_i\right]\hat{n}_i \delta(f) &= -\frac{\partial}{\partial x_j}\left[p\delta_{ij} - \sigma_{ij}\right]\hat{n}_i \delta(f) - \frac{\partial}{\partial x_j}\left[\rho u_i u_j\right]\hat{n}_i \delta(f) \\ &= -\frac{\partial T_{ij}}{\partial x_j}\hat{n}_i \delta(f) - a_\circ^2 \frac{\partial \rho'}{\partial n}\delta(f) \end{aligned} \tag{3.10}$$

Note also that

$$\frac{\partial^2}{\partial x_i \partial x_j}\left[T_{ij} H(f)\right] = \frac{\partial}{\partial x_i}\left[T_{ij}\hat{n}_j \delta(f)\right] + \frac{\partial T_{ij}}{\partial x_j}\hat{n}_i \delta(f) + H(f)\frac{\partial^2 T_{ij}}{\partial x_i \partial x_j} \tag{3.11}$$

The combination of equations (3.8)through (3.11) leads to

$$\begin{aligned} \Box^2\left[a_\circ^2 \rho' H(f)\right] &= \Box^2\left[p' H(f)\right] \\ &= -\left(\frac{\partial p'}{\partial n} + \frac{1}{a_\circ} M_n \frac{\partial p'}{\partial t_x}\right)\delta(f) \\ &\quad - \frac{1}{a_\circ}\frac{\partial}{\partial t}\left[M_n p' \delta(f)\right] - \frac{\partial}{\partial x_i}\left[p'\hat{n}_i \delta(f)\right] \\ &\quad + H(f)\frac{\partial^2 T_{ij}}{\partial x_i \partial x_j} \end{aligned} \tag{3.12}$$

The subscript x on the temporal derivative in the first term is included to denote derivation with respect to the observer time, with the observer coordinates held fixed. Note that the first three terms on the right side of (3.12) are identical to those on the right side of (2.21), with $\phi = p' = a_\circ^2 \rho'$. The nomenclature and similarities between the Kirchhoff and FWH approaches are shown in figure 3.1.

The equivalence of (3.12) and (3.7) indicates that the Ffowcs Williams–Hawkings and Kirchhoff integrals are equivalent solutions to the same equation.

The traditional Kirchhoff integral, from the previous chapter, is a solution to the homogeneous wave equation, while the FWH equation is a solution to an inhomogeneous (Lighthill's) wave equation. Ffowcs Williams and Hawkings[18] mention that the impermeable surface forms of (3.12) and (3.7) are identical, while Farassat[36] says there is "considerable cancellation and simplification of the source terms" in going from equation (3.12) to (3.7). Much of the simplification is lost when the surface is not impermeable.

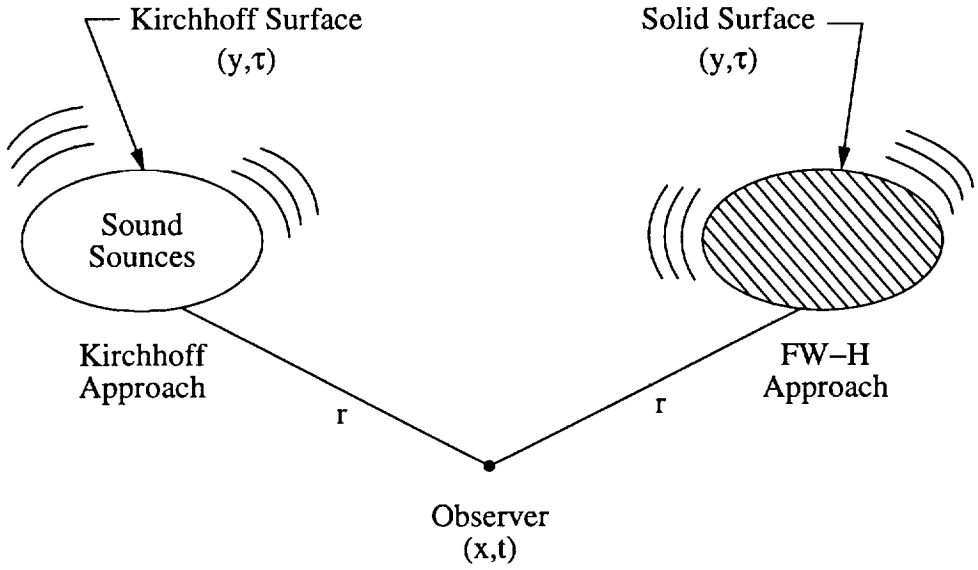

Figure 3.1. Schematic of similarities between Kirchhoff and Ffowcs Williams–Hawkings methods.

3.2.1 Time Domain – 3D

Equation (3.12) can now be solved to produce a formulation the authors have referred to as the modified Kirchhoff formula. The derivation is similar to that of Farassat and Myers,[27] and the previous chapter. The free space Green's function is

used to solve (3.12),

$$\begin{aligned} 4\pi\tilde{p}(\vec{x},t) = &- \int \frac{1}{r}\Big(\frac{\partial p'}{\partial n} + \frac{1}{a_o}M_n\frac{\partial p'}{\partial \tau_y}\Big)\delta(f)\delta(g)\,d\vec{y}\,d\tau \\ &- \frac{1}{a_o}\frac{\partial}{\partial t}\int \frac{1}{r}M_n p'\delta(f)\delta(g)\,d\vec{y}\,d\tau \\ &- \frac{\partial}{\partial x_i}\int \frac{1}{r}p'\hat{n}_i\delta(f)\delta(g)\,d\vec{y}\,d\tau \\ &+ H(f)\frac{\partial^2}{\partial x_i \partial x_j}\int \frac{T_{ij}}{r}\delta(g)d\vec{y}\,d\tau \end{aligned} \tag{3.13}$$

Where $\tilde{p} = p'H(f)$. Through the use of equation (2.23) the divergence operator can be converted to a temporal derivative in the source time. This leads to

$$\begin{aligned} 4\pi\tilde{p}(\vec{x},t) = &- \int \frac{1}{r}\Big(\frac{\partial p'}{\partial n} + \frac{1}{a_o}M_n\frac{\partial p'}{\partial \tau_y}\Big)\delta(f)\delta(g)\,d\vec{y}\,d\tau \\ &+ \int \frac{1}{r^2}\left(p'\cos\theta\right)\delta(f)\delta(g)\,d\vec{y}\,d\tau \\ &+ \frac{1}{a_o}\frac{\partial}{\partial t}\int \frac{1}{r}\Big[(\cos\theta - M_n)\,p'\Big]\delta(f)\delta(g)\,d\vec{y}\,d\tau \\ &+ H(f)\frac{\partial^2}{\partial x_i \partial x_j}\int \frac{T_{ij}}{r}\delta(g)d\vec{y}\,d\tau \end{aligned} \tag{3.14}$$

The temporal derivative is transformed to source time and brought inside the integral. $\vec{y}$ is transformed to (u^1, u^2, u^3), and τ is transformed to g. The Jacobians of the transformations are 1 and $1/(1 - M_r)$ respectively. Integration over $\vec{u}$ and g gives

$$\begin{aligned} 4\pi\tilde{p}(\vec{x},t) = &\int_{D(S)}\Bigg\{-\frac{1}{r(1-M_r)}\left(\frac{\partial p'}{\partial n} + \frac{1}{a_o}M_n\frac{\partial p'}{\partial \tau_y}\right)\sqrt{g_{(2)}} \\ &+ \frac{(p'\cos\theta)}{r^2(1-M_r)}\sqrt{g_{(2)}} \\ &+ \frac{1}{a_o r\,(1-M_r)}\frac{\partial}{\partial\tau}\left[\frac{(\cos\theta - M_n)\,p' +}{(1-M_r)}\sqrt{g_{(2)}}\right]\Bigg\}_{\tau^*} du^1\,du^2 \\ &+ \int\limits_{f=u^3>0}\left[\frac{1}{r(1-M_r)}\frac{\partial^2 T_{ij}}{\partial u^i \partial u^j}\right]_{\tau^*} du^1\,du^2\,du^3 \end{aligned} \tag{3.15}$$

Because $u^3 \neq 0$ in the volume integral, the retarded time τ^* is now the root of

$$g = \tau - t + \frac{|\vec{x} - \vec{y}(u^1, u^2, u^3, \tau)|}{a_o} = 0 \tag{3.16}$$

The temporal derivative can be evaluated analytically, to obtain the moving, porous surface version of the modified Kirchhoff formula,

$$4\pi a_o^2 \tilde{\rho}(\vec{x},t) = 4\pi \tilde{p}(\vec{x},t) = \int_{D(S)} \left[\frac{E_1 \sqrt{g_{(2)}}}{r\,(1-M_r)} + \frac{p'\,E_2 \sqrt{g_{(2)}}}{r^2\,(1-M_r)} \right. \\ \left. + \int_{u^3>0} \left[\frac{1}{r(1-M_r)} \frac{\partial^2 T_{ij}}{\partial y_i \partial y_j} \right]_{\tau^*} du^1\,du^2\,du^3 \right. \tag{3.17}$$

E_1 and E_2 are presented in the previous chapter, equation (2.28). (In E_1, ϕ must be replaced by $p' = a_o^2 \rho'$.) The form of (3.17), without the volume integral, was presented by Farassat and Myers.[27] The addition of the volume integral represents a new formulation, and is of major significance for this report. This additional term can readily be added to an existing Kirchhoff prediction code to make it more applicable in cases where the Kirchhoff surface can not be placed in a linear region. A simplified form of (3.17) for a stationary, rigid surface was presented by the authors in reference 32. The full form was presented in reference 33. Recently, di Francescantonio[54] presented a formulation equivalent to (3.7). He refers to this formulation as the "Kirchhoff–FWH" equation.

3.2.2 Frequency Domain – 2D

The modified Kirchhoff integral formula for a stationary, rigid, porous Kirchhoff surface can also be derived for the two dimensional Helmholtz equation. The derivation follows that presented above and in the previous chapter. The generalized Kirchhoff equation in the frequency domain is

$$\frac{\overline{\partial}^2}{\partial x_i^2}\left(\hat{p}H(f)\right) + k^2 \hat{p} H(f) = -\frac{\partial \hat{p}}{\partial n}\delta(f) - \frac{\overline{\partial}}{\partial x_i}\left[\hat{p}\hat{n}_i \delta(f)\right] \\ + H(f)\frac{\partial^2 T_{ij}}{\partial x_i \partial x_j} \tag{3.18}$$

where $\hat{p}$ is the Fourier transform of p'. Solution of this equation with the appropriate free-space Green's function (2.12), gives the modified Kirchhoff formula in the 2D frequency domain,

$$\begin{aligned} 4i\hat{p}(\vec{x},\omega)H(f) = &- \int \frac{\partial \hat{p}}{\partial n} H_0^{(2)}(kr)\delta(f)\, d\vec{y} - \frac{\overline{\partial}}{\partial x_i} \int \hat{p}\hat{n}_i\, H_0^{(2)}(kr)\delta(f)\, d\vec{y} \\ &+ H(f)\frac{\partial^2}{\partial x_i \partial x_j} \int_{f>0} \hat{T}_{ij} H_0^{(2)}(kr)\, d\vec{y} \end{aligned} \tag{3.19}$$

The divergence operators act only on the Hankel functions, so (3.19) can be written as

$$\begin{aligned} 4i\hat{p}(\vec{x},\omega)H(f) = &- \int_S \left[\frac{\partial \hat{p}}{\partial n} H_0^{(2)}(kr) - \cos\theta\, k\, \hat{p}\, H_1^{(2)}(kr)\right] dS \\ &+ \int_{f>0} \hat{T}_{ij} \left[k^2 \hat{r}_i \hat{r}_j\, H_2^{(2)}(kr) - \frac{k}{r}\delta_{ij}\, H_1^{(2)}(kr)\right] dV \end{aligned} \tag{3.20}$$

where the integral over S is again understood to be a line integral, and that over V a surface integral in two dimensional space.

3.3 Uniform Rectilinear Motion

3.3.1 Time Domain

The techniques used in the previous chapter to present the traditional Kirchhoff integral for the case of uniform rectilinear motion can now be used to present the modified Kirchhoff integral for the same case. This development was presented by the authors in reference 33. The control surface is again assumed to be rigid. Setting $\dot{M}$, $\dot{\sigma}$, $\dot{n}$, etc. to zero, and expressing the integrals in a frame of reference which is moving with the surface and observer allows equation (3.17) to be expressed as

$$\begin{aligned} 4\pi\tilde{p}(\vec{x},t) = 4\pi a_o^2 \tilde{\rho}(\vec{x},t) = &\int_S \left[\frac{\tilde{E}_1}{r\,(1-M_r)} + \frac{p' E_2}{r^2\,(1-M_r)}\right]_{\tau^*} dS \\ &+ \int_{f>0} \left[\frac{1}{r(1-M_r)} \frac{\partial^2 T_{ij}}{\partial y_i \partial y_j}\right]_{\tau^*} dV \end{aligned} \tag{3.21}$$

$\tilde{E}_1$ and E_2 are the same as presented previously in equations (2.28)and (2.32). (ϕ must be equal to p'.) The retarded time is again the root of equation (2.30). This modified Kirchhoff formula is useful in studies of jet noise in which there is a non–zero free stream velocity, and significant nonlinearities at and outside of the Kirchhoff surface.

3.3.2 Frequency Domain

The frequency domain counterpart to equation (3.21) is easily derived through the use of the preceding analysis. This equivalent is given by

$$\begin{aligned} 4\pi\hat{p}(\vec{x},\omega)H(f) &= 4\pi a_\circ^2\hat{\rho}(\vec{x},\omega)H(f) \\ &= \int_S e^{i\omega r/a_\circ}\left[\frac{K_1}{r\,(1-M_r)} + \frac{\hat{p}\,E_2}{r^2\,(1-M_r)}\right]dS \\ &+ \int_{f>0} e^{i\omega r/a_\circ}\left[\frac{1}{r(1-M_r)}\frac{\partial^2 T_{ij}}{\partial y_i \partial y_j}\right]dV \end{aligned} \tag{3.22}$$

where $\hat{\rho}$ is the Fourier transform of ρ'. K_1 was presented earlier in equation (2.34). Thus, both frequency domain and time domain formulations are available for use in jet noise calculations.

3.4 Volume Integral

To this point little mention has been made of the volume integral that arises from the development of the modified Kirchhoff integral formulation. Solution of this volume integral is identical to solution of the integrals that arise from the use of Lighthill's acoustic analogy.[10] Because of this, some methods previously used in jet noise studies which employed acoustic analogy predictions may be of use. Here a modified form of the exact volume integral is presented, as well one means of approximation of the volume integral solution.

3.4.1 Exact Solution

As presented in (3.17), the volume integral is the equivalent to that presented by Lighthill in his original work.[10] However, it is possible to cast this integral in a different form. The new form makes it possible to obtain more accurate predictions from approximations to T_{ij}. The volume integral contribution to the overall solution is

$$4\pi p'_v(\vec{x},t) = \frac{\partial^2}{\partial x_i \partial x_j} \int \frac{T_{ij}}{r} \delta(g) d\vec{y}\, d\tau \tag{3.23}$$

Farassat and Brentner[55] showed that the double divergence can be expressed in terms of temporal derivatives

$$\begin{aligned} \frac{\partial^2}{\partial x_i \partial x_j}\left[\frac{\delta(g)}{r}\right] = \frac{1}{a_\circ^2}\frac{\partial^2}{\partial t^2}\left[\frac{\hat{r}_i\hat{r}_j\delta(g)}{r}\right] + \frac{1}{a_\circ}\frac{\partial}{\partial t}\left[\frac{(3\hat{r}_i\hat{r}_j - \delta_{ij})\,\delta(g)}{r^2}\right] \\ + \frac{(3\hat{r}_i\hat{r}_j - \delta_{ij})\,\delta(g)}{r^3} \end{aligned} \tag{3.24}$$

Using the relation

$$\left.\frac{\partial}{\partial t}\right|_x = \left[\frac{1}{(1-M_r)}\left.\frac{\partial}{\partial \tau}\right|_x\right]_{\tau^*}$$

allows (3.23) to be cast in terms of temporal derivatives at the source time,

$$\begin{aligned} 4\pi p'_v(\vec{x},t) = \frac{1}{a_\circ^2}\int\left\{\frac{1}{(1-M_r)}\frac{\partial}{\partial\tau}\left[\frac{1}{(1-M_r)}\frac{\partial}{\partial\tau}\left(\frac{T_{rr}}{r(1-M_r)}\right)\right]\right\}_{\tau^*} d\vec{y} \\ + \frac{1}{a_\circ}\int\left[\frac{1}{(1-M_r)}\frac{\partial}{\partial\tau}\left(\frac{3T_{rr}-T_{ii}}{r^2(1-M_r)}\right)\right]_{\tau^*} d\vec{y} \\ + \int\left(\frac{3T_{rr}-T_{ii}}{r^3(1-M_r)}\right)_{\tau^*} d\vec{y} \end{aligned} \tag{3.25}$$

where $T_{rr} = \hat{r}_i T_{ij} \hat{r}_j$. Here M_r is the local Mach number of the motion of the source coordinate system with respect to a stationary reference frame, in the radiation direction. After analytical derivation and some algebra (3.25) can be expressed as

$$4\pi p'_v(\vec{x},t) = \int_{f>0}\left[\frac{B_1}{a_\circ^2 r(1-M_r)^3} + \frac{B_2}{a_\circ r^2(1-M_r)^2} + \frac{B_3}{r^3(1-M_r)}\right]_{\tau^*} dV \tag{3.26}$$

The terms B_1, B_2, and B_3 are presented in the appendix to this chapter. The contribution from B_1 in (3.26) is the often used far–field approximate solution to Lighthill's equation. B_2 and B_3 are important only in the near–field and mid–field. Their contribution is significant, because it allows for acoustic predictions in a region where CFD or empirical data (the data used on the Kirchhoff surface) is available. A comparison can then be used to validate the surface integral methodology. Brentner[56] has derived an expression equivalent to (3.26) for use in Ffowcs Williams–Hawkings based aeroacoustic predictions.

3.4.2 Source Approximations

In many cases, it will not be possible to determine T_{ij} in the entire region where it has significant magnitude. If it is possible, the Kirchhoff surface can be extended to include the entire source region, and the volume integration will not be necessary. One means of approximating T_{ij} outside of the control surface, and solving the subsequent volume integrals, is presented here. A similar approximation was presented by Mitchell, et. al.[30]

For simplicity, T_{ij} is expressed as $\widehat{T}_{ij}$ through Fourier transformation, and the Kirchhoff surface is assumed to be rigid, and either stationary or in rectilinear motion. τ^* is then uniquely defined, and the effect of the temporal derivatives is simplified considerably. For example,

$$\int_{f>0} \frac{\hat{r}_i \ddot{T}_{ij} \hat{r}_j}{a_\circ^2 r (1-M_r)^3} dV = -\frac{1}{2\pi} \int_{-\infty}^{\infty} \frac{\omega^2}{a_\circ^2} \int_{f>0} \frac{\hat{r}_i \widehat{T}_{ij} \hat{r}_j e^{i\omega r/a_\circ}}{r(1-M_r)^3} d\vec{u}\, d\omega$$

If enough of the sound production region is contained within the surface, $\widehat{T}_{ij}$ in the remaining region can be approximated by

$$\widehat{T}_{ij} \simeq \widehat{T}_{ij_s} e^{i\kappa_{ij} u^3} \tag{3.27}$$

where $\hat{T}_{ij_s}$ is $\hat{T}_{ij}$ evaluated at the control surface, and κ_{ij} is a complex wavenumber with positive imaginary part. (Repeated indices on κ_{ij} are not summed.) This approximation is crude, at best, and most likely not applicable over a wide range of problems, but it serves to demonstrate one means of solving the volume integral with data which is available on the Kirchhoff surface. κ_{ij} is assumed to be constant with u^3 and

$$\kappa_{ij} = -i\frac{\partial \hat{T}_{ij}/\partial u^3}{\hat{T}_{ij}}\bigg|_S$$

Expanding the integrand in a Taylor series about $u^3 = 0$, and retaining dominant terms yields

$$\int_{f>0} \frac{\hat{r}_i \ddot{T}_{ij} \hat{r}_j}{a_\circ^2 r(1-M_r)^3} dV = -\frac{1}{2\pi}\int_{-\infty}^{\infty} \frac{\omega^2}{a_\circ^2} \iint \hat{T}_{ij_s} \sum_{n=0}^{\infty} \Big[\Big(\frac{\omega \cos\theta}{a_\circ}\Big)^n \times \int_0^{\infty} \frac{\big(-iu^3\big)^n}{n!} e^{i\kappa_{ij}u^3} du^3 \Big] \frac{\hat{r}_i \hat{r}_j e^{i\omega r/a_\circ}}{r(1-M_r)^3}\, du^1\, du^2\, d\omega$$

where r, $\hat{r}_i$, $\hat{r}_j$ and θ are now evaluated at the surface. The integral over u^3 is Euler's integral[40]

$$\Gamma(z) = \int_0^{\infty} \zeta^{z-1} e^{-\zeta} d\zeta$$

$$\Gamma(n+1) = n!$$

Using this in the summation with $z = n+1$ gives

$$\int_{f>0} \frac{\hat{r}_i \ddot{T}_{ij} \hat{r}_j}{a_\circ^2 r(1-M_r)^3} dV = -\frac{1}{2\pi}\int_{-\infty}^{\infty} \frac{\omega^2}{a_\circ^2} \iint \frac{i\hat{T}_{ij}}{\kappa_{ij}} \sum_{n=0}^{\infty} \Big(\frac{\omega \cos\theta}{a_\circ \kappa_{ij}}\Big)^n \frac{\hat{r}_i \hat{r}_j e^{i\omega r/a_\circ}}{r(1-M_r)^3}\, du^1\, du^2\, d\omega$$

If $|\omega \cos\theta / a_\circ \kappa_{ij}| < 1$ then the summation can be expressed in closed form,

$$\int_{f>0} \frac{\hat{r}_i \ddot{T}_{ij} \hat{r}_j}{a_\circ^2 r (1 - M_r)^3} dV = -\frac{1}{2\pi} \int_{-\infty}^{\infty} \frac{i\omega^2}{a_\circ^2} \int \left(1 - \frac{\omega \cos\theta}{a_\circ \kappa_{ij}}\right)^{-1} \frac{\hat{r}_i \hat{T}_{ij} \hat{r}_j \, e^{i\omega r / a_\circ}}{\kappa_{ij} r (1 - M_r)^3} \, dS \, d\omega \tag{3.28}$$

The volume integral is now expressed in terms of quantities available on the Kirchhoff surface. The other integrals in (3.26) can be approximated in a similar fashion. If $|\omega \cos\theta / a_\circ \kappa_{ij}| \geq 1$, the assumption of exponential decay in the source terms in equation (3.27) is not valid. This may thus be used as one criterion in the determination of a suitable location for the Kirchhoff surface.

Other volume integral approximations may be more appropriate. Brentner[56] gives one means of calculating the quadrupole noise in rotorcraft high speed impulsive noise studies. Wu and Akay[57] have re–written the volume integral terms in the Ffowcs Williams–Hawkings equation to show their effect on sound radiated by vibrating solid bodies in motion. They found that the quadrupole terms in the volume integral can cancel some terms in the surface integrals. While this cancellation is most likely lost when dealing with a porous surface, their analysis, and that of Brentner, may be useful in developing new techniques for approximating and calculating the volume integral in the modified Kirchhoff formulation.

3.5 Significance of Developments

At this point it is necessary to stress the significance of the developments presented in this chapter. First, note the equivalence of equations (3.7) and (3.17). This equivalence indicates a unification between Lighthill's acoustic analogy,[10] the Ffowcs Williams–Hawkings equation,[18] and the Kirchhoff formulation.[27] Thus, if

there is no surface in the modified Kirchhoff equation, the resultant equation is identical to Lighthill's equation. If the surface is solid, the equation is then equivalent to the Ffowcs Williams–Hawkings equation. Also, if the surface is placed in a linear region, the equation is equivalent to the traditional Kirchhoff formulation.

A versatile code which can switch freely between Ffowcs Williams–Hawkings and Kirchhoff based predictions can be developed. This will allow for the most efficient and accurate calculations for any given CFD input. The development of the modified Kirchhoff integral was also presented in Fourier space, and in two dimensions, to aid in predictions where those requirements or special conditions hold. One means of estimating the volume integral portion of the modified Kirchhoff of Ffowcs Williams–Hawkings predictions was presented as well.

3.6 Validation Calculations

Test calculations have been performed in order to validate the theory and numerical implementation of the modified Kirchhoff method. Results of these calculations are presented in this section.

3.6.1 Stationary Kirchhoff Surface

To determine the validity of the modified Kirchhoff method it is necessary to compare known solutions to the governing equations with the results obtained through the Kirchhoff integral. The calculations shown were developed with jet noise predictions in mind, but the derivations above remain applicable for general acoustics problems.

A source distribution which resembles that encountered in jet noise predictions

can be defined by

$$\widehat{T}_{ij} = \exp\left[i\,\kappa_{ij}\,|y_1 - y_o| - R/h\right] \tag{3.29}$$

where (y_1, R) are the near–field source cylindrical coordinates. If κ and ω_o are chosen properly, (3.29) loosely approximates the source distribution in a round jet forced at frequency ω_o. Figure 3.2 shows the amplitude of $\widehat{T}_{11}$ on the centerline, $(R = 0)$. If the source distribution is defined by (3.29) then equation (3.27) is exact. The radiated sound can then be determined through a solution of Lighthill's equation. The volume integration is not a burden, so long as only one frequency, ω_o, is considered. The geometry of the volume integration, with respect to the cylindrical control surface and source distribution, are shown in figure 3.3.

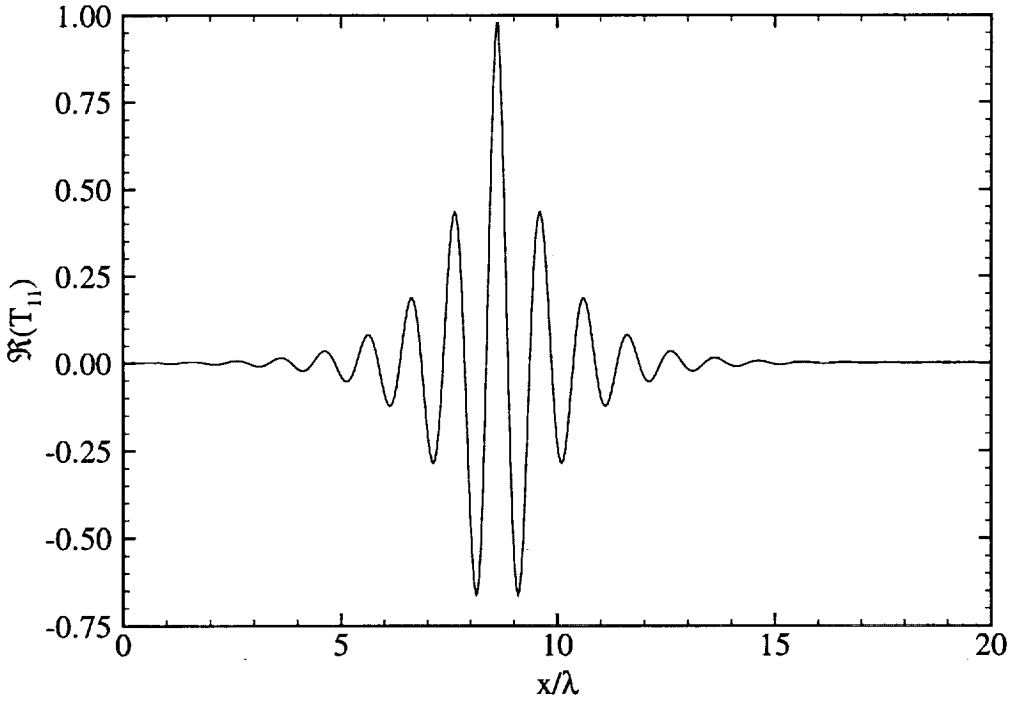

Figure 3.2. Centerline amplitude of $\widehat{T}_{11}$, calculated with equation (3.29).

Figure 3.4 shows the real part of $\widehat{p}$ for $\kappa = (6.26 + i\,0.838)/\lambda$. The distribution is stationary. ω_o is chosen to correspond to the forcing frequency of a jet simulated previously by the authors.[32] The sound field is symmetric about $x_o = 8.62\,\lambda$, and h is set to $0.133\,\lambda$. The necessary volume and surface integrals were calculated with first order mid–panel quadrature.[50] To ensure that the entire source region is captured, the dimensions of the volume integration domain, and number of quadrature points, are double those of the Kirchhoff surface. (The volume integral domain is a cylinder of length $34.48\,\lambda$, and radius $2.66\,\lambda$. 260, 80, and 108 quadrature points were used in the axial, radial and azimuthal directions.) Use of a larger domain does not change the volume integral solution. For the purposes of the comparisons here, it is considered exact.

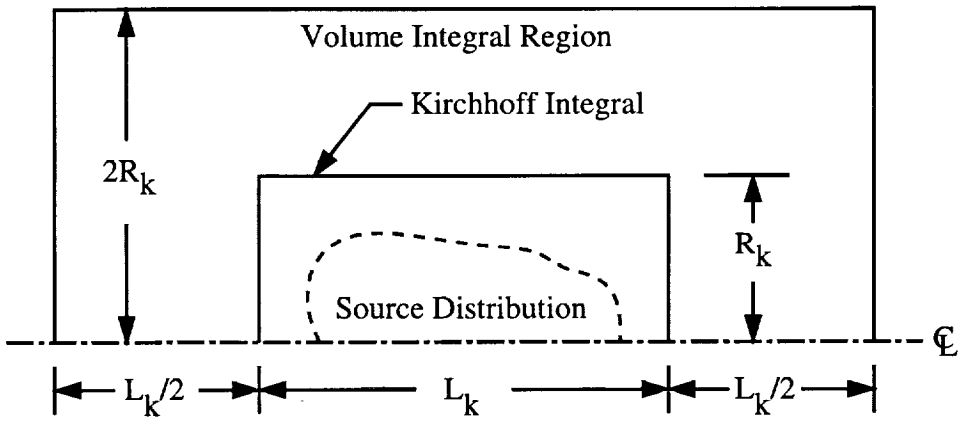

Figure 3.3. Kirchhoff surface and volume integral geometry.

The source distribution described above (3.29) was initially used as an additional test of the traditional Kirchhoff formulation. If the entire source region is enclosed within the Kirchhoff surface, then equation (2.31) should be able to predict the mid–field and far–field sound. Figure 3.5 shows the predicted and exact acous-

tic signals at $(x, R) = (20\,\lambda, 2.5\,\lambda)$. The Kirchhoff surface was a cylinder of length $L_k = 17.24\,\lambda$ and radius $R_k = 1.33\,\lambda$. The amplitude of $\widehat{T}$ is very small beyond the ends of the cylinder. Thus, noise production in these regions can be ignored with no effect on the calculated sound signals. The surface was discretized with 130, 40, and 54 uniformly spaced points in the axial, radial and azimuthal directions. The addition of more quadrature points on the surface had little effect on the solution.

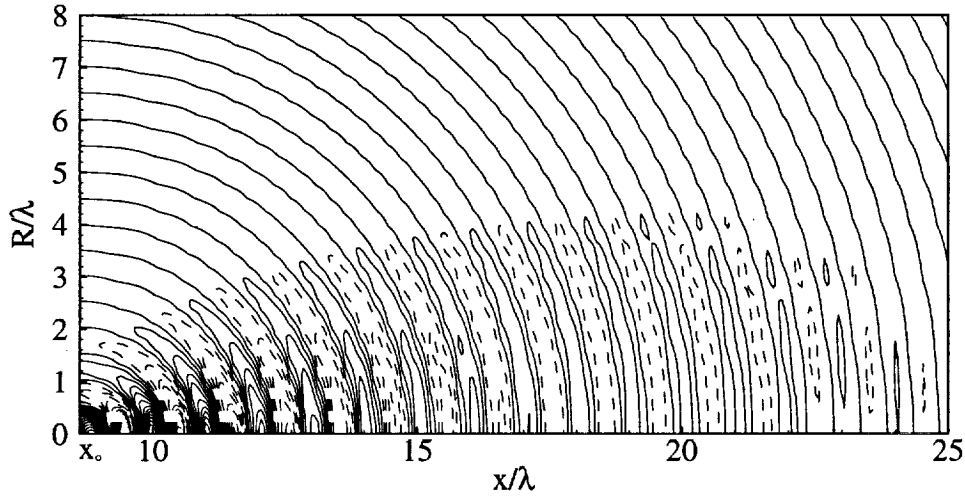

Figure 3.4. Exact sound field (real part), calculated with equation (3.29). Contours: min $= -0.340$, max $= 0.340$, increment $= 0.0283$. Negative contours are dashed. $M = 0.00$.

The excellent agreement between the "exact" and Kirchhoff solutions serves to validate the Kirchhoff methodology when the computational surface is placed in a fully linear region. Also shown in the figure is the signal calculated with a cylindrical Kirchhoff surface without the end surfaces. The prediction which employed a partial Kirchhoff surface gave substantial amplitude and phase errors. "Open–surface" Kirchhoff methods (e.g. those used in references 29 and 30) are not appropriate

acoustic prediction tools when the observation point lies close to the jet axis.

Next, the Kirchhoff surface was reduced in size, so that it no longer enclosed the entire source distribution. The length of the cylindrical surface was reduced to $L_k = 10.61\,\lambda$, while the radius, and number of discrete points on the surface remained the same.

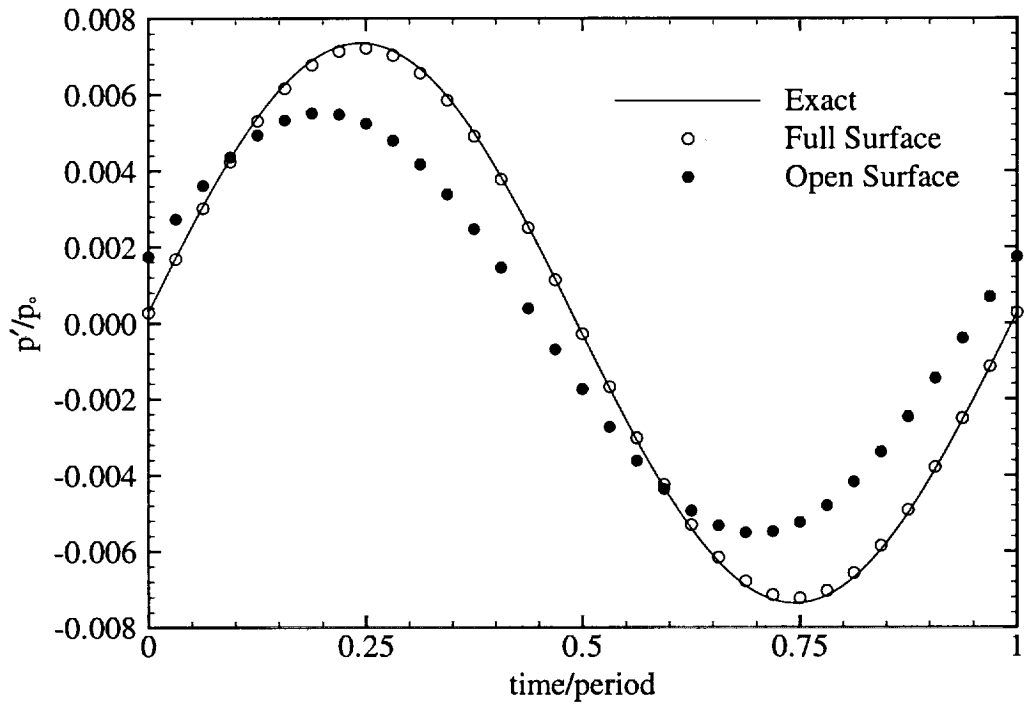

Figure 3.5. Predicted and exact acoustic signals calculated with the traditional Kirchhoff method at $(x, R) = (20\,\lambda, 2.5\,\lambda)$. $M = 0.00$.

Figure 3.6 shows the exact and predicted sound signals, at the same observation point, obtained with the modified Kirchhoff method. Two levels of approximation in the volume integration, as well as the traditional Kirchhoff solution, are shown. Omission of the volume integral leads to large amplitude errors, while the approxi-

mation given in equations (3.27) and (3.28) slightly over–predicts the amplitude and reduces the error considerably. If the "exact" volume integral solution (outside of the Kirchhoff surface) to Lighthill's equation is used in (2.31), the error is reduced to almost zero. This validates the modified Kirchhoff formulation for this simplified test case, and a stationary surface.

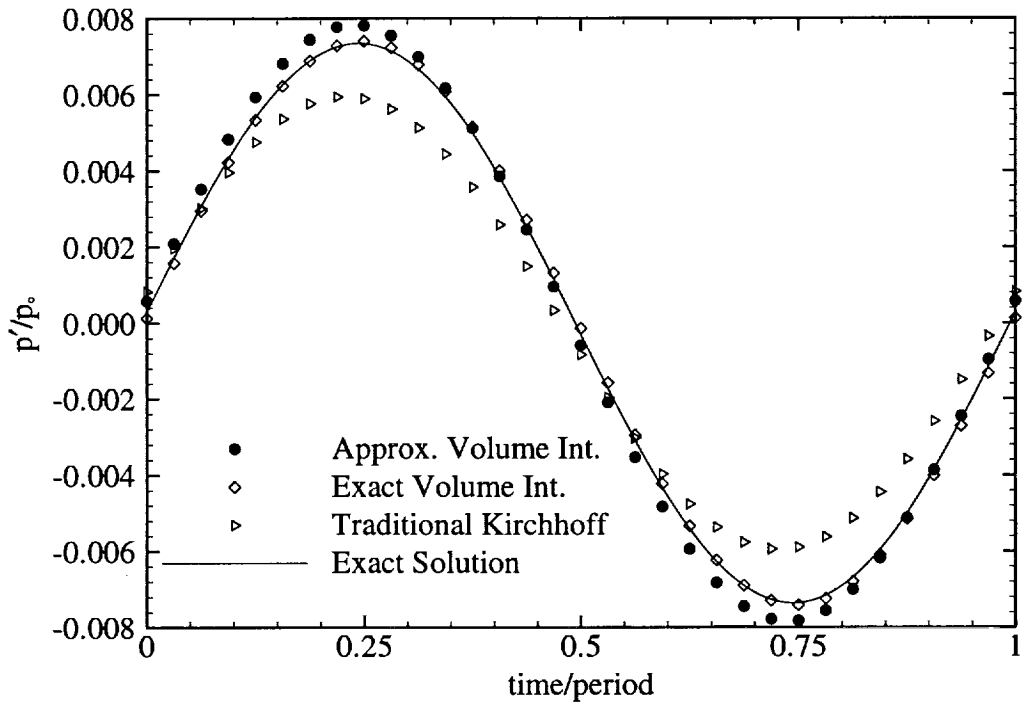

Figure 3.6. Predicted and exact acoustic signals calculated with the modified Kirchhoff method at $(x, R) = (20\,\lambda, 2.5\,\lambda)$. $M = 0.00$.

The error field $(\widehat{p}_{calc} - \widehat{p}_{exact})$ to the right of an open Kirchhoff surface ($L_k = 10.61\,\lambda$) is shown in figure 3.7. It is evident that jet noise calculations using an open surface will not be acceptable in the region downstream of the surface. Figure 3.8 shows the error field produced by the full modified Kirchhoff method, using the

approximate volume integral and the full Kirchhoff surface. The error is reduced considerably. (Note the change in contour spacing.)

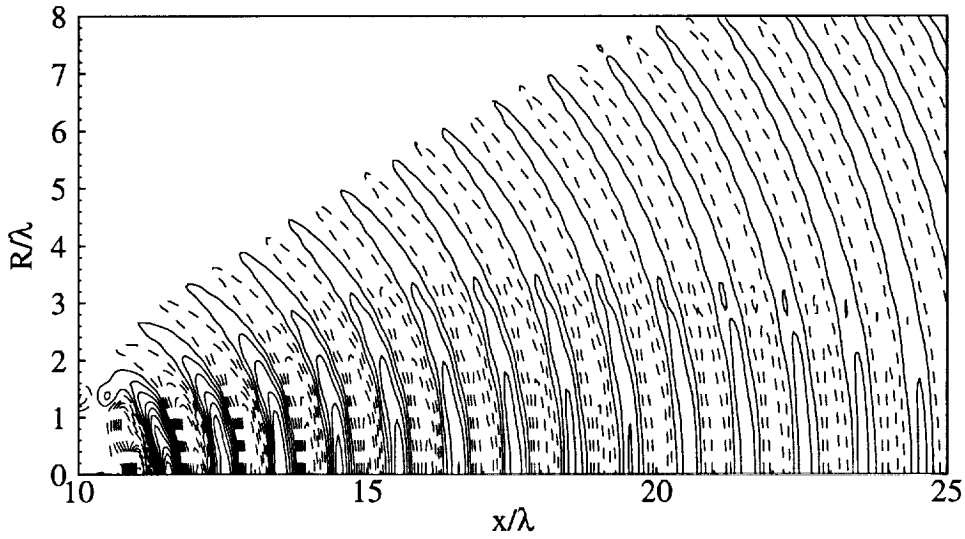

Figure 3.7. Error field (real part) obtained using an open Kirchhoff surface and the traditional Kirchhoff method. Contours: min = −0.270, max = 0.190, increment = 0.020. $M = 0.00$. Negative contours are dashed.

3.6.2 Rectilinear Motion

The test calculations presented above were also applied to a source distribution in rectilinear motion. The source distribution given by (3.29), the Kirchhoff surface, and all observer points, are assumed to be moving in the $-y_1$ direction at $M = 0.40$. Figure 3.9 shows the real part of $\hat{p}$ for $\kappa_{ij} = (16.67 + i0.40)/\lambda$ for all (i, j). $\hat{p}$ is normalized by the maximum amplitude of $\widehat{T}_{11}$ in the source distribution. y_o and h are now set to $8\,\lambda$ and $0.088\,\lambda$ respectively.

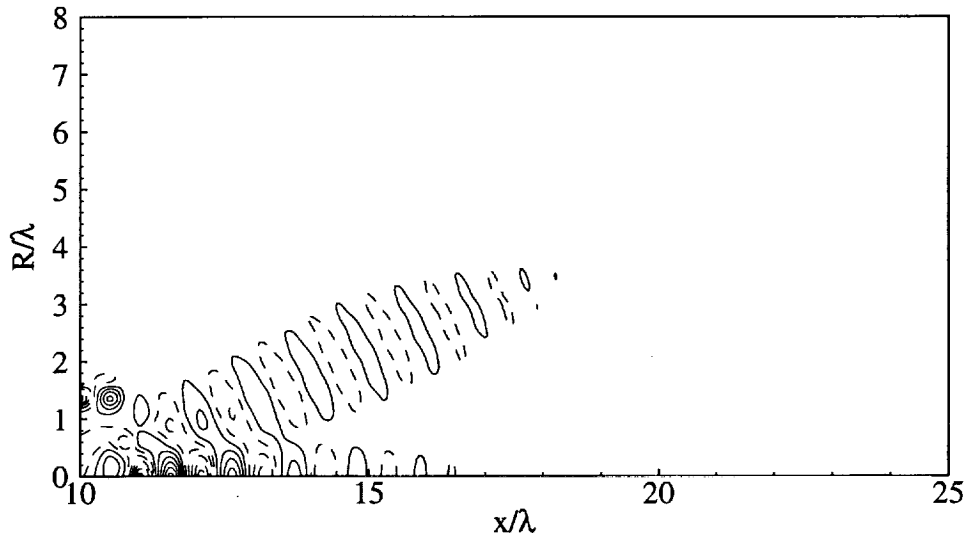

Figure 3.8. Error field (real part) obtained using a closed Kirchhoff surface and the full modified Kirchhoff integral. Contours: min = −0.055, max = 0.075, increment = 0.010. $M = 0.00$. Negative contours are dashed.

The source distribution is again used to validate the traditional Kirchhoff integral formulation. If the entire source region is enclosed within the Kirchhoff surface, then equation (2.27) should be able to completely predict the sound radiated to the far–field. Figure 3.10 shows the predicted and exact acoustic signals at $(x_1, R) = (18\,\lambda, 1.0\,\lambda)$. The signals are normalized by the maximum disturbance amplitude at the observation point. The Kirchhoff surface is a cylinder of length $L_k = 17.0\,\lambda$ and radius $R_k = 1.2\,\lambda$. The surface is discretized with 130, 30 and 90 uniformly spaced quadrature points in the axial, radial, and azimuthal directions. These values are chosen so that the order of accuracy in the numerical quadrature has little effect on the calculated signals. Mid–panel first order quadrature[50] is again used to solve the integrals numerically.

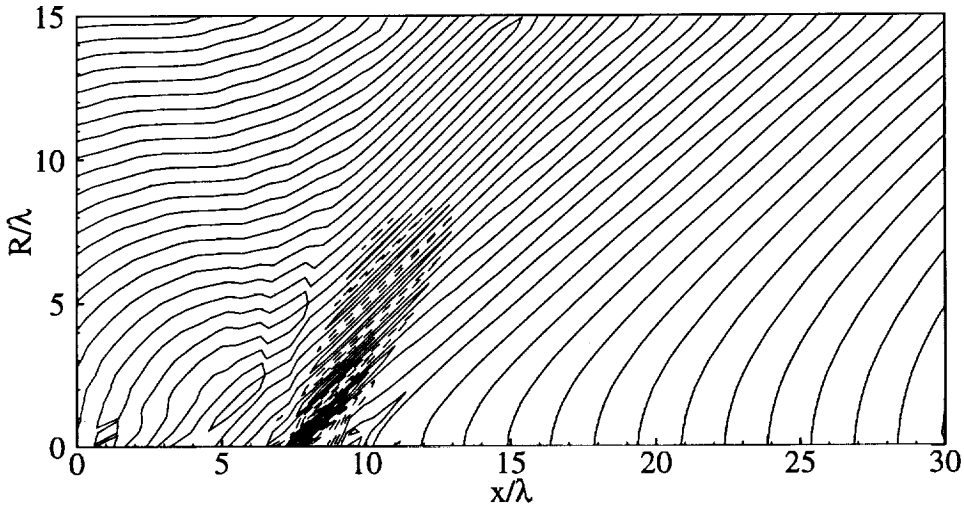

Figure 3.9. Exact sound field (real part), calculated with equation (3.29). Contours: min = −0.045, max = 0.045, increment = 3.75×10^{-3}. $M = -0.40$. Negative contours are dashed.

As discussed in the previous chapter, higher order quadrature schemes with "enrichment"[52] have been programmed, but the numerical scheme used was determined to be sufficient to validate the theoretical development here. Also shown in the figure is the signal calculated with a cylindrical control surface without the end surfaces (the region where traditional Kirchhoff predictions lose validity in jet noise calculations). The prediction which employs the full control surface is nearly exact, while the partial surface gives substantial amplitude and phase errors. "Open–surface" Kirchhoff methods are again shown to be inappropriate in cases where the observation point lies in a region near the jet axis.

Following the process described above, the control surface is decreased in size, so that it no longer encloses the entire source distribution. The length of the cylin-

drical surface is reduced to $L_k = 10\,\lambda$, while the radius of the surface remains constant. The number of discrete points in the axial direction is reduced to 75. Figure 3.11 shows the exact and predicted sound signals, at $(x_1, R) = (18\,\lambda, 1.0\,\lambda)$, obtained with the modified Kirchhoff method. The open surface is again seen to produce large amplitude and phase errors. The approximated volume integral slightly reduces this amplitude error, as well as the phase error. If the "exact" volume integral solution (i.e. that solved numerically outside the Kirchhoff surface) is used in the modified Kirchhoff formulation, the amplitude and phase errors are reduced to almost zero. This serves to validate the modified Kirchhoff formulation for surfaces in rectilinear motion. The signals shown are insensitive to the value of L_k, since (3.27) is exact for the given source distribution.

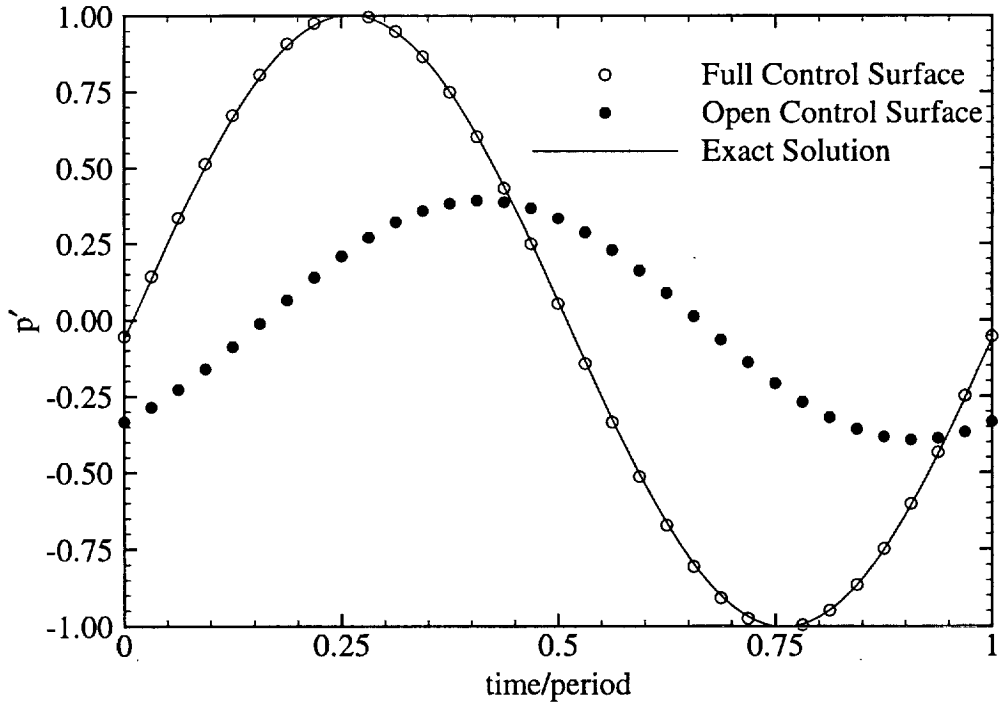

Figure 3.10. Predicted and exact acoustic signals at $(x_1, R) = (18\,\lambda, 1.0\,\lambda)$.

Figure 3.12 shows normalized signals produced with the modified Kirchhoff integral at $(x_1, R) = (8\,\lambda, 5\,\lambda)$. At this observer location, most of the signal is produced by the constant R side of the cylindrical Kirchhoff surface, so even the open surface can produce an effective signal. The approximate volume integral is again seen to improve the signal, and the "exact" volume integral produces almost no error.

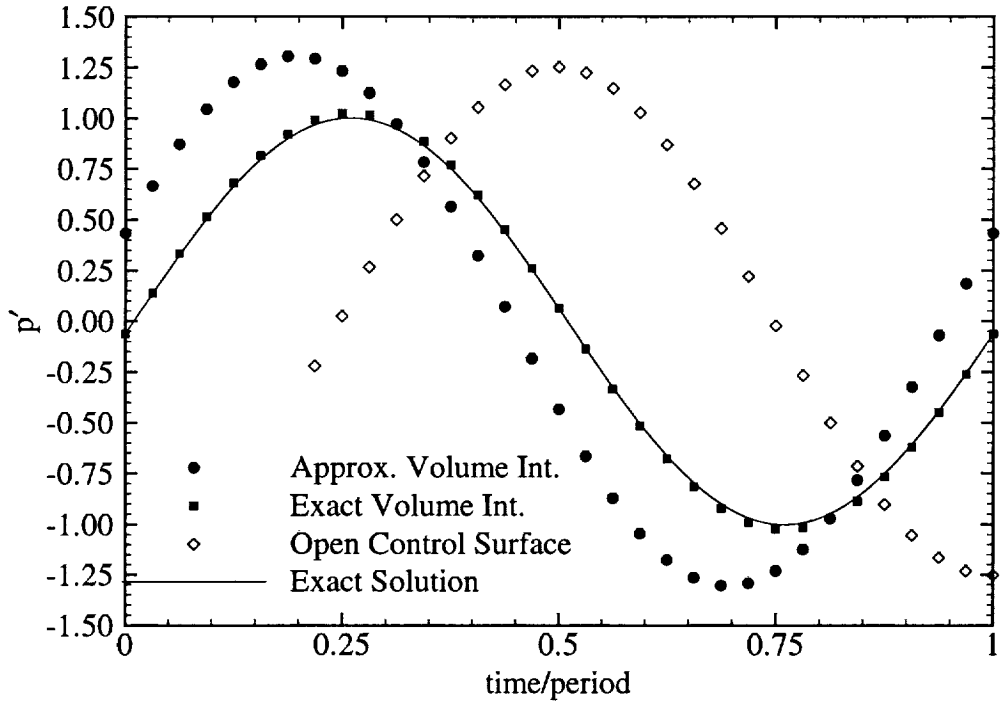

Figure 3.11. Predicted and exact acoustic signals at $(x_1, R) = (18\,\lambda, 1.0\,\lambda)$.

The error field $(\widehat{p}_{calc} - \widehat{p}_{exact})$ produced with an open Kirchhoff surface ($L_k = 10.0\,\lambda$) is shown in figure 3.13. The control surface is shaded. It is evident that aerodynamically generated noise calculations using an open Kirchhoff surface in rectilinear motion will not be acceptable in some regions. Figure 3.14 shows the

error field produced by the full modified Kirchhoff method, using the approximate volume integral. The error is reduced considerably.

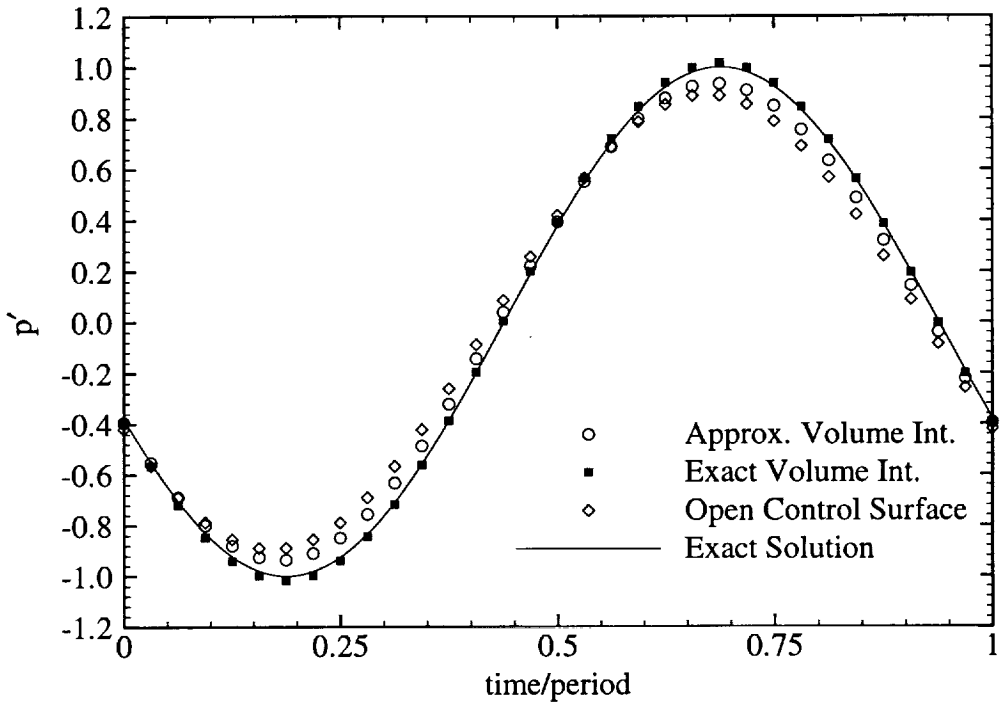

Figure 3.12. Predicted and exact acoustic signals at $(x_1, R) = (8\,\lambda, 5\,\lambda)$.

The simple source distributions used in these calculations do not closely match those found in real jets, but it serves to verify the validity of the use of the modified Kirchhoff integral in certain cases. These cases include those where the source region is extensive enough to prohibit placement of the Kirchhoff such that it surrounds all sources. The results presented in this section were all produced with the frequency domain formulation of the three dimensional modified Kirchhoff integral. Similar results have been obtained with the time domain, and two dimensional versions of the Kirchhoff integral. Results of predictions of the noise due axisymmetric and

two dimensional supersonic jets are presented in the next chapter.

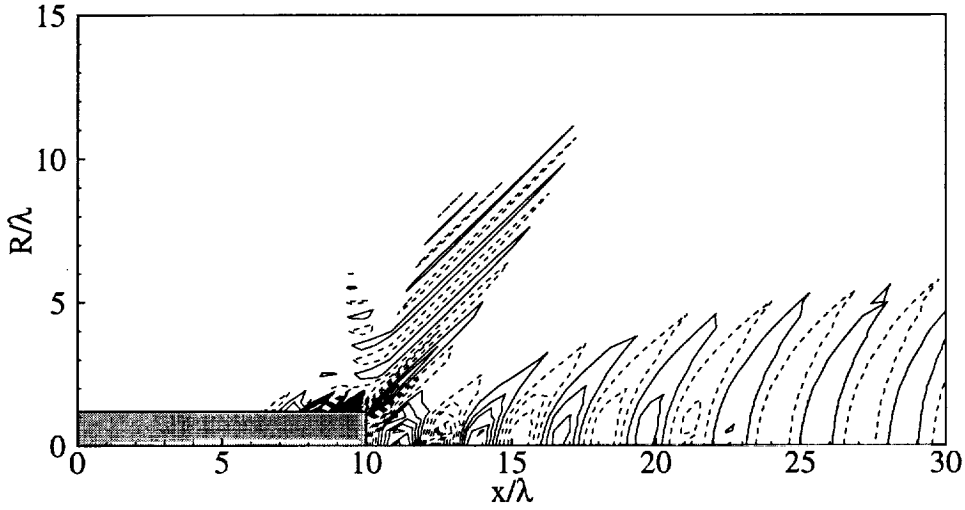

Figure 3.13. Error field (real part) using an open control surface. Contours: min = -0.01, max = 0.01, increment = 8.70×10^{-4}. Negative contours are dashed.

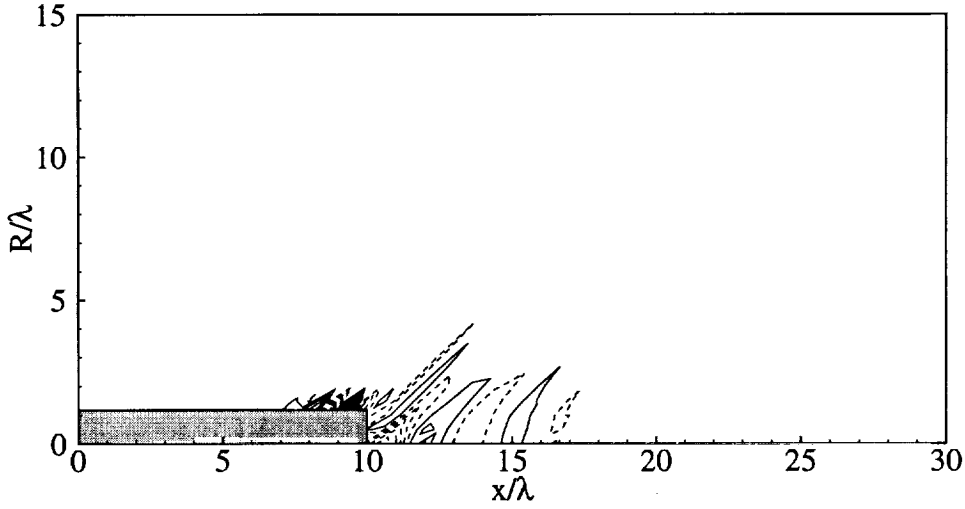

Figure 3.14. Error field (real part) with approximate volume integral. Contours: min = -0.01, max = 0.01, increment = 8.70×10^{-4}. Negative contours are dashed.

Appendix

The terms B_1, B_2, and B_3 in equation (3.26) are as follows.

$$
\begin{aligned}
B_1 &= \hat{r}_i \ddot{T}_{ij} \hat{r}_j + \frac{1}{(1-M_r)} \left(3\dot{M}_r + \ddot{M}_r\right) T_{rr} + \frac{1}{(1-M_r)^2} \left(3\dot{M}_r^2 T_{rr}\right) \\
B_2 &= 3\hat{r}_i \dot{T}_{ij} \hat{r}_j \\
&\quad + \frac{1}{(1-M_r)} \Big[\dot{M}_r \left(3T_{rr} - T_{ii}\right) - T_{ij} \left(\dot{M}_i \hat{r}_j + \dot{M}_j \hat{r}_i\right) - \dot{T}_{ii} \\
&\qquad\qquad + \dot{T}_{ij} \left(M_r \hat{r}_i \hat{r}_j - M_i \hat{r}_j - M_j \hat{r}_i\right)\Big] \\
&\quad + \frac{1}{(1-M_r)^2} \Big[\dot{T}_{ij} \hat{r}_i \hat{r}_j \left(M_r^2 - M^2 - 3M_r\right) - 3T_{ij} \dot{M}_r \left(M_i \hat{r}_j + M_j \hat{r}_i\right) \\
&\qquad\qquad + T_{rr} \left(3\dot{M}_r + 12 M_r \dot{M}_r - M_i \dot{M}_i + 2M\dot{M}\right)\Big] \\
&\quad + \frac{1}{(1-M_r)^3} \Big[4\dot{M}_r T_{rr} \left(M_r^2 - M^2\right)\Big] \\
B_3 &= 3T_{rr} - T_{ii} \\
&\quad + \frac{1}{(1-M_r)} \Big[M_r \left(9T_{rr} - 2T_{ii}\right) - 3T_{ij} \left(M_i \hat{r}_j + M_j \hat{r}_i\right)\Big] \\
&\quad + \frac{1}{(1-M_r)^2} \Big[T_{rr} \left(12M_r^2 - 3M^2\right) - T_{ii} \left(M_r^2 - M^2\right) \\
&\qquad\qquad + T_{ij} \left(2M_i M_j - 6M_r \left(M_i \hat{r}_j + M_j \hat{r}_i\right)\right)\Big] \\
&\quad + \frac{1}{(1-M_r)^3} \Big[T_{rr} \left(M_r^2 - M^2\right) \left(9M_r + 3\right) \\
&\qquad\qquad + T_{ij} \left(M_r^2 - M^2\right) \left(1 - 3\left(M_i \hat{r}_j + M_j \hat{r}_i\right)\right)\Big] \\
&\quad + \frac{1}{(1-M_r)^4} \Big[3T_{rr} \left(M_r^2 - M^2\right)\Big]
\end{aligned}
$$

Chapter 4

Jet Noise Predictions

The mathematical and numerical methods and techniques derived in the previous chapters have been applied in sample jet noise calculations. The results of these calculations are presented in this chapter.

4.1 Axisymmetric Round Jet

The authors have obtained data from a near–field jet noise calculation performed at the NASA Lewis Research Center. The calculations were performed using the Large Scale Simulation code of Mankbadi, et. al.,[7,8] based on the 2–4 MacCormack method of Gottlieb and Turkel.[58] The calculations simulated an excited, Mach 2.1, cold (jet total temperature = ambient temperature = $294K$), round jet of Reynolds Number $Re = 70000$. The jet exit variables were perturbed at a single axisymmetric mode at a Strouhal number of $St = 0.20$. The amplitude of the perturbation was 2% of the mean. The jet flow field and all observers were

assumed to be static. These conditions were imposed in order to approximate the experimental conditions in the study of Troutt and McLaughlin.[59] However, since the numerical simulation assumed axi–symmetry in the flow and acoustic fields, the correlation between numerically predicted and experimentally measured acoustic properties can only be qualitative. The flow data was then converted to the frequency domain at all spatial points using a Fast Fourier Transform algorithm.[60] The CFD mesh used in the calculation extended from $5\,R_j$ to $70\,R_j$ in the axial direction and from 0 to $32.2\,R_j$ in the radial direction, where R_j is the jet nozzle radius. The CFD mesh consisted of 390 × 280 grid points in the axial and radial directions.

Figures 4.1 and 4.2 show the axial variation of $\Re(\widehat{T}_{11})$ and $\Im(\widehat{T}_{11})$ on the jet centerline from 5 to 70 jet radii (the extent of the available data), for the first and second Fourier wave modes, which correspond to $St = 0.20$ and $St = 0.40$, ($\Re$ and $\Im$ denote the real and imaginary parts respectively). All variables are normalized by jet nozzle conditions. Higher order wave modes show similar results. It is evident that the disturbance amplitude is quite large at the end of the computational domain. Thus, a prediction of the disturbances in the region downstream of the computational domain, e.g. equation (3.27), is required.

Output from the numerical jet simulation was used to determine p', ρ', and the necessary derivatives on a cylindrical Kirchhoff surface. The surface was chosen to match lines in the mesh used for the CFD calculations, so that $L_k = 64.67\,R_j$, and $R_k = 8.56\,R_j$. These values were deemed to be the best choices among the available data, based on mesh spacing and the assumed linearity of disturbances near the surface. (The surface extends axially from $x = 5\,R_j$ to $x = 69.67\,R_j$.) There are 389 axial, 167 radial, and 90 azimuthal quadrature points on the Kirchhoff

surface. These points correspond to points in the CFD mesh. The radial mesh is exponentially stretched about $R = R_j$. First order, mid-panel quadrature[50] was again used in the determination of the integral solutions. On the constant R portion of the Kirchhoff surface, the number of quadrature points is approximately equal to 10 points per wavelength of the fourth Fourier mode. This is around the lower limit found to be sufficient for accurate predictions in previous chapters. Thus, only the first four Fourier modes are used in the calculations shown here.

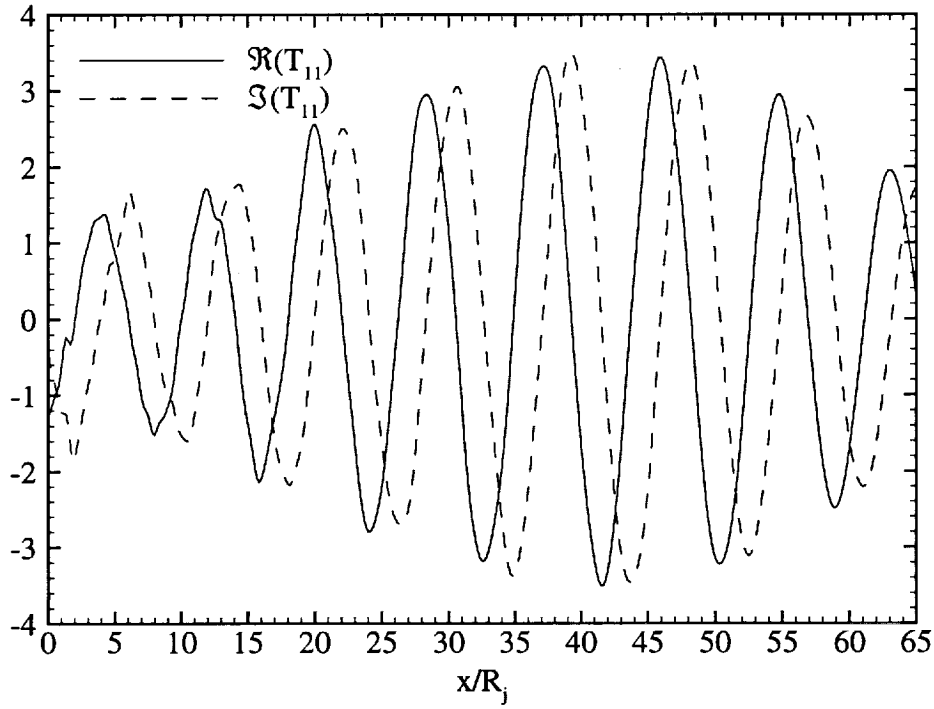

Figure 4.1. Computed centerline axial variations of $\widehat{T}_{11}$ at $St = 0.20$.

Figure 4.3 shows the acoustic signals generated by two levels of approximation, as well as the signal generated with the first four Fourier modes of the CFD prediction, at $(x, R) = (63.17\,R_j, 9.18\,R_j)$. Both levels of approximation match the

CFD calculations reasonably well, at this observation point. The volume integral in the modified Kirchhoff equation does not have much effect in this region, as the majority of the sound prediction comes from the terms of the traditional Kirchhoff integral, on the constant R portion of the Kirchhoff surface. Shih, et. al.[34] have shown that predictions obtained with the modified Kirchhoff integral match very closely with other prediction schemes in this region.

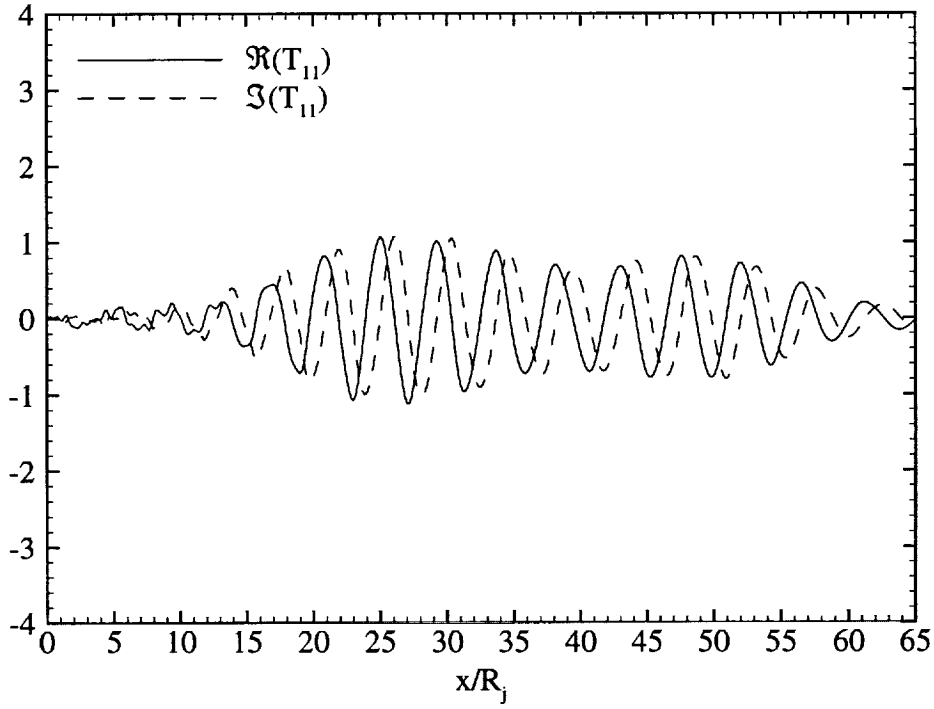

Figure 4.2. Computed centerline axial variations of $\widehat{T}_{11}$ at $St = 0.40$.

Figure 4.4 shows a snapshot of instantaneous pressure disturbance contours. The disturbances shown above the centerline were calculated with the modified Kirchhoff method on a closed surface ($p' = a_o^2 \rho'$). Those shown below the centerline were calculated with the traditional Kirchhoff method on an open surface ($p' =$

$p - p_o$). (The traditional Kirchhoff method is not valid on the closed surface near the jet centerline.) The figure shows that the modifications have a substantial effect in the region downstream of the Kirchhoff surface. The modified Kirchhoff method produces disturbances which appear to propagate spherically from an equivalent source located near $x_s \approx 30\, R_j$.

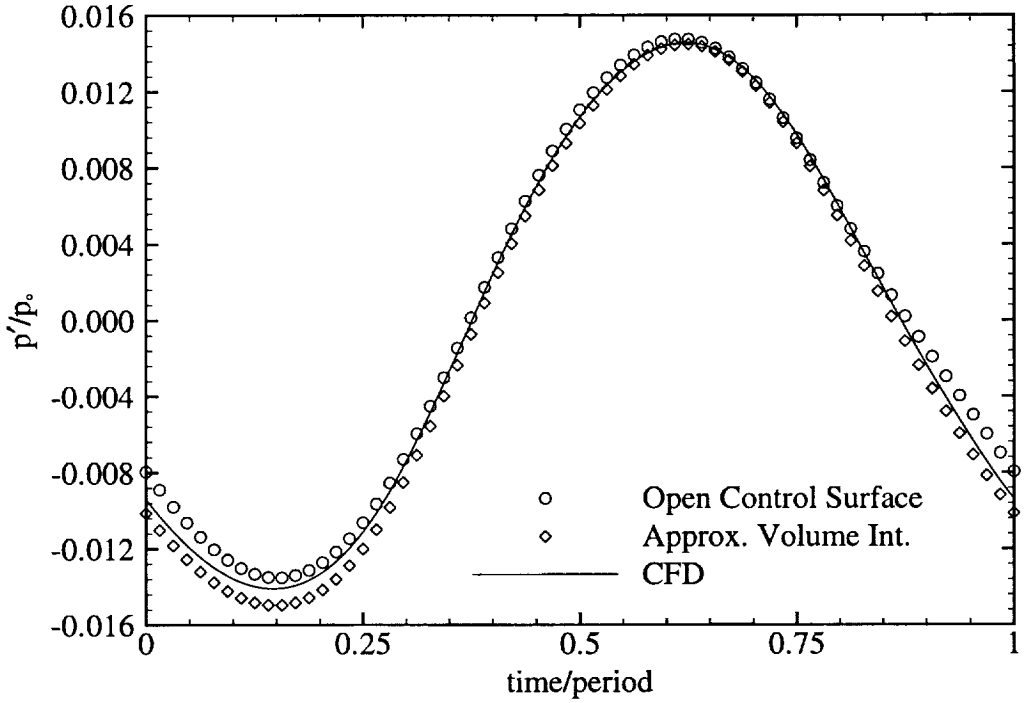

Figure 4.3. Predicted acoustic signals from the CFD calculations and Kirchhoff methods at $(x, R) = (63.17\, R_j, 9.18\, R_j)$.

There is a large zone of relative silence in the traditional Kirchhoff prediction caused by the omission of noise generated at and downstream of the surface. A smaller zone of silence near the jet centerline should be evident in the predictions. This zone of silence is caused by mean flow refraction of the sound. However, no means

on approximating the physical processes involved in this refraction are currently included in the Kirchhoff methodology. Both predictions appear to adequately capture the Mach wave radiation in the region $R \geq 10\, R_j$.

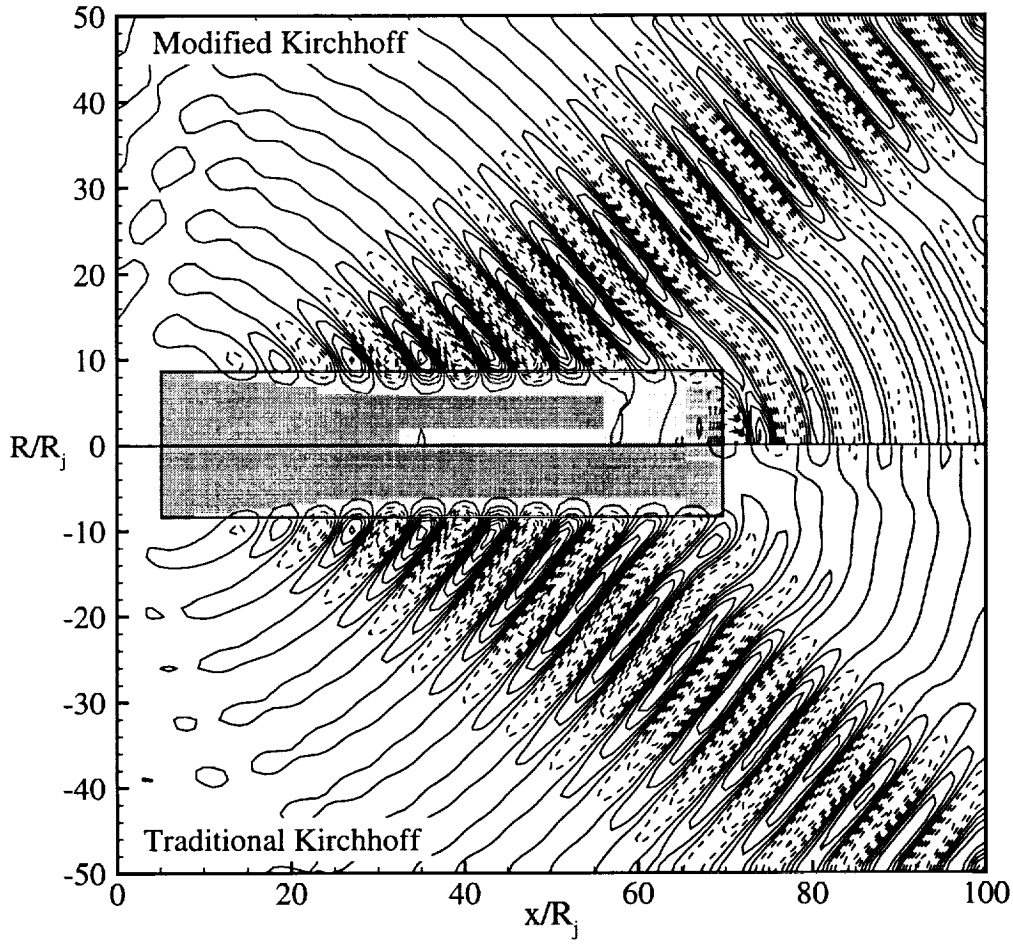

Figure 4.4. Snapshot of instantaneous pressure contours (normalized by free stream pressure) predicted with the modified and traditional Kirchhoff methods. Contours: min = −0.020, max = 0.020, increment = 0.002. Negative contours are dashed. The Kirchhoff surface is shaded

The effects of the newly derived modifications to the Kirchhoff integral are

also clearly shown in figure 4.5. The figure shows sound pressure level contours calculated from the two cases described above. The levels are scaled relative to the experimental data given by Troutt and McLaughlin.[59] The differences between the two predictions are clearly evident in the region downstream of the computational surface. The predictions show qualitative agreement with the results presented in reference 59, and also those presented by Mankbadi, et. al.[61] However, it should be noted again that the calculations shown here were based on an axisymmetric CFD calculation. The experimental data in reference 59 is made up of axisymmetric and helical disturbance modes, so that a direct quantitative comparison is not possible.

In the future, as more accurate and efficient numerical methods become available for the near–field acoustics predictions, the modified Kirchhoff method should be able to predict mid–field and far–field acoustics in regions where the traditional Kirchhoff method other prediction schemes lose validity. The modified method should also be useful in the prediction of other types of aerodynamically generated noise as well.

4.2 Two Dimensional Plane Jet

A second set of jet CFD calculation data has been made available to the authors. These calculations numerically simulated the flow field of a two–dimensional rectangular slot jet. The calculations were performed in an effort to approximate the experimental conditions of Raman,[62] and to investigate the instability modes excited by natural screech tones.

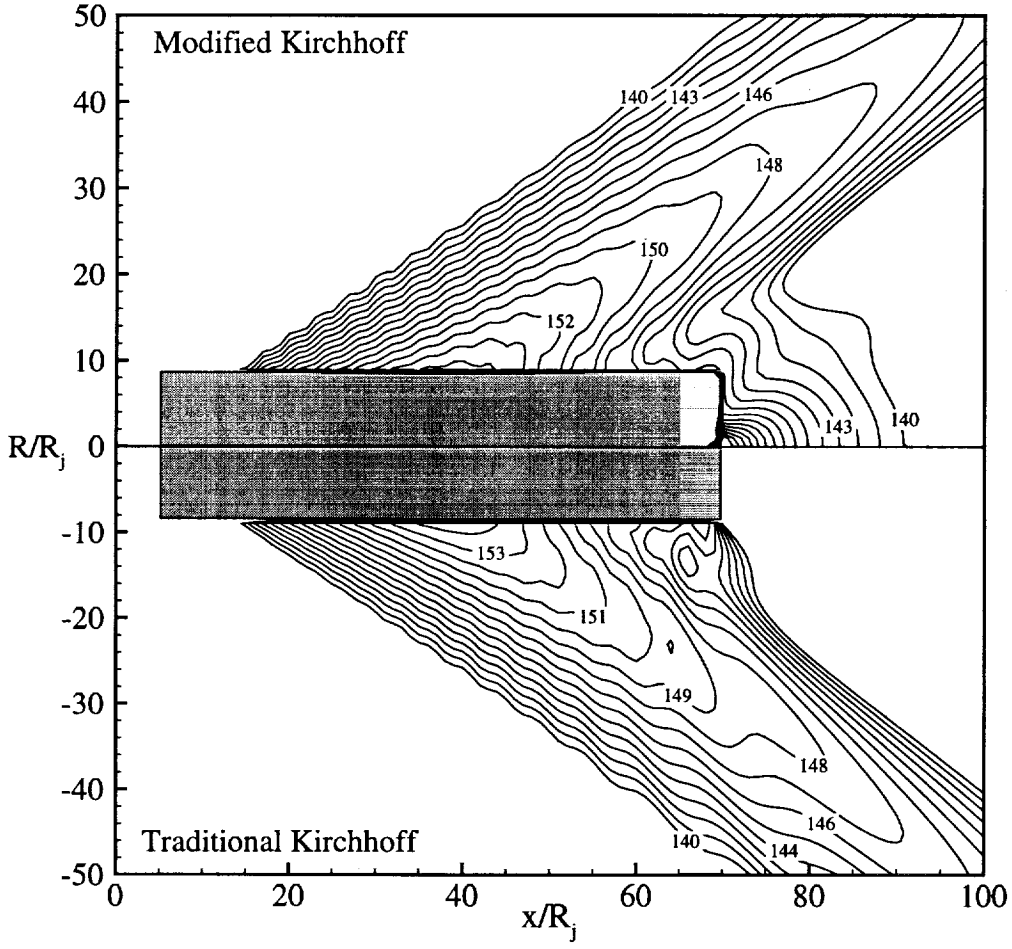

Figure 4.5. Sound pressure level contours predicted with the modified and traditional Kirchhoff methods. The Kirchhoff surface is shaded

The computational study, which was performed at the Ohio State University, solved the unsteady, two dimensional, Navier–Stokes equations. The numerical algorithm used to solve the equations was the MacCormack method, which is second order accurate in both space and time.[63] The calculations were performed to simulate a jet exiting a converging rectangular nozzle with an aspect ratio of 9.63. In the experimental and numerical studies, the jet was in an underexpanded condition,

so that the plume contained shock waves. The jet Mach number, just downstream of the initial expansion system, was $M = 1.6$. The numerical simulations assumed that the ambient conditions were that of a standard atmosphere. The numerical simulation was allowed to progress temporally from the initial conditions (those of the experiment) to a state where the period of the jet's flapping mode was nearly constant. The jet was not numerically excited. For the sake of the predictions shown here, the jet flow field was assumed to be periodic with a frequency equal to that of the flapping mode. The calculations were performed with a computational mesh that extended $70\,h$ in the streamwise direction, and from $-20\,h$ to $20\,h$ is the spanwise direction. Here, h is the width of the jet nozzle opening. A sample computational mesh, similar to that used in the calculations, is shown in figure 4.6.

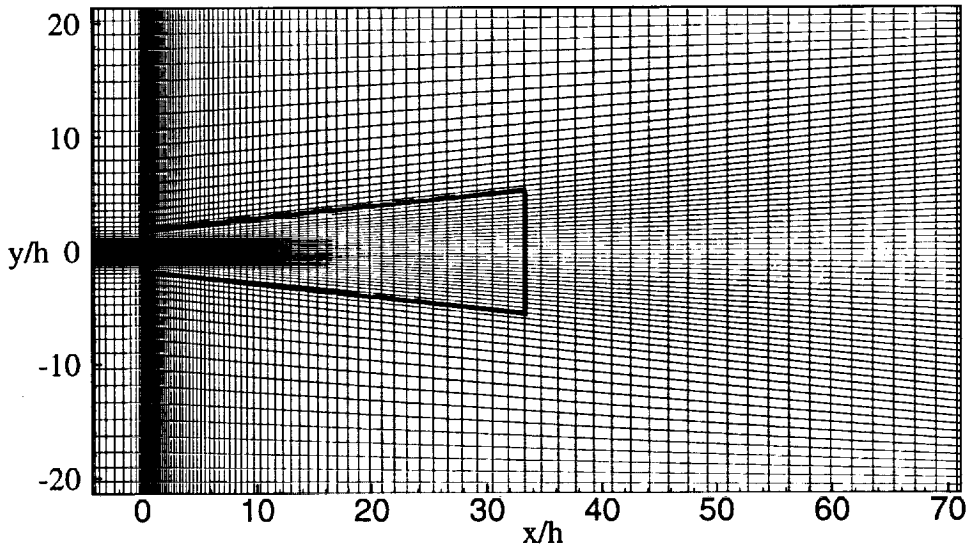

Figure 4.6. Computational mesh used in the 2D jet simulations. For clarity, every other point is shown.

Figures 4.7 and 4.8 show the streamwise variation of the real and imaginary parts of

$\widehat{T}_{11}$ at $y = 0$, for the first two Fourier modes. The two modes correspond to Strouhal Numbers ($St_m = \omega_m h/2\pi U_j$) of approximately 0.125 and 0.250 respectively. Here U_j is the RMS averaged jet velocity at the nozzle. The values of T_{ij} are normalized by the jet dynamic pressure, $q_j = \rho_j U_j^2$.

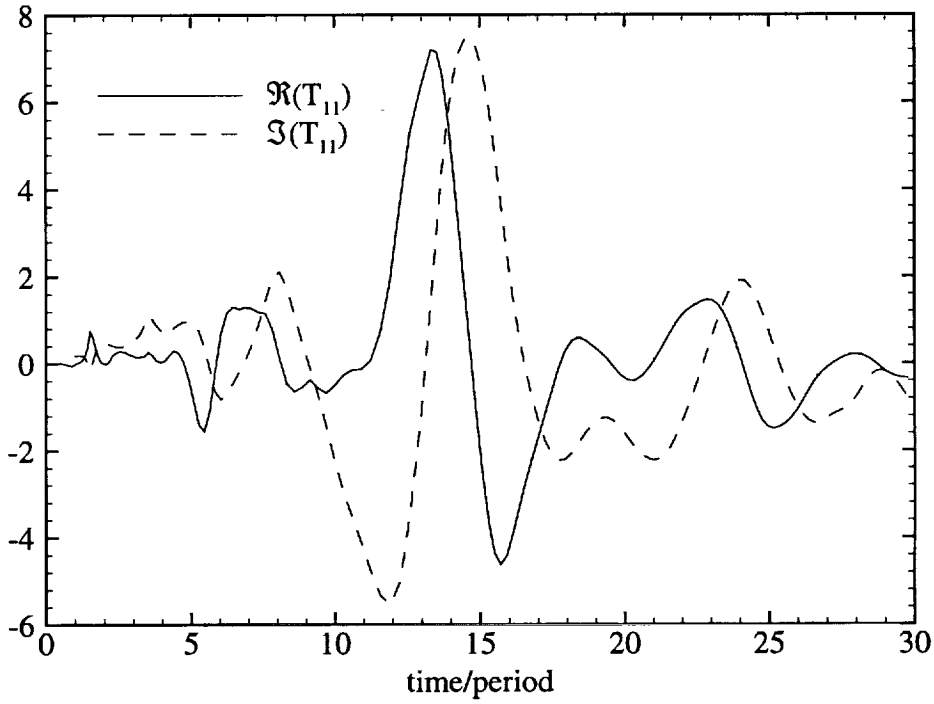

Figure 4.7. Computed streamwise variations of $\widehat{T}_{11}$ at $y = 0$. $St = 0.125$.

A Kirchhoff surface was chosen to surround the majority of the noise producing region of the jet flow. A sample Kirchhoff surface is shown with a heavy line in figure 4.6. Surface data was taken directly from the CFD mesh, and transformed via FFT. The surface extended from 0 to $26.9\,h$ in the spanwise direction. Data in the simulation downstream of $26.9\,h$ was judged to be unreliable in acoustics predictions, due to spurious waves reflected into the computational domain at the

downstream end of the domain. The portions of the Kirchhoff surface just above or below the shear layer were chosen to match match one line in the CFD mesh. On the upstream side of the surface, it is located at $y \simeq \pm 2.25\, h$, and at the downstream end at $y \simeq \pm 6.76\, h$. There are 134 quadrature points in the streamwise direction and 74 points in the spanwise direction on the surface. Data at these points was taken directly from the CFD calculations.

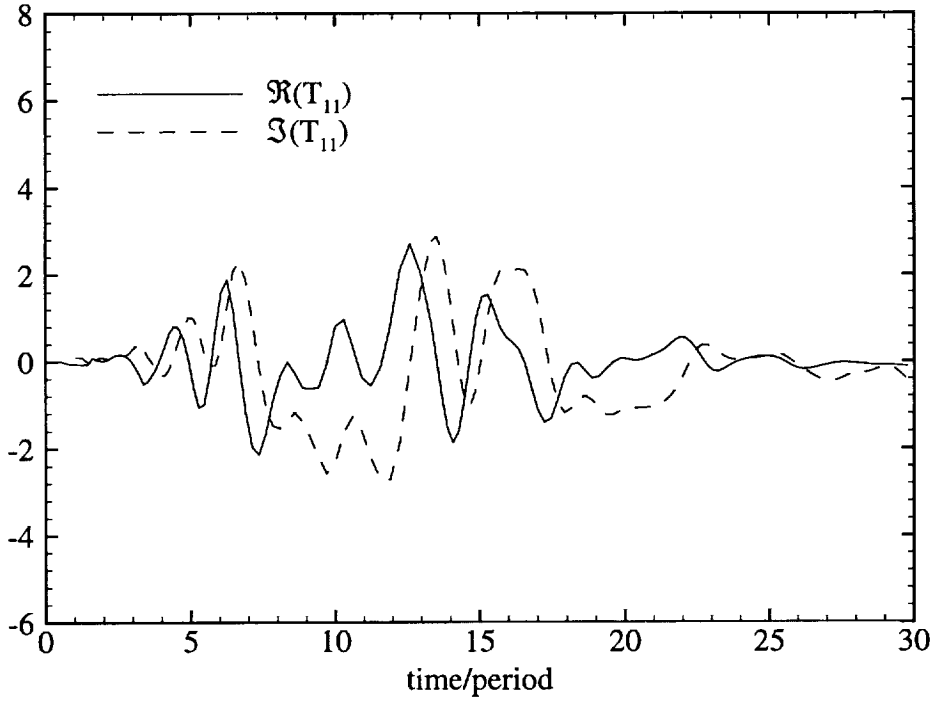

Figure 4.8. Computed streamwise variations of $\widehat{T}_{11}$ at $y = 0$. $St = 0.250$.

The two dimensional frequency domain version of the modified Kirchhoff method, equation (3.20), was used to calculate near–field and mid–field the noise produced by this jet. Experience has shown that the two dimensional modified Kirchhoff formulation is sensitive to the accuracy of the surface normal derivatives.

No means of increasing the accuracy of these calculations was available, so acoustics predictions suffer somewhat from derivatives which are calculated in regions where the CFD mesh is more coarse. The enrichment procedure discussed in previous chapters was programmed into the two dimensional code to help alleviate this problem somewhat. Additionally, since the jet was not numerically excited, the data used on the Kirchhoff surface is not completely periodic in nature. This periodicity is an implicit assumption in the development of the frequency domain formulations of the Kirchhoff integrals. So, while the CFD data is not periodic, the Kirchhoff predictions are, resulting in a lack of correlation. These caveats aside, the jet simulation data can be used to demonstrate the usefulness of Kirchhoff method for the prediction of jet noise in cases where a two dimensional simulation is appropriate.

Figure 4.9 shows calculated acoustic signals at $(x, y) = (28.57\,h, 6.56\,h)$, while figure 4.10 shows signals at $(x, y) = (14.43\,h, -4.14\,h)$. The temporal signal produced by the first two Fourier modes of the CFD prediction data is also shown for comparison. Only the first and second Fourier wave modes were used in the Kirchhoff predictions. Use of higher order modes produced oscillations in the calculated signals. These oscillations can be explained by the requirement of ~ 20 points per wavelength on the surface, as was determined in Chapter 2. In these calculations, there are approximately 24 quadrature points per wavelength of the first mode on the Kirchhoff surface. For the second mode, the number drops to 12 points per wavelength. For higher modes, with shorter wavelengths, there are not enough quadrature points to adequately resolve the integrands in the Kirchhoff integral.

These figures show the ability of the modified Kirchhoff method to determine, at least in a qualitative sense, the near–field and mid–field acoustics due to a two

dimensional planar jet.

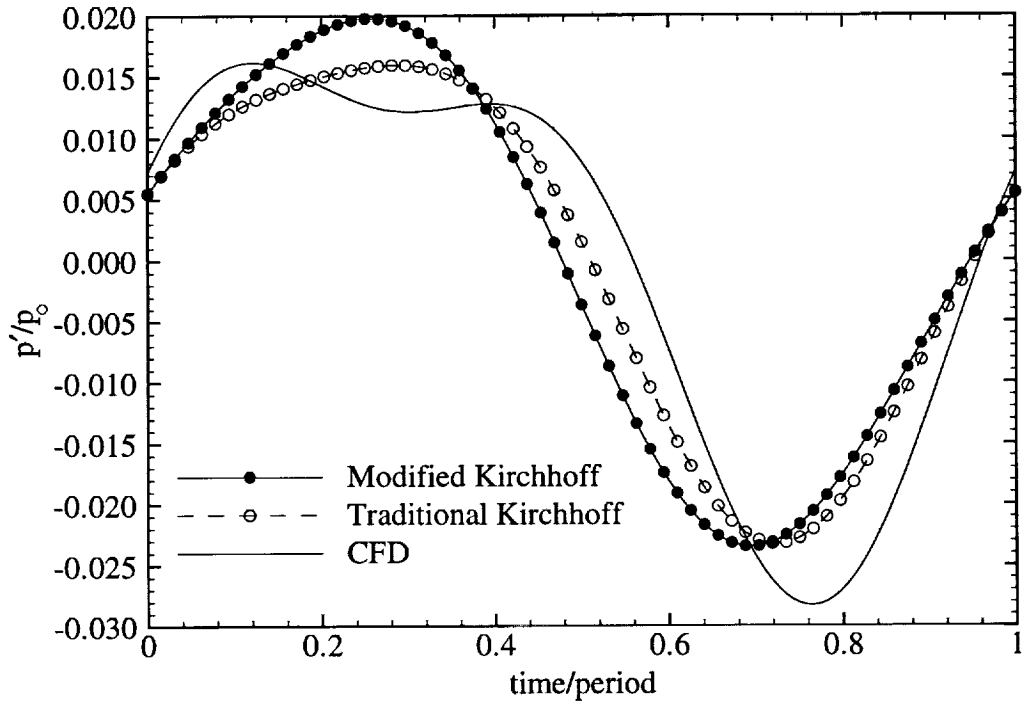

Figure 4.9. Temporal acoustic signatures from the Kirchhoff methods and CFD calculation, at $(x, y) = (28.57\,h, 6.56\,h)$.

The signals calculated with the CFD code are not periodic, while those of the Kirchhoff method are. Also, the signals generated with the Kirchhoff method have zero mean pressure disturbance, while those from the CFD calculations do not. This is due to the nature of the Hankel functions in the 2D modified Kirchhoff formulation. The Hankel function with zero argument (i.e. $k = 0$) is singular, so an asymptotic approximation should be used. However, in these calculations, $H^{(2)}(0)$ is set to zero. A comparison of the signals generated with the first two Fourier modes of the CFD prediction, and the full CFD prediction (shifted to zero mean

pressure disturbance) at $(x, y) = (28.57\,h, 6.56\,h)$ is shown in figure 4.11.

The modified Kirchhoff method seems to do a better job of matching the prediction from the CFD codes, at least at these observer points. The traditional Kirchhoff calculations used an open Kirchhoff surface, again because that formulation is not valid otherwise.

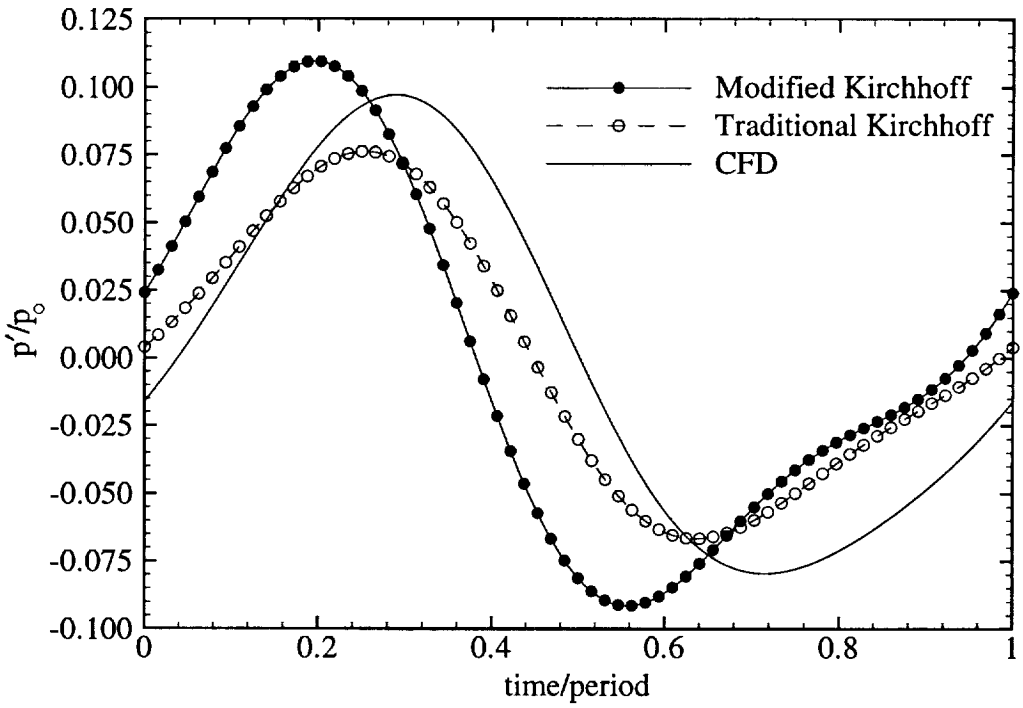

Figure 4.10. Temporal acoustic signatures from the Kirchhoff methods and CFD calculation, at $(x, y) = (14.43\,h, -4.14\,h)$.

Figures 4.12 and 4.13 show contours of $\hat{p}/p_\circ$ in the acoustic near–field and mid–field due to the jet. Figure 4.12 shows contours at the first Fourier Mode, $St = 0.125$, while figure 4.13 has contours at $St = 0.250$. The contours were calculated with the traditional Kirchhoff method and an open control surface. The

form of outward propagating waves is apparent, but there is no means, other than the results presented in the previous two figures, of determining if these waves represent any physical reality.

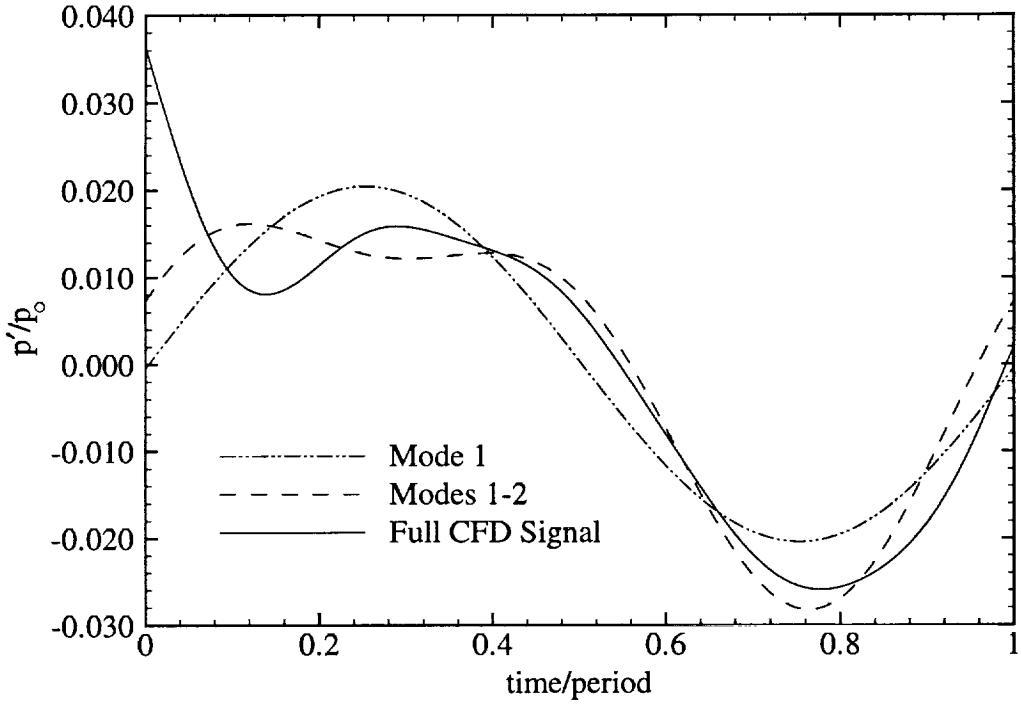

Figure 4.11. Comparison of CFD–generated Fourier modes at $(x, y) = (28.57\,h, 6.56\,h)$.

The same contour plots are presented again in figures 4.14 and 4.15. However, in this case the modified Kirchhoff method was used to generate the acoustic signals. The wave forms appear to be more sharply defined in this case, but the general trend shown by the traditional method contours holds here as well. Note that the null field expected inside the Kirchhoff surface is not calculated as it should be. This is most likely caused by the mesh spacing used to calculate $\partial\hat{p}/\partial n$ on the Kirchhoff

surface.

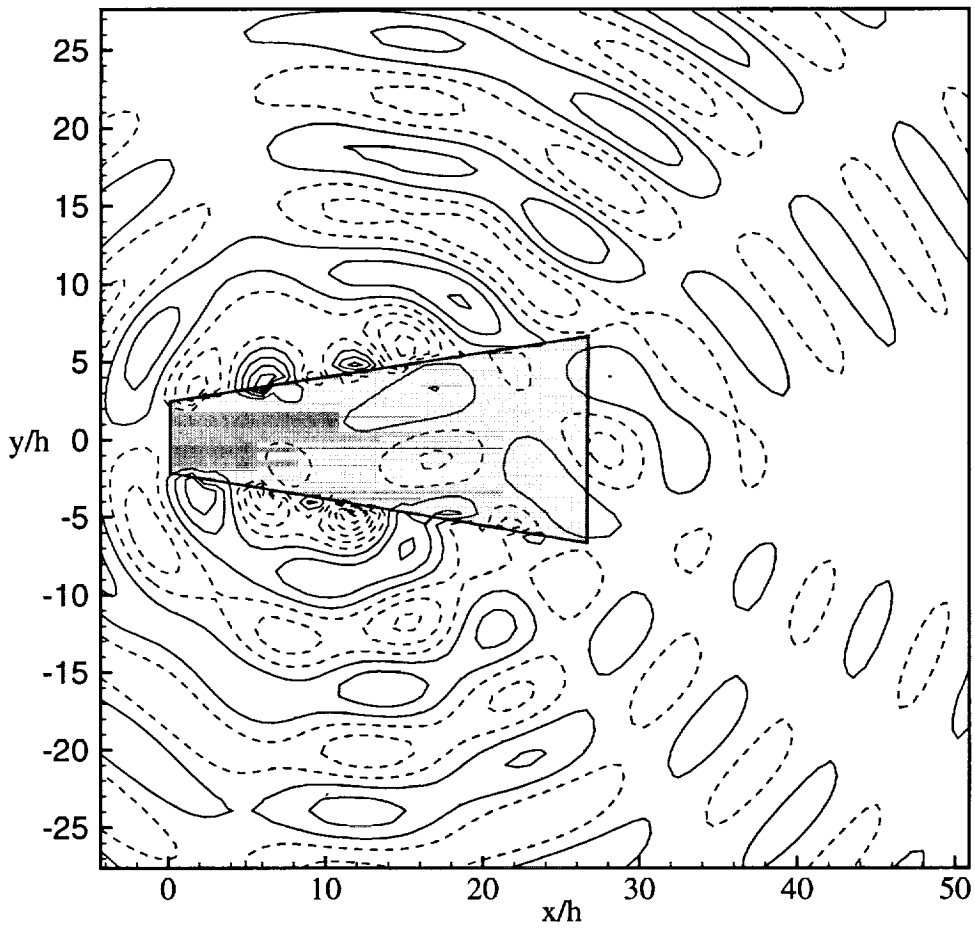

Figure 4.12. Contours of $\widehat{p}/p_o$ (Real part) calculated with the traditional Kirchhoff method. First Fourier mode, $St = 0.125$. Contours: min $= -3.00$, max $= 3.00$, increment $= 0.40$. Negative contours are dashed. The Kirchhoff surface is shaded.

The effects of grid spacing on the Kirchhoff predictions were investigated further by calculating the acoustic field of a point acoustic source placed inside a Kirchhoff surface identical to that used in the calculations presented above. The source was place at $(x, y) = (11.14\,h, 0.0)$. The relative error, as a function of Δx,

the mesh spacing used in the derivative calculations, is shown in figure 4.16. At this observer location, $(x, y) = (11.14\,h, 6.63\,h)$, with the mesh spacing used in the CFD calculations, the relative error is $\sim 0.20\%$. (This point is indicated in the figure with an arrow.)

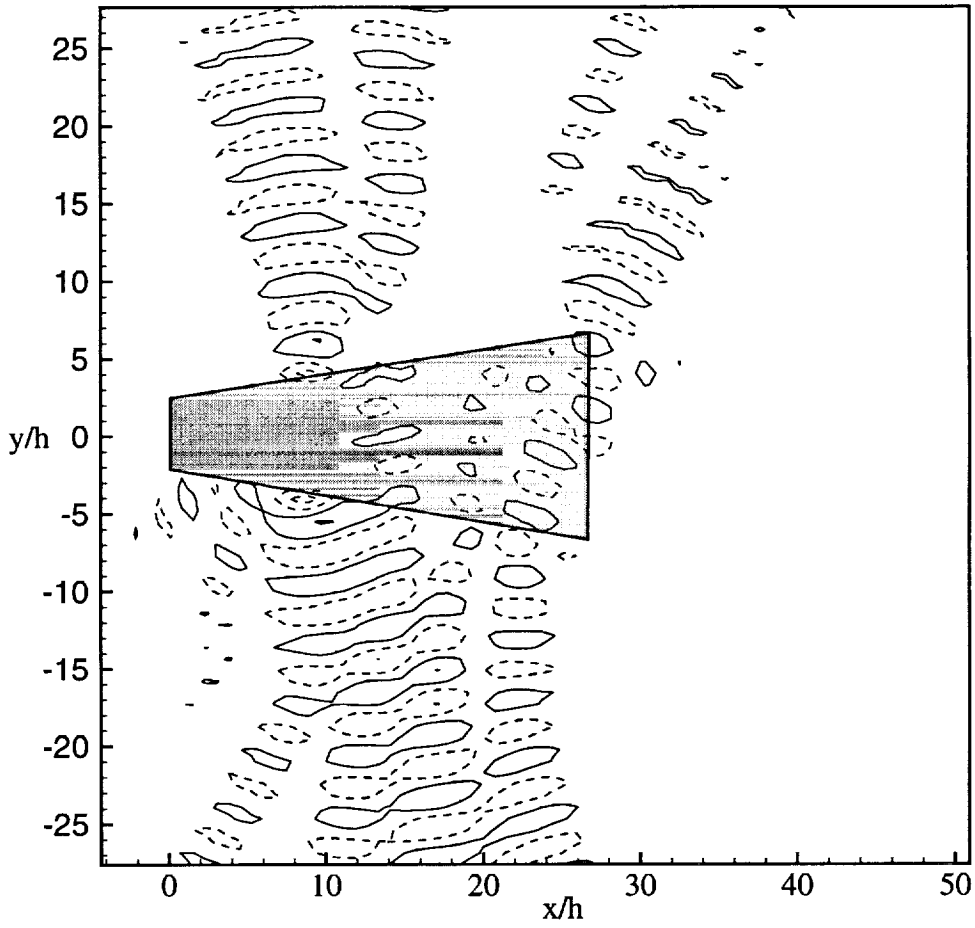

Figure 4.13. Contours of $\widehat{p}/p_o$ (Real part) calculated with the traditional Kirchhoff method. Second Fourier mode, $St = 0.250$. Contours: min $= -3.00$, max $= 3.00$, increment $= 0.40$. Negative contours are dashed. The Kirchhoff surface is shaded.

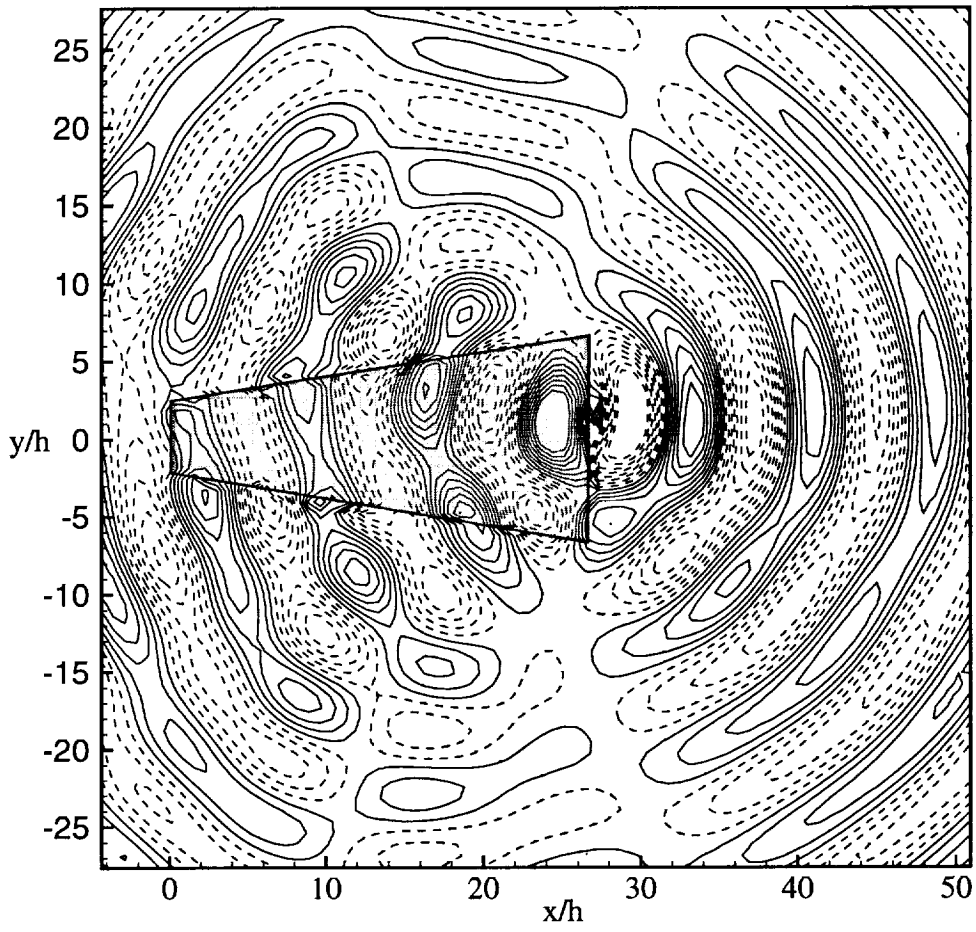

Figure 4.14. Contours of $\widehat{p}/p_o$ (Real part) calculated with the modified Kirchhoff method. First Fourier mode, $St = 0.125$. Contours: min $= -3.00$, max $= 3.00$, increment $= 0.40$. Negative contours are dashed. The Kirchhoff surface is shaded.

The effects of the error caused by coarse mesh spacing are shown in figure 4.17. This figure shows contours of the real part of the predicted monopole signal. The Kirchhoff surface and mesh spacing used were identical to those used in the CFD calculations shown earlier. The signals show many characteristics similar to those generated with the CFD calculations. The expected null field inside the Kirchhoff

surface is not obtained, and there are many nodes and anti–nodes in the acoustic field. When a very fine spacing was used to calculate the derivatives on this same surface, the predictions were very nearly exact. So, the errors presented here, and in the previous figures, are due to the coarse mesh used in the CFD calculations. Use of a very fine mesh in the CFD calculations should alleviate most of this error.

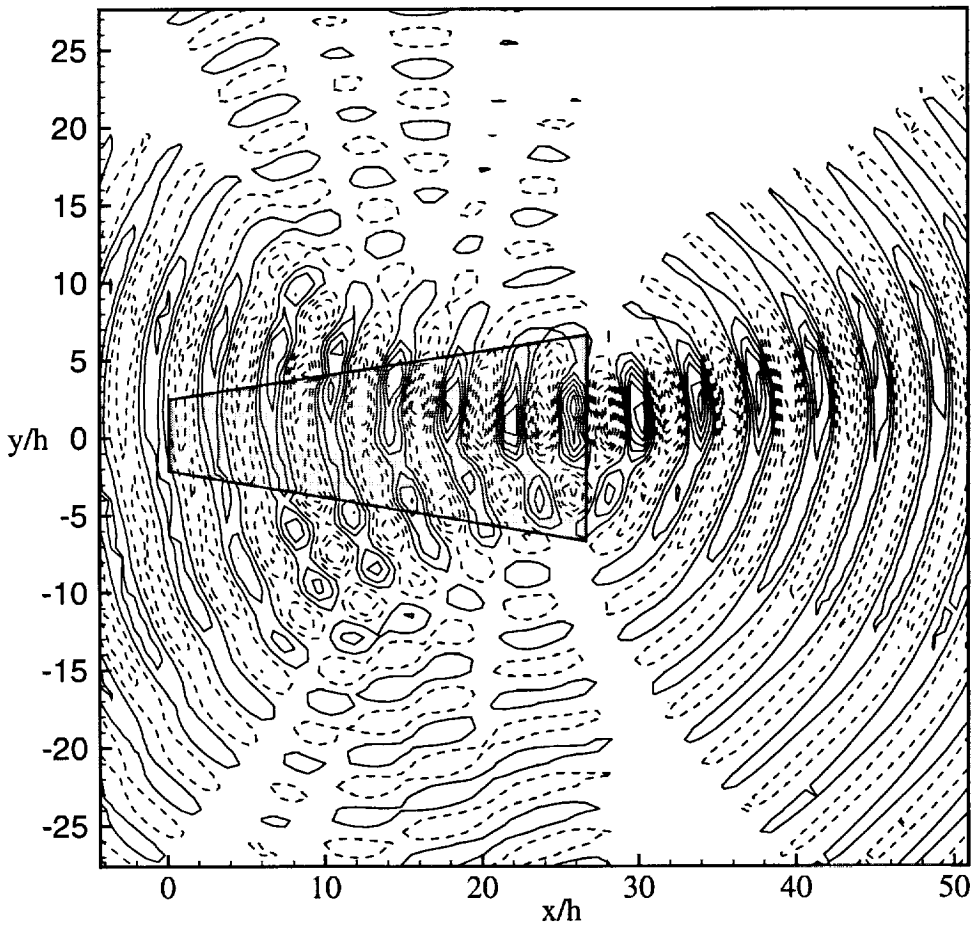

Figure 4.15. Contours of $\widehat{p}/p_o$ (Real part) calculated with the modified Kirchhoff method. Second Fourier mode, $St = 0.250$. Contours: min $= -3.00$, max $= 3.00$, increment $= 0.40$. Negative contours are dashed. The Kirchhoff surface is shaded.

More research into the effects of mesh spacing and quadrature implementation in the two dimensional Kirchhoff formulations is required before they can be used with confidence in jet noise predictions. The physical conditions used as a basis for the CFD calculations are inherently three dimensional, so the best future course of action may be to develop accurate 3D CFD calculations, and use the 3D Kirchhoff formulations. Some of the results of this section were presented by the authors in reference 35.

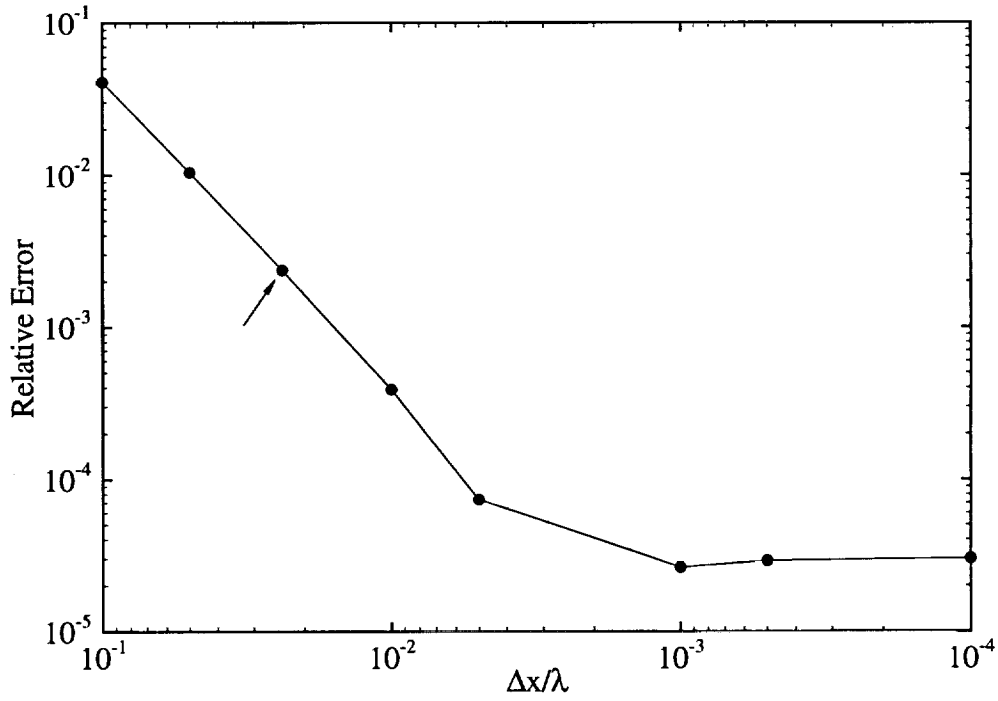

Figure 4.16. Relative Error, $|\widehat{\phi} - \widehat{\phi}_{exact}|/\widehat{\phi}_{exact}$, verses mesh spacing. $M = 0.0$.

The results presented in this chapter show that surface integral methods, the Kirchhoff method and Ffowcs Williams–Hawkings based methods, can be used in the prediction of jet noise. The modifications presented in the previous chapter

are necessary for these formulations to be valid. Accurate Kirchhoff surface data (e.g. from CFD/CAA calculations) is essential for valid predictions.

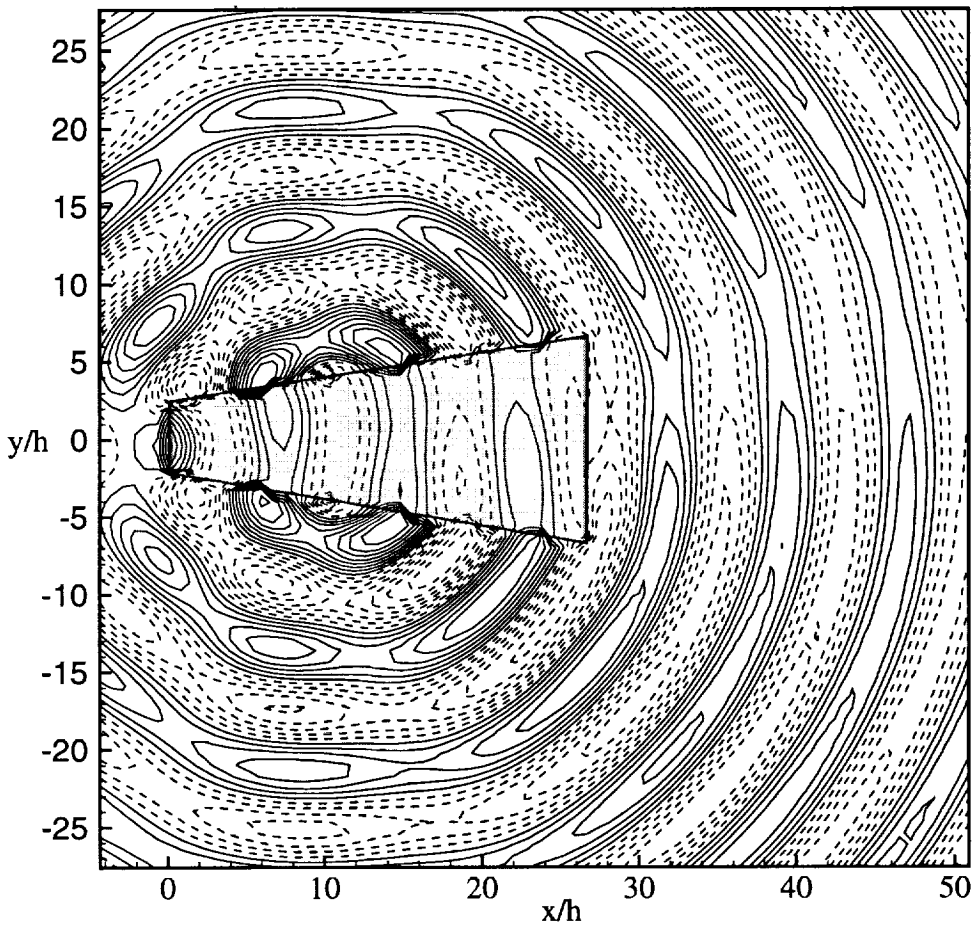

Figure 4.17. Real part of predicted 2D acoustic monopole field, $\Re(\widehat{\phi}/A)$. Contours: min $= -0.010$, max $= 0.010$, increment $= 0.0133$. Negative contours are dashed. $M = 0.00$.

Chapter 5

Refraction Corrections

As discussed in earlier chapters, the Kirchhoff method has been used successfully in the prediction of jet noise by several researchers recently.[29,30,34,35,61,64] Shih, et. al.[34] showed that the Kirchhoff method can predict results nearly identical to those obtained with a direct calculation method, with a substantial savings in CPU time. However, there are some difficulties involved with using the Kirchhoff method, and related methods, for jet aeroacoustic problems. For an accurate prediction, the Kirchhoff control surface must completely enclose the aerodynamic source region. This is often difficult or impossible to accomplish with the source regions found in jet acoustics problems. The validity of predictions is also dependent on the control surface being placed in a region where the linear wave equation is valid. Difficulties meeting this criterion frequently arise in jet acoustics studies. Additionally, the existence of a steady mean flow outside the Kirchhoff surface will cause refraction of the propagating sound. Failure to account for this refraction will also lead to errors when the observer location is near the jet axis.

This chapter outlines the preliminary development of corrections to the modified Kirchhoff method to account for the difficulties caused by mean flow refraction. The corrections are based on geometric acoustics principles, with the steady mean flow approximated as an axisymmetric parallel shear flow. Sample calculations are presented which show the corrections to predict a "zone of silence" in qualitative agreement with experimental observations. These developments were presented by the authors in reference 65.

5.1 Refraction Effects

The Kirchhoff formulas presented in (2.27) and (3.17) can efficiently and accurately predict aerodynamically generated noise, as long as the Kirchhoff surface surrounds the entire source region. In jet noise predictions, however, it is usually impossible, with current numerical methods, to determine the entire near–field source region. This is due to time and memory limitations imposed by the computer architecture, as well as dispersion and dissipation constraints. Thus, a significant nonlinear source region, as well as a steady mean flow, will exist outside of the Kirchhoff surface. The jet flow field and Kirchhoff surface for a circular jet are depicted in figure 5.1.

The large extent of the source region described above can be seen in axisymmetric jet numerical data discussed in the previous chapter. It is evident from figures 4.1 and 4.2 that the disturbance amplitude is quite large at the end of the computational domain. Thus, some approximation of the sources in the region downstream of the Kirchhoff surface is necessary. One possible approximations was presented by the authors in chapter 3. In this chapter, the emphasis will be on the refraction

caused by the steady mean flow, so any nonlinear sources outside the Kirchhoff surface will be ignored. In the future, the nonlinear source approximations should be included along with the refraction corrections derived here.

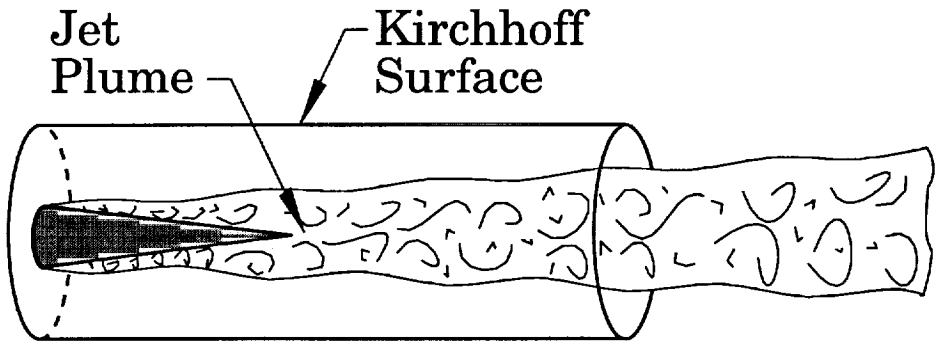

Figure 5.1. Jet flow and Kirchhoff surface.

Even if the unsteady sound sources outside of the Kirchhoff surface can be ignored, there is still a substantial steady mean flow in the region near the jet axis, downstream of the Kirchhoff surface. Figure 5.2 shows the decay of averaged axial velocity along the jet axis. At the downstream end of the Kirchhoff surface the mean axial velocity is still over 98% of the jet exit value. The linear wave equation (2.1) is not valid for acoustic propagation through the region near the jet axis, downstream of the Kirchhoff surface. Thus, some means of approximating the effects of this steady flow are required if an acoustic prediction is desired for observer points lying near the jet axis.

5.2 Flow Approximation and Effects

A suitable approximation to the downstream flow is necessary, in order to determine the refraction effects. In the past, several researchers have used an axisymmetric parallel shear flow model to determine sound produced by point acoustic

sources within circular jets.[66–69] This approach is adopted here as well. A real jet has non–zero radial velocity, but the refracting effect of this component is minimal, and can safely be ignored. The numerical simulations used to determine the near–field source terms on the Kirchhoff surface are axisymmetric in nature, so the lack of azimuthal variation in the parallel shear flow approximation will not have an effect here. The value of the axial velocity to be used in the shear flow approximation can be taken directly from the near–field numerical simulation, at the downstream end of the Kirchhoff surface, as an average of the time dependent axial velocity at each radial grid point.

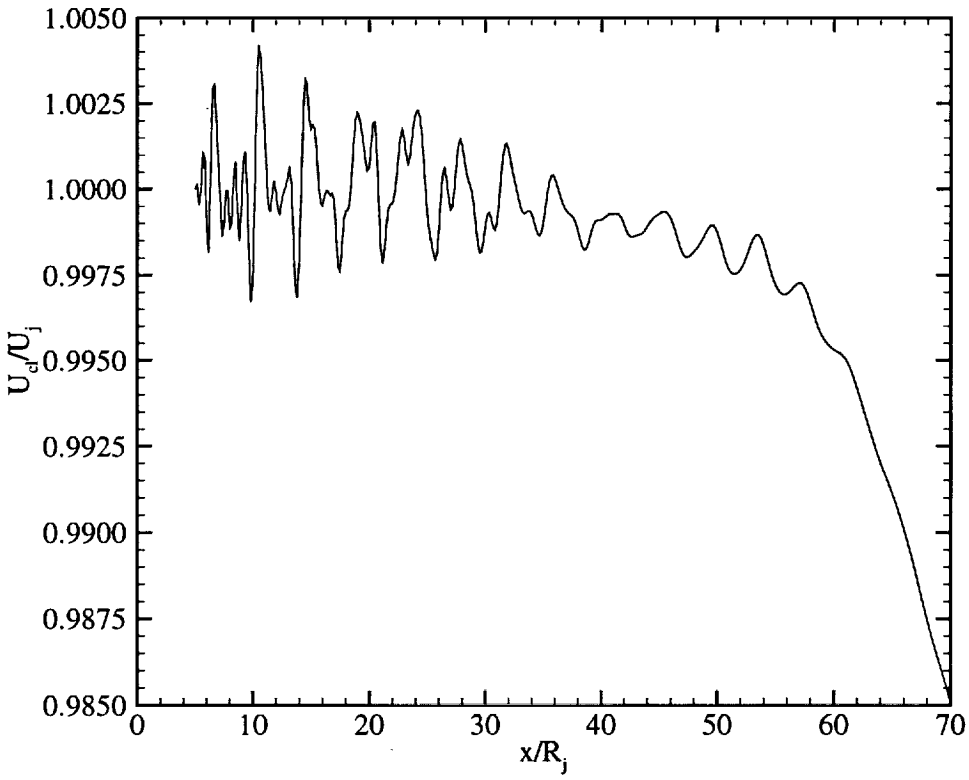

Figure 5.2. Decay of averaged centerline axial velocity.

The refraction problem now consists of a collection of point acoustic sources (the integrands of (2.27) or (3.17)) acting at radial location R, scaled by differential area $\Delta S = R\Delta R\Delta\varphi$, (where φ is the azimuthal angle), and the parallel shear flow with U determined at each R. If the acoustic wavelength, $\lambda = 2\pi a_o/\omega$, is assumed to be small compared to the shear layer thickness δ, then geometric acoustics principles hold.

If the steady velocity at the downstream end of the Kirchhoff surface is denoted U_s, the sound emission angle with respect to the jet axis ϑ_s, and the emission angle in the stagnant, ambient air is denoted ϑ_o, then the axial acoustic phase speeds are preserved by the stratified flow, i.e.[68]

$$\frac{a_o}{\cos\vartheta_o} = U_s + \frac{a_o}{\cos\vartheta_s} \tag{5.1}$$

Here it is assumed that the speed of sound at the source is equivalent to that in the ambient air. This equation can be rearranged to show that there is a critical angle, ϑ_c defined by

$$\vartheta_c = \cos^{-1}\left(\frac{1}{1+M_s}\right) \tag{5.2}$$

If the the observer angle ϑ_o is greater than ϑ_c than no sound emitted at the source on the Kirchhoff surface can reach the observer. This criterion is easily added to the stationary surface Kirchhoff program. (Note that M_s is the Mach number of the mean shear flow, and not the Kirchhoff surface, which is assumed stationary.)

An additional correction is necessary to accurately account for the mean flow refraction. Imposing the local "zone of silence" condition described above can allow a surface source at a relatively large radial location to radiate sound into and through the shear flow. This is because the local "zone of silence" decreases in size with the radial location of the source, because of the decrease in source Mach number.

The simple correction is to set the source strength to zero if the observation point is located closer to the jet axis than the source point on the Kirchhoff surface,

$$\Delta S = \begin{cases} R\Delta R\Delta\varphi & R_o \geq R_s \\ 0 & R_o < R_s \end{cases} \tag{5.3}$$

It should be noted that the azimuthal variation between the source and observer points has been ignored in the analysis presented here. The azimuthal variation should have some effect, but it is most likely secondary to those effects described above. (Though the near–field CFD calculations are axisymmetric, the Kirchhoff surface is a full three dimensional cylinder, so discrepancies between source and observer azimuthal location can exist.) Also, the geometric acoustics approximation is only valid for $\delta/\lambda > 1$. It is assumed here that the downstream end of the cylindrical Kirchhoff surface is located far enough downstream of the jet potential core that the shear layer thickness is large compared with the acoustic wavelength. Regardless, Morfey and Szewczyk[68] have shown that jet mixing noise can be effectively modeled with geometric acoustics principles even when $\delta/\lambda < 1$.

5.3 Sample Validation Calculation

As an initial test of the refraction corrections for the Kirchhoff method, a simple acoustic monopole was placed inside a cylindrical Kirchhoff control surface. The monopole was located at $(x, R) = (5\,\lambda, 0)$. The cylindrical Kirchhoff surface had dimensions $(L_k, R_k) = (10\,\lambda, 1.5\,\lambda)$. The surface was discretized with 130, 40 and 90 quadrature points, in the axial radial and azimuthal directions respectively. The value of the Kirchhoff integrands was determined analytically on the Kirchhoff surface at each quadrature point. For comparison, the radiated sound field was first

calculated in the absence of a mean shear flow. Then, a parallel shear flow was imposed in the region downstream of the Kirchhoff surface. The flow velocity was governed by

$$U_s(R) = M_s a_o \exp\left[-\left(R^2/b^2\right)\right]$$

where $M_s = 1.4$, and $b = 0.153\,\lambda$. This is not a realistic scenario, as the shear flow is created at the end of the Kirchhoff surface, and no refractive effects are included in the analytical determination of the Kirchhoff integrands, but it serves the purpose of demonstrating the nature of the proposed corrections.

Figure 5.3 shows instantaneous contours of ϕ calculated with the Kirchhoff method for the case described above. The contours shown above the centerline are those obtained with no refracting flow field, while those shown below the centerline were obtained with with refraction corrections described above. The effect of the parallel shear flow is seen in the region downstream of the Kirchhoff surface the propagating sound waves are bent away from the centerline by the imposed shear flow. This causes a "zone of silence" near the centerline. Note that a null sound field is calculated inside the Kirchhoff surface in both cases. As discussed in earlier chapters, this is a result of the outgoing radiation condition imposed by the Green's function solution of the wave equation, and serves as a validation of the numerical implementation of the Kirchhoff algorithm.

5.4 Jet Noise Calculation

The axisymmetric near–field jet CFD calculations discussed above and in the previous chapter were used to determine the integrands in the Kirchhoff integral formula, and also to predict the parallel shear flow downstream of the Kirchhoff

surface. The surface was chosen to match lines in the mesh, and was identical to that discussed in the previous chapter.

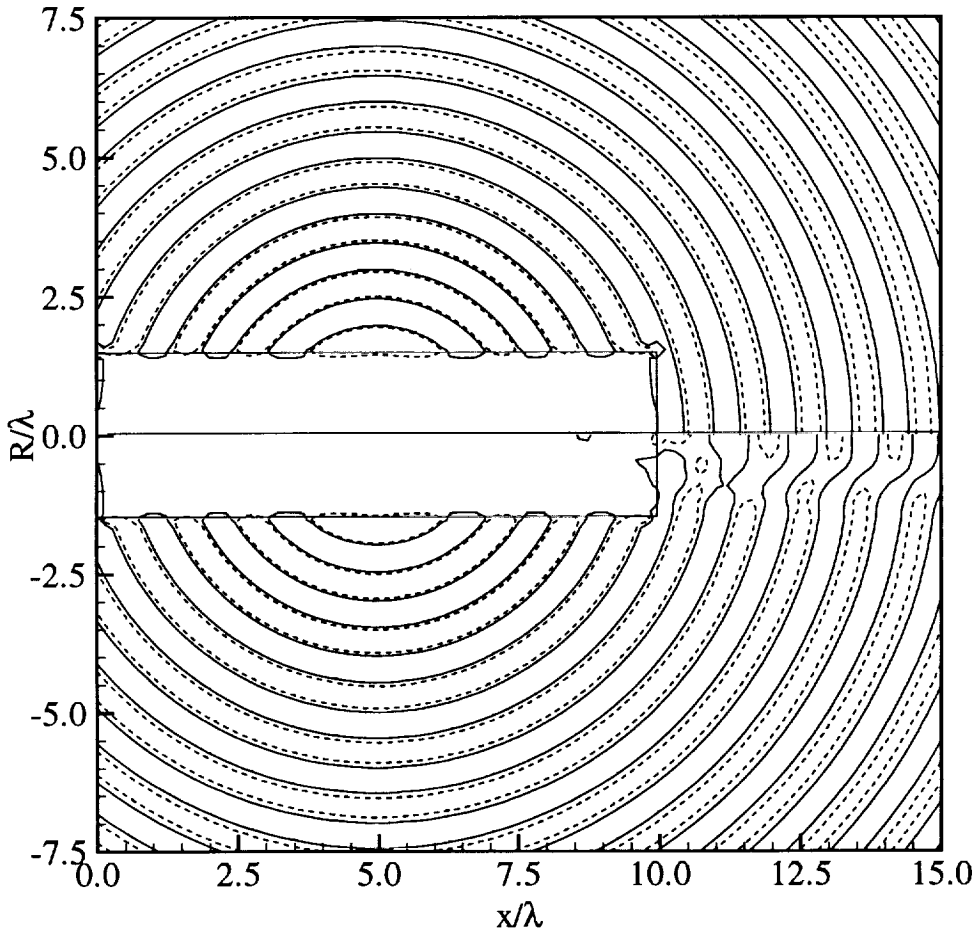

Figure 5.3. Instantaneous contours of ϕ. $R > 0$: No shear flow. $R < 0$: Shear flow imposed at Kirchhoff surface.

The effect of the refraction corrections on this jet noise prediction is shown in figure 5.4. The figure shows instantaneous contours of $a_\circ^2 \rho'/p_\circ$ on a plane passing through the jet axis, calculated with the modified Kirchhoff method and the

numerical data described above. The contours shown above the jet axis are those obtained when the mean flow refraction effects were ignored. The contours shown below the jet axis were calculated in an identical fashion, except that the effects of mean flow refraction were included in sound generated at the downstream end of the Kirchhoff surface.

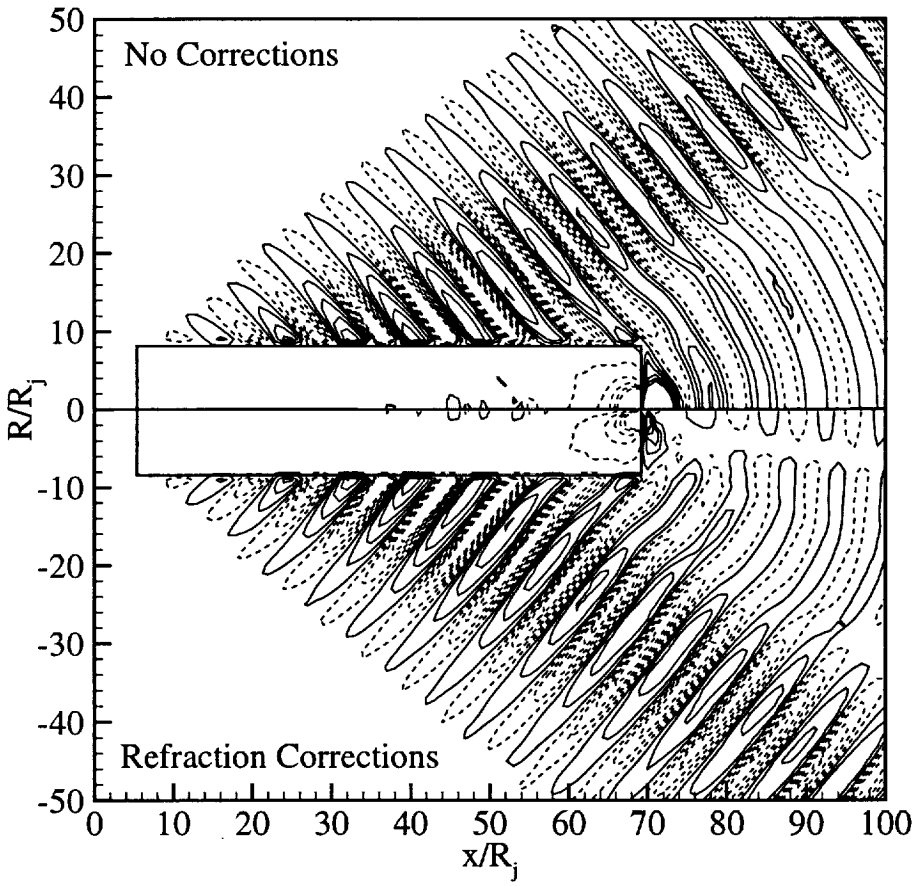

Figure 5.4. Instantaneous contours of $a_o^2\rho'/p_o$. $R > 0$: No refraction corrections. $R < 0$: Refraction corrections imposed.

Both calculations capture the Mach wave radiation in the region $R > 10\,R_j$ identically. The steady mean flow has little effect on the radiation in this region. Downstream of the Kirchhoff surface, the sound waves appear to propagate away spherically from an equivalent source located near $x \approx 30\,R_j$. In the prediction without refraction correction, the sound waves have large amplitude near the end of the Kirchhoff surface, and propagate as through a uniform stationary medium. The corrections, however, reduce the amplitude in the region near the jet axis, and adjust the phase of each disturbance. The corrected sound waves propagate away from the axis at a modest angle. This creates a "zone of silence" near the axis, similar in nature to those observed experimentally. The zone of silence is also evident in figure 5.5, which shows sound pressure level contours in the near and mid acoustic fields. The reduction in amplitude near the jet axis caused by the refraction corrections is again evident. Also noteworthy is the prediction of sound inside the Kirchhoff surface. As discussed earlier, a null acoustic field should be calculated inside the surface. The sound field inside the surface shown here is a result of several factors. Among these factors are numerical roundoff errors, and the interpolation routine used by the graphics program. Also, the upstream end of the Kirchhoff surface was left open in the predictions.

In the past, researchers utilizing Kirchhoff methods to predict jet noise have ignored sound generated at and outside of the downstream end of the Kirchhoff surface.[29,30,64] If the observer lies in an area in which a majority of the sound is predicted by the constant radius portion of the Kirchhoff surface, then this omission may not pose a problem. However, the authors have shown that "open surface" Kirchhoff methods are not acceptable for jet acoustics predictions when the observer is in the region downstream of the Kirchhoff surface. The refraction corrections

presented here can aid in the accurate prediction of sound in this region. While these corrections are crude, and most likely overly simplified, they do represent a first step towards efficient, accurate determination of acoustic propagation at and near a jet axis. Further development of the corrections is required. Emphasis should be focused on inclusion of azimuthal and amplitude variations in the refraction effects.

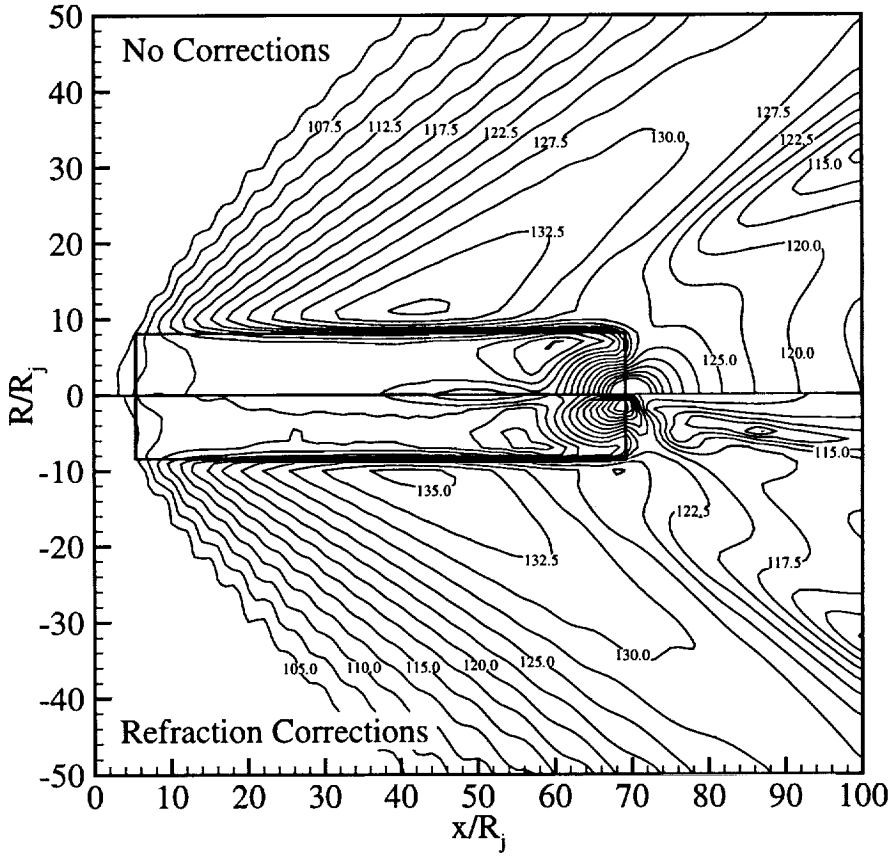

Figure 5.5. Sound Pressure Level contours (Re: 2×10^{-5} Pa). $R > 0$: No refraction corrections. $R < 0$: Refraction corrections imposed.

Chapter 6

Concluding Remarks

This report is concerned with the development of improvements to the Kirchhoff method and Ffowcs Williams–Hawkings methods used in computational aeroacoustics. This chapter briefly summarizes the main results and developments of this work, and presents some recommendations for future related research.

6.1 Conclusions of This Work

Aerodynamically generated noise is now and will continue to be a source of annoyance for the general public. Thus, efficient and accurate means of predicting this noise are required. Direct calculation of aerodynamic sound through the use of a CFD like algorithm is possible. But, the requirements imposed by dissipation and dispersion errors, as well as limitations on computer time and memory, make this an impractical method for the calculation of mid–field and far–field sound. It is usually necessary to separate the noise generation problem into two parts, one in

which the noise sources are calculated, and another in which the sound propagation to the mid–field and far–field is determined.

This separation of the aerodynamic noise generation problem is the basis of Lighthill's acoustic analogy.[10] In the acoustic analogy, sound sources are determined through a CFD or empirical process. Then, a volume integral is numerically solved to determine the mid–field and far–field sound. If the source region is non–compact, as in most important problems, this volume integration leads to prohibitive computation times and memory requirements.

An alternative to the burden of the volume integrations in the acoustic analogy can be found in the Kirchhoff method.[19,26] In the Kirchhoff method, a control surface surrounds all noise sources. Through the use of Green's theorem, a surface integral over this surface can be used to determine the acoustics at any point outside the surface. The reduction in dimension from a volume integral to surface integral represents a tremendous savings in required computer time and memory. The Kirchhoff method has been used successfully in the prediction of noise from helicopter rotors, turbomachinery and other aerodynamic problems where the source region is relatively small, and easily contained within the Kirchhoff surface.[28]

However, the noise generated by jet flows is a very important exception. These flows generally have very extensive source regions. As shown in chapter 4, these source regions usually extend beyond the extent of the numerical domain used in near–field CFD calculations. In this case, the Kirchhoff surface is not able to enclose all sound sources. This leaves Kirchhoff predictions invalid in some portions of the acoustic field. However, the open–surface Kirchhoff methodology has been successfully used jet noise calculations.[28,30] It is desirable to develop a Kirchhoff

integral that is valid over all portions of the acoustic field. Development of this integral, valid in the entire acoustic field, is the main goal of this work.

Several important points concerning this integral, and associated developments are presented in this report. There are listed here again for clarity:

1. *Equivalence of FWH and Kirchhoff Formulations*:

In Chapter 2, the Ffowcs Williams–Hawkings equation[18] and the Kirchhoff integral equation[27] were rigorously shown to be equivalent to one another, under certain conditions. In fact, the Ffowcs Williams–Hawkings equation is a special case of Kirchhoff's formula. That case being for an inhomogeneous (Lighthill's) wave equation, with the density perturbation as the wave variable. This fact was noted by Ffowcs Williams and Hawkings,[18] and Farassat,[36] but was not shown.

1.1 *Noise Generation by Porous Surfaces*:

The developments of Ffowcs Williams and Hawkings,[18] and subsequent applications of Farassat[24] and others assume the noise generating surface is solid, and impermeable. This assumption is mathematically equivalent to placing a Kirchhoff control surface such that it surrounds all sound sources. As, discussed above, this is often not possible in jet noise studies. Blowing and suction on an airfoil blade will also alter the noise generation. For these reasons, porous surface versions of the Kirchhoff integral equation and the Ffowcs Williams–Hawkings equation were developed, and shown to be equivalent. These versions became what is referred to as the modified Kirchhoff method.

2. *Development of Useful Algorithm Extensions*:

The porous surface versions of the Kirchhoff integral and Ffowcs Williams–Hawkings equation discussed above were expressed in such a way as to make them

easily applicable in existing aeroacoustic prediction codes. In the development of the modified Kirchhoff method, the E_1, E_2... nomenclature of Farassat and Myers[27] was adopted. Thus, a computer program currently based on the Farassat and Myers formulation of the Kirchhoff integral can easily by extended to the modified Kirchhoff integral with the use of $p' = a_o^2\rho'$ as the dependent variable, and the addition of a volume integral. The similarities between the two formulations allow for the development of a versatile code which can predict aerodynamically generated noise using the most appropriate algorithm (Kirchhoff or Ffowcs Williams–Hawkings) for the problem at hand.

2.1 *Volume Integral Equivalent and Approximation*:

The integrand of the volume integral which appears in the modified Kirchhoff formulation, the Ffowcs Williams–Hawkings formulations, and the solution of Lighthill's equation is written in a new, equivalent form. This form allows for more accurate numerical determination of the integral solution. It also facilitates the approximate integral solutions presented in chapter 3.

2.2 *Frequency Domain and 2D Developments*:

The traditional and modified Kirchhoff methods were presented in the frequency domain and for two dimensional aeroacoustics problems. The traditional Kirchhoff method has been used in these cases previously, but all the formulations have not yet been presented together in one work, as is done here.

2.3 *Refraction Corrections*:

Simplified refraction corrections, for use in jet noise studies, were developed. These corrections can be used to improve jet noise calculations in the region near the jet axis.

Based on these developments, the modified Kirchhoff method has potential to become a popular and valuable tool for aeroacoustic analysis.

6.2 Recommendations for Future Work

Development of the integral methods presented in this work is ongoing. This work will continue as long as surface integral methods are used in aerodynamic noise prediction. Some particular areas on interest for work in the near future are discussed next.

The refraction corrections developed in chapter 5 are preliminary and simplified. The corrections should be extended to account for azimuthal variations, and non–parallel flow effects.

The volume integral approximations presented in chapter 3 are crude and very simplified. Development of new approximations, which are more universally applicable, should be a priority in any extensions of this work. Work on these extensions should be performed in conjunction with the refraction corrections as well.

Bibliography

[1] Hardin, J.C., and Hussaini, M.Y., eds., *Computational Aeroacoustics*, Springer–Verlag, New York, 1993.

[2] Reynolds, W.C., "The Potential and Limitations of Direct and Large Eddy Simulations," in *Whether Turbulence? or Turbulence at the Crossroads*, Cornell University, Ithaca, New York, March 21-24, 1989.

[3] Mankbadi, R.R., "The Self Noise from Ordered Structures in a Low Mach Number Jet, " *ASME Journal of Applied Mechanics*, Vol. 57, 1990, pp. 241-246.

[4] Tam, C.K.W., and Burton, D.E., "Sound Generated by Instability Waves of Supersonic Flows, Part 1. Two–Dimensional Mixing Layers," *Journal of Fluid Mechanics*, Vol. 138, 1984, pp. 249-271.

[5] Tam, C.K.W., and Burton, D.E., "Sound Generated by Instability Waves of Supersonic Flows, Part 2. Axisymmetric Jets," *Journal of Fluid Mechanics*, Vol. 138, 1984, pp. 273-295.

[6] Tam, C.K.W., "Jet Noise Generated by Large–Scale Coherent Motion," in

Aeroacoustics of Flight Vehicles: Theory and Practice, Volume 1: Noise Sources, H.H. Hubbard ed., NASA Reference Publication No. 1258, August 1991.

[7] Mankbadi, R.R., Hayder, M.E. and Povinelli, L.A., "Structure of Supersonic Jet Flow and Its Radiated Sound," *AIAA Journal*, Vol. 32, No. 5, May 1994, pp. 897-906.

[8] Mankbadi, R.R., Shih, S.H., Hixon, R. and Povinelli, L.A., "Direct Computation of Sound Radiation by Jet Flow Using Large–Scale Equations," AIAA Paper No. 95-0680, January 1995.

[9] Tam, C.K.W., and Webb, J.C., "Dispersion–Relation–Preserving Finite Difference Schemes for Computational Aeroacoustics," *Journal of Computational Physics*, Vol. 107, 1993, pp.262-283.

[10] Lighthill, M.J., "On Sound Generated Aerodynamically I. General Theory," *Proceedings of the Royal Society of London*, Vol. A211, 1952, pp. 564-587.

[11] Lighthill, M.J., "On Sound Generated Aerodynamically II. Turbulence as a Source of Sound," *Proceedings of the Royal Society of London*, Vol. A222, 1954, pp. 1-32.

[12] Phillips, O.M., "On the Generation of Sound by Supersonic Turbulent Shear Layers," *Journal of Fluid Mechanics*, Vol. 9, No. 1, September 1960, pp.1-28.

[13] Lilley, G.M., "On the Noise From Jets," *Noise Mechanisms*, AGARD–CP–131, March 1974, pp. 321-349.

[14] Ribner, H.S., "New Theory of Jet–Noise Generation, Directionality, and Spectra," *Journal of the Acoustical Society of America*, Vol. 31, No. 2, February 1959, pp. 245-246.

[15] Ribner, H.S., "Perspectives on Jet Noise," *AIAA Journal*, Vol. 19, No. 12, December 1981, pp. 1513-1526.

[16] Lilley, G.M., "Jet Noise Classical Theory and Experiments," in *Aeroacoustics of Flight Vehicles: Theory and Practice, Volume 1: Noise Sources*, H.H. Hubbard ed., NASA Reference Publication No. 1258, August 1991.

[17] Curle, N., "The Influence of Solid Boundaries Upon Aerodynamic Sound," *Proceedings of the Royal Society of London*, Vol. A231, 1955, pp. 505-514.

[18] Ffowcs Williams, J.E., and Hawkings, D.L., "Sound Generation by Turbulence and Surfaces in Arbitrary Motion," *Philosophical Transactions of the Royal Society of London*, Vol. 264A, May 1969, pp. 321-342.

[19] Kirchhoff, G.R. "Zur Theorie der Lichtstrahlen," *Annalen der Physik und Chemie*, Vol. 18, 1883, pp. 663-695.

[20] Morgans, W.R., "The Kirchhoff Formula Extended to a Moving Surface," *Philosophical Magazine*, Vol. 9, 1930, pp. 141-161.

[21] Khromov, V.A., "Generalization of Kirchhoff's Theorem for the Case of a Surface Moving in an Arbitrary Way," *Soviet Physics – Acoustics*, Vol. 9, 1963, pp. 68-71.

[22] Hawkings, D.L., "Comments on 'Extension of Kirchhoff's Formula to Radiation From Moving Surfaces,'" *Journal of Sound and Vibration*, Vol. 133, No. 1, 1989, pp. 189.

[23] Farassat, F., and Myers, M.K., "Authors' Reply to 'Comments on Extension of Kirchhoff's Formula to Radiation From Moving Surfaces,'" *Journal of Sound and Vibration*, Vol. 133, No. 1, 1989, pp. 190.

[24] Farassat, F., and Succi, G.P., "The Prediction of Helicopter Rotor Discrete Frequency Noise," *Vertica*, Vol. 7, No. 4, 1983, pp. 309-320.

[25] Brentner, K.S., "Prediction of Rotor Discrete Frequency Noise – A Computer Program Incorporating Realistic Blade Motions and Advanced Acoustic Formulation," NASA TM 87721, October 1986.

[26] Hawkings, D.L., "Noise Generation by Transonic Open Rotors," *Westland Research Paper No. 599*, 1979.

[27] Farassat, F., and Myers, M.K., "Extension of Kirchhoff's Formula to Radiation From Moving Surfaces," *Journal of Sound and Vibration*, Vol. 123, No. 3, 1988, pp. 451-460.

[28] Lyrintzis, A.S., "Review, The Use of Kirchhoff's Method in Computational Aeroacoustics," *ASME Journal of Fluids Engineering*, Vol. 116, December 1994, pp. 665-676.

[29] Lyrintzis, A.S., and Mankbadi, R.R., "Prediction of the Far–Field Jet Noise Using Kirchhoff's Formulation," *AIAA Journal*, Vol. 34, No. 2, Feb. 1996, pp. 413-416.

[30] Mitchell, B.E., Moin, P. and Lele, S.J., "Direct Computation of the Sound Generated by Vortex Pairing in an Axisymmetric Jet," AIAA Paper No. 95-0504, January 1995.

[31] Freund, J.B., Lele, S.K. and Moin, P., "Calculation of the Radiated Sound Field Using an Open Kirchhoff Surface," *AIAA Journal*, Vol. 34, No. 5, May 1996, pp. 909-916.

[32] Pilon, A.R., and Lyrintzis, A.S., "An Improved Kirchhoff Method for Jet Aeroacoustics," AIAA Paper No. 96-1709, May 1996. Submitted for review

to *AIAA Journal.*

[33] Pilon, A.R., and Lyrintzis, A.S., "Surface Integral Methods for Computational Aeroacoustics," AIAA Paper No. 97-0020, January 1997. Submitted for review to the *Journal of Sound and Vibration.*

[34] Shih, S.H., Mankbadi, R.R., Hixon, D.R., Pilon, A.R., and Lyrintzis, A.S., "Evaluation of Far–Field Jet Noise Prediction Methods," AIAA Paper No. 97-0282, January 1997.

[35] Scott, J.N., Pilon, A.R., Lyrintzis, A.S., and Rozmajzl, T.J., "A Numerical Investigation of Noise from a Rectangular Jet," AIAA Paper No. 97-0285, January 1997.

[36] Farassat, F., "Discontinuities in Aerodynamics and Aeroacoustics: The Concept and Applications of Generalized Derivatives," *Journal of Sound and Vibration*, Vol. 55, No. 2, 1977, pp. 165-193.

[37] Farassat, F., "Introduction to Generalized Functions With Applications in Aerodynamics and Aeroacoustics," NASA TP-3428, May 1994.

[38] Farassat, F., "The Kirchhoff Formulas for Moving Surfaces in Aeroacoustics – The Subsonic and Supersonic Cases," NASA TM-110285, September 1996.

[39] Haberman, R., *Elementary Applied Partial Differential Equations*, Prentice Hall, Englewood Cliffs, New Jersey, 1983.

[40] Abramowitz, M., and Stegun, I.A., *Handbook of Mathematical Functions*, Dover, New York, 1965.

[41] Morino, L., "Mathematical Foundations of Integral Methods," in *Computational Methods in Potential Aerodynamics*, L. Morino ed., Springer–Verlag,

New York, 1985.

[42] Pierce, A.D., *Acoustics: An Introduction to Its Physical Principles and Applications*, Acoustical Society of America, Woodbury, New York, 1994.

[43] Atassi, H.M., Dusey, M., and Davis, C.M., "Acoustic Radiation from a Thin Airfoil in Nonuniform Subsonic Flows," *AIAA Journal*, Vol. 31, No. 1, January 1993, pp. 12-19.

[44] Fang, J., and Atassi, H.M., "Direct Calculation of Sound Radiated from a Loaded Cascade in a Gust," in *Computational Aero- and Hydro-Acoustics*, R.R. Mankbadi, A.S. Lyrintzis, O. Baysal, L.A. Povinelli, M.Y. Hussaini eds., ASME FED Vol. 147, 1993, pp. 111-116.

[45] Patrick, S.M., Davis, C.M., and Atassi, H.M., "Acoustic Radiation from a Lifting Airfoil in Nonuniform Subsonic Flows," in *Computational Aero- and Hydro-Acoustics*, R.R. Mankbadi, A.S. Lyrintzis, O. Baysal, L.A. Povinelli, M.Y. Hussaini eds., ASME FED Vol. 147, 1993, pp. 41-46.

[46] Aris, R., *Vectors, Tensors and the Basic Equations of Fluid Mechanics*, Dover, New York, 1962.

[47] Farassat, F., and Myers, M.K., "The Kirchhoff Formula for a Supersonically Moving Surface," CEAS/AIAA Paper No. 95-062, May 1995.

[48] Myers, M.K., and Hausmann, J.S., "On The Application of the Kirchhoff Formula for Moving Surfaces," *Journal of Sound and Vibration*, Vol. 139, No. 1, 1990, pp. 174-178.

[49] Myers, M.K., and Hausmann, J.S., "Computation of Acoustic Scattering from a Moving Rigid Surface," *Journal of the Acoustical Society of America*, Vol. 91, No. 5, May 1992, pp. 2594-2605.

[50] Brentner, K.S. "Numerical Algorithms for Acoustic Integrals – the Devil is in the Details," AIAA Paper No. 96-1706, May 1996.

[51] Press, W.H., Teukolsky, S.A., Vetterling, W.T., and Flannery, B.P., *Numerical Recipes in Fortran: The Art of Scientific Computing*, Cambridge University Press, Cambridge, 1992.

[52] Meadows, K.R., and Atkins, H.L., "Towards a Highly Accurate Implementation of the Kirchhoff Approach for Computational Aeroacoustics," *Journal of Computational Acoustics*, Vol. 4, No. 2, June 1996.

[53] Crighton, D.G., Dowling, A.P., Ffowcs Williams, J.E., Heckl, M., and Leppington, F.G., *Modern Methods in Analytical Acoustics: Lecture Notes*, Springer–Verlag, London, 1992.

[54] di Francescantonio, P., "A New Kirchhoff Formulation for Transonic Rotor Noise," Presented at the 22nd European Rotorcraft Forum, Brighton, UK, Sept. 1996.

[55] Farassat, F., and Brentner, K.S., "The Uses and Abuses of the Acoustic Analogy in Helicopter Rotor Noise Prediction," *Journal of the American Helicopter Society*, Vol. 33, No. 1, 1988, pp. 29-36.

[56] Brentner, K.S. "An Efficient and Robust Method for Predicting Rotor High–Speed Impulsive Noise," AIAA Paper No. 96-0151, January 1996.

[57] Wu, X.-F., and Akay, A., "Sound Radiation from Vibrating Bodies in Motion," *Journal of the Acoustical Society of America*, Vol. 91, No. 5, May 1992, pp. 2544-2555.

[58] Gottlieb, D. and Turkel, E., "Dissipative Two–Four Methods for Time–Dependant Problems," *Mathematics of Computation*, Vol. 30, No. 136, October

1976, pp. 703-723.

[59] Troutt, T.R., and McLaughlin, D.K., "Experiments on the Flow and Acoustic Properties of a Moderate–Reynolds–Number Supersonic Jet," *Journal of Fluid Mechanics*, Vol. 116, 1982, pp. 123-156.

[60] Press, W.H., Teukolsky, S.A., Vetterling, W.T., and Flannery, B.P., *Numerical Recipes in Fortran: The Art of Scientific Computing*, Cambridge University Press, Cambridge, 1992.

[61] Mankbadi, R.R., Shih, S.H., Hixon, R., Stuart, J.T. and Povinelli, L.A., "Extension of Near Field to Far Field Jet Noise Prediction," AIAA Paper No. 96-2651, July 1996.

[62] Raman, G., "Cessation of Screech in Underexpanded Jets," AIAA Paper No. 96-1719, May 1996.

[63] Scott, J.N., and Hankey, W.L., "Numerical Simulation of Cold Flow in an Axisymmetric Centerbody Combustor," *AIAA Journal*, Vol. 23, No. 5, May 1985, pp. 641-649.

[64] Chyczewski, T.S., and Long, L.N., "Numerical Prediction of the Noise Produced by a Perfectly Expanded Rectangular Jet," AIAA Paper No. 96-1730, May 1996.

[65] Pilon, A.R., and Lyrintzis, A.S., "Refraction Corrections For The Kirchhoff Method," AIAA Paper No. 97-1654, May 1997.

[66] Amiet, R.K., "Refraction of Sound by a Shear Layer," *Journal of Sound and Vibration*, Vol. 58, No. 4, 1978, pp. 467-482.

[67] Schlinker, R.H., and Amiet, R.K., "Shear Layer Refraction and Scattering of

Sound," AIAA Paper No. 80-0973, June 1980.

[68] Morfey, C.L., and Szewczyk, V.M., "Jet Noise Modelling by Geometric Acoustics, Part 1. Theory and Prediction Outside the Cone of Silence," *ISVR Technical Report No. 91*, Sept. 1977.

[69] Tester, B.J., and Morfey, C.L., "Developments in Jet Noise Modeling – Theoretical Predictions and Comparisons with Measured Data," *Journal of Sound and Vibration*, Vol. 46, No. 1, 1976, pp. 79-103.